# EXPERIMENTAL INVESTIGATIONS OF PSEUDOSPARK DISCHARGE AND PSEUDOSPARK PRODUCED INTENSE ELECTRON BEAMS

by

JING HU

A DISSERTATION

Presented to the Faculty of the Graduate School of the

MISSOURI UNIVERSITY OF SCIENCE AND TECHNOLOGY

In Partial Fulfillment of the Requirements for the Degree

DOCTOR OF PHILOSOPHY

in

AEROSPACE ENGINEERING

2012

Approved by

Joshua L. Rovey, Advisor
Kakkattukuzhy M. Isaac,
David W. Riggins,
Scott M. Kovaleski
Carlos H. Castano

## PUBLICATION DISSERTATION OPTION

This dissertation has been prepared in three papers for publication in the style used by Missouri University of Science and Technology. Three journal articles which have been published or are under review are presented in this dissertation on various topics of the pseudospark discharge. Paper 1 “Experimental investigation of formation time in single-gap pseudospark discharge” has been published in *Journal of Physics D: Applied Physics*, 45(2012) 465023. Paper 2 “Faraday cup with nanosecond response and adjustable impedance for fast electron beam characterization” has been published in Review of Scientific Instruments, 82 (7) 073504. Paper 3 “Experiment investigation of time-resolved electron beam energy distributions generated in a transient hollow cathode discharge” has been submitted to Journal of Applied Physics and is currently under review.

## ABSTRACT

This dissertation focuses on the pseudospark discharge, a pulsed discharge discovered for the first time in 1970's. This dissertation is prepared as three journal articles in the style used by Missouri University of Science and Technology. A high voltage pseudospark discharge experiment setup, and discharge and electron beam diagnostic system are constructed and presented in this work. Three journal articles which have been published or are under review are presented in this dissertation on various topics of the pseudospark discharge.

Paper 1 "Experimental investigation of formation time in single-gap pseudospark discharge" is focused on experimental investigations of the time-dependent characteristics of single gap pseudospark discharge device in order to understand the initiation of the discharge current increase and build-up of a highly conductive channel during the high current main discharge phase, which is important for pseudospark performance as a switching device. Paper 2 "Faraday cup with nanosecond response and adjustable impedance for fast electron beam characterization" presents a specifically designed Faraday cup diagnostic with fast response time of 8.6 ns that is used to determine the time-resolved electron beam energy distribution function by the self-biased method. Paper 3 "Experimental investigation of time-resolved electron beam energy distributions generated in a transient hollow cathode discharge" describes a more accurate method to determine time-resolved electron energy spectrum of pseudospark electron beams using a retarding potential energy analyzer (RPEA) specifically designed for pulsed electron beams within the pressure range of tens of mTorr. The time-dependent electron beam energy spectrum generated by multi-gap pseudospark discharge, and the dependence of generated electron energy on external parameters are presented in this work. Experimental investigations under applied potential of 5 kV, 10 kV, 15 kV and 20 kV were carried out and the time-resolved electron energy distributions are constructed. Additionally, the energy efficiency of pseudospark produced electrons is also calculated for energy cost evaluation and compared with the requirement of intense electron beam applications in this work.

## ACKNOWLEDGMENTS

I wish to express my most sincere gratitude to my advisor Dr. Joshua Rovey. Without his patience, insightful guidance and encouragement, this work would not be possible. I must acknowledge my appreciation to all the members of my dissertation committee, Dr. Kakkattukuzhy Isaac, Dr. David Riggins, Dr. Scott Kovaleski, and Dr. Carlos Castano for all the interesting discussions on pulse power and charge particle physics issues and inspiring supervision of this work. I would also like to express my thanks to all my colleagues in the Aerospace Plasma Laboratory at Missouri S&T for their encouragement, assistance, and enlightening conversations.

On a personal level, I must express my gratitude to my boyfriend Keyou for his endless patience and encouragement. I could never complete my research work without his support. I would also like to express my appreciation to my parents Qingli and Xiurong for their support.

# TABLE OF CONTENTS

SECTION

# LIST OF ILLUSTRATIONS

Figure Page

SECTION

PAPER II



PAPER III

# LIST OF TABLES

Table Page

# 1. INTRODUCTION

In this chapter, the introduction of pseudospark discharge will be presented in the following sections. The fundamental mechanism, basic configuration, and development process are described in Section 1.1. In Section 1.2, the applications of pseudospark in various research and industrial areas as both a discharge device and electron beam source are reviewed and summarized according to the previous research work. In addition to the great research interest of pseudospark discharge, a discussion of current challenges, limitations, and problems to be determined is presented in Section 1.3. Finally, the objective and outline of this dissertation, and a brief introduction of three journal articles in this work is summarized in Section 1.4.

## 1.1 MECHANISM AND CONFIGURATION OF PSEUDOSPARK DISCHARGE

The pseudospark discharge was first discovered in the late 1970's, as an axially symmetric, high voltage gas discharge operating at low pressure regime located on the left hand side of the Paschen curve as illustrated in Figure 1.1 [1], which is based on the principles of a hollow cathode discharge. The fundamental discharge configuration consists of planar anode and cathode, or multi-gap electrodes, as illustrated in Figure 1.2 and Figure 1.3. The central hole in the middle of the electrodes makes the effective distance of the discharge path a maximum in the region of the bore hole on the axial center of electrodes and cathode cavity. Thus the gas discharge is concentrated in the region around the axis of the central holes [1-2]. Then the high electric field ($10^6$ V/m) concentrated in the central axis across the electrode gap and the charge carrier multiplication taking place in the hollow cathode cause the final ignition of high voltage high current gas breakdown. According to the previous research works [1, 3-8], the pseudospark discharge with a hollow cathode configuration can be divided into five different processes as illustrated in Figure 1.4.

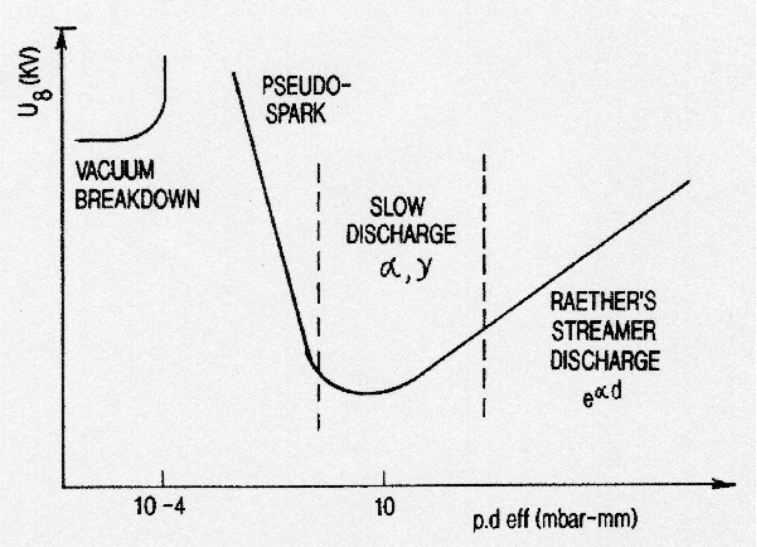


Figure 1.1. Gas breakdown curve (Paschen curve) under various pressure regions [1]

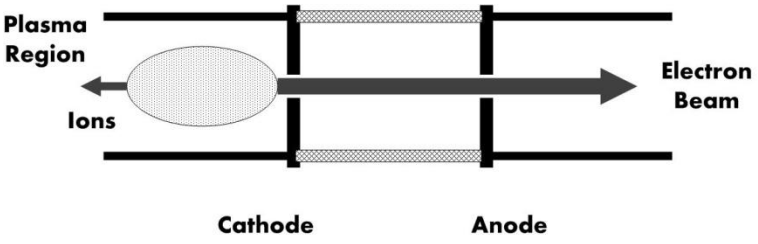


Figure 1.2. Single-gap pseudospark discharge chamber

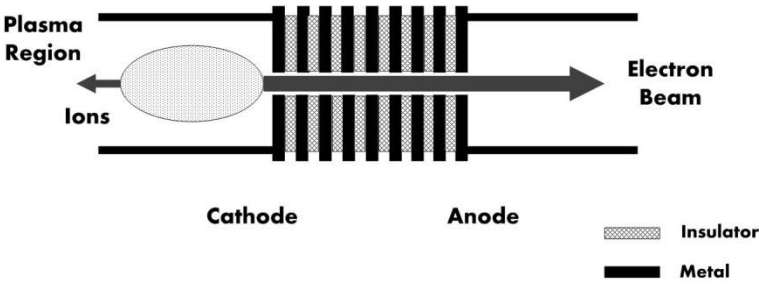


Figure 1.3. Multi-gap pseudospark discharge chamber

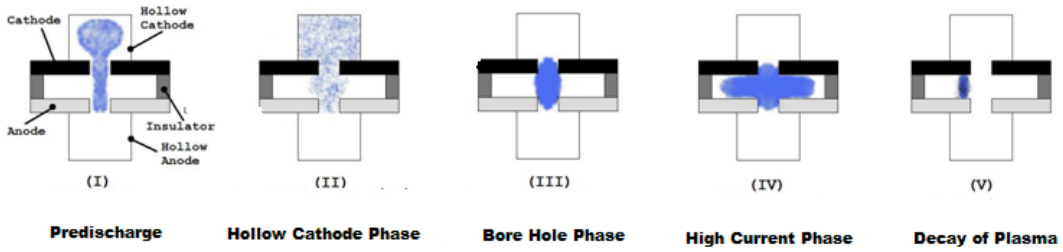


Figure 1.4. Different stages in pseudospark discharge

**1.1.1. Predischarge.** This stage is the initiation of pseudospark discharge. The pseudospark discharge is originated from the large charge carrier multiplication in the region of hollow cathode. Thus the electrons released from the hollow cathode region generated by the particle impact or photo-effect depending on the trigger type cause a strong avalanche growth in the cathode backspace and accelerated into the gap between anode and cathode. Then a dense plasma emerges at the center path in the intergap region as illustrated in Figure 1.4 [1].

**1.1.2. Hollow Cathode Discharge.** In some research work, the hollow cathode discharge (phase II in Figure 1.4.) and bore hole phase (phase III in Figure 1.4.) are assumed to be one phase, since they are both characterized by ionization enhancement in the gap region and plasma propagation from cathode region toward anode space [1]. In this phase, the charge multiplication is further enhanced and the hollow cathode phase is filled with plasma working as a virtual cathode for the electron extraction from the cathode backspace. The extracted electrons from cathode backspace are accelerated and propagated under the effect of electric field potential in the intergap region between anode and cathode. This phase is characterized by the start of electron emission from pseudospark discharge. Additionally, the voltage breakdown across the pseudospark gap and increase of discharge current can be easily observed by electrical measurements in this phase [1-2].

**1.1.3. High Current Main Discharge.** This phase is of great interest in gas switching applications [2, 4] due to its capability to establish high current of kA within very short time of $10^{-9}$-$10^{-7}$ seconds, leading to a current rising rate of $10^{10}$-$10^{11}$ A/second. The mechanism for pseudospark to achieve such a high current is still not well determined. In the work of Hartmann and Gundersen [4], the high current pseudospark discharge is assumed to be a form of superdense glow discharge. In [4], gas particles are released from the cathode surface by ion impact and thermal desorption. The electrode surface is then heated by ion impact to a temperature of 3000-4000 K within 30-100 ns. Additionally, an estimation of field-enhanced thermionic electron emission (Schottky emission) was presented in [4] to show its capability to deliver the measured high current density. However, in some other work [2], the parameters of high current in pseudospark were assumed to be mainly determined by the external circuit consisting of trigger, capacitance and inductance, and pulse charging mode.

**1.1.4. Decay of Plasma.** At this stage, the decay and recovery of plasma in pseudospark is of specific interest due to their effect on the recovery strength and repetition rate of pseudospark device [9]. When the time interval between single shot of pseudospark discharge exceeds the limit of decay and recovery time of plasma in given pseudospark device, residual ionization in the gap can cause the discharge to become unstable and breakdown of the gas occurs at lower voltages, i.e., during charging of the storage capacitors [9-10]. During this phase, the main processes that remove the residual ionization in the pseudospark device are plasma bulk recombination and diffusion toward the wall [1, 9]. The research work presented in [9] shows that the ambipolar diffusion of electrons inside the hollow cathode is the main limiting factor for the decay and recovery time of pseudospark discharge. And the recovery time of pseudospark device presented in [9] was fitted as a function of hollow cathode length and radius of gas volume in the given configuration:

$$t_{rec} \propto \left[\left(\frac{2.405}{r_0}\right)^2 + \left(\frac{\pi}{L}\right)^2\right] \quad (1)$$

where $t_{rec}$ is the minimum limit of recovery time for a pseudospark device, $r_0$ is the radius of gas vessel volume in the given device, and $L$ is the length of hollow cathode.

## 1.2 APPLICATIONS OF PSEUDOSPARK DISCHARGE

The specific property of the pseudospark to establish a high current and intense charge particles in a gas discharge within very short time (normally within $10^{-9}$-$10^{-6}$ second) make this specific discharge configuration be potential and of great interest in many research areas, including fast gas switches, intense electron beam sources, and even aerospace applications.

**1.2.1 Fast Gas Switches.** As stated in previous section, pseudospark discharge is a pulsed gas discharge in which the gas discharge can obtain tens to hundres of kV voltage hold-off capability and kA discharge current during total time of discharge of tens to hundreds ns, and several ns rise time. The physical volume of pseudospark discharge chamber is tens of $cm^3$. Thus the pseudospark device can obtain the tens of kV hold-off voltage and high current rising rate of $10^{10}$ to $10^{11}$ A/s within a 10s of $cm^3$ volume, which makes it suitable for compact pulsed power drive with a large total charge transfer, high repetition rates and low jitter values compared with hydrogen thyratrons [2-4, 6-7, 11-13]. Besides the high voltage high current hold-off capability, the pseudospark is a low-pressure gas discharge operated on the left branch of Paschen curve. Thus unlike high pressure spark gaps, this device is free from mercury and electrode erosion to achieve longer lift time. A pseudospark switch presented in [2] shows the switching capability of high pulse energy and high peak currents of up to 3.5 kJ per pulse at up to 200 kA peak current per switch, with lifetime in excess of $10^5$ shots at high repetition rate, and lifetime of up to $10^{10}$ shots under normal operating conditions. Additionally, due to the simple and symmetric configuration of pseudospark device, the possibility of paralleling several discharge channels to obtain higher current rise and lifetime can be easily achieved. Ref [14] presents a radial multi-channel pseudospark configuration which was tested up to $10^5$ kA peak current and charge transfer of 78 coulomb under pulsed operation.

**1.2.2 Intense Electron Beam Source.** Another important feature of pseudospark is the capability of plasma-produced intense electron beam generation. During gas breakdown, electrons are multiplied rapidly because of the hollow cathode effect. Then the electrons are accelerated by high electric field and extracted from the exit at anode side. This electron beam is a highly pinched electron beam with high current density ($10^3$ A/cm$^2$) and high energy (keV-tens keV).

The outstanding characteristics of pseudospark produced charge particles have been successfully applied in multiple applications [15-22]. In [17-19], the intense electron beams were developed for ultraviolet and x-ray production. A pulsed electron beam of 10A was generated from an 8-gap pseudospark (PS) discharge. The beam was used to produce coherent microwave radiation via a Cherenkov interaction between the electron beam and the $TM_{01}$ mode of a 60-cm long alumina-lined waveguide. A gain of $29 \pm 3$ dB was measured and an output power of $2 \pm 0.2$ kW in the frequency range 25.5-28.6 GHz [21-22]. In [23-25], the pulsed electron beam with estimated power density of $10^9$ W/cm$^2$ was determined to be a good candidate for material processing compared with common pulsed lasers. Specifically, some results of copper thin films are presented in [23-24].

**1.2.3 Specific Applications of Intense Electrons Beams in Aerospace Area.** Pulsed intense electron beams characterized by a very fast time duration and high charge numbers also have applications in aerospace area. Electron beam fluorescence is a relevant example. The electron beam fluorescence (EBF) technique for gas specie density measurement has been developed since 1968 [26]-[30]. As illustrated in Figure 1.5 [31], in this technique, local number density measurement using the electron beam technique is determined by a unique relationship between the local gas number density and the spontaneous fluorescence of the beam-excited atomic states [27]. Compared to the laser-induced fluorescence (LIF) technique used in gas density and temperature measurements, the extra seed gas or multi-photon excitation is not required in EBF techniques.

However, in both LIF and EBF techniques, the quenching collision in an unknown environment is a big challenge for the applications in relatively dense air flow,

since the collisional quenching at greater densities can cause a nonlinearity between intensity and density, leading to increase of measurements uncertainty as the density rises [26, 28]. Thus, in [26, 28-30], the pulsed electron beam fluorescence (PEBF) technique was developed and the advantages of pulsed electron beam compared with DC electron beam in fluorescence technique were analyzed and validated. Compared with the DC electron beams, pulsed electron beams consume small amount of total energy and can be packaged in a small volume. In addition, background light levels which are the bane of high enthalpy diagnostics can be minimized since the signal integration time is small in PEBF techniques [26]. Initial experimental study of pulsed electron beam fluorescence was obtained in a pseudospark discharge device [26, 28-30]. A 150-A pulsed electron beam is applied for both rotational temperature and gas density measurements in static, room temperature nitrogen at pressures between 5 mTorr and 150 mTorr.

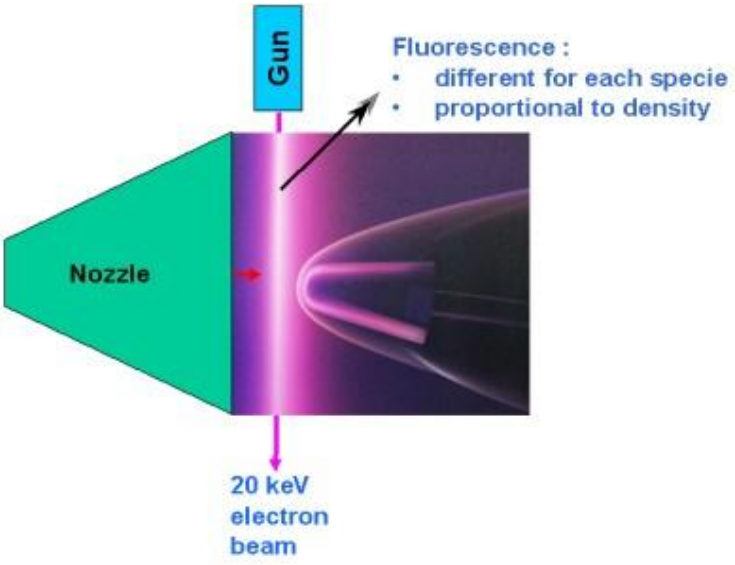


Figure 1.5. Typical setup of EBF in a wind tunnel [31]

Plasma generation is another important application which requires high energy intense electron beams. An example is the Magnetohydrodynamic (MHD) effect. Two

main applications related with MHD effect are MHD flow control and MHD power generation. Figure 1.6 shows the two different views of schematic of a MHD channel for flow control [32]. Production of plasma is a critical issue in the relevant applications, which may require highly efficient neutral gas ionization by high energy intense electron beams. In [33], the feasibility of electron beam generated plasmas in hypersonic MHD channel control was discussed. In [33-35], the MHD control of hypersonic flow and scramjet inlets by electron beam ionization was developed and validated. Electron beams are assumed to be the most efficient way of ionizing cold gases. Specifically, it shows that compared to low-energy (1-3 eV) electrons in conventional discharges that dissipate most of their energy in nonionizing inelastic collisions, the ionizing electrons with comparatively high energy from tens of electronvolts to thousand of electronvolts minimize the power required to sustain weakly ionized plasmas, which can be easily achieved by the presented pseudospark discharge [1, 8, 35].

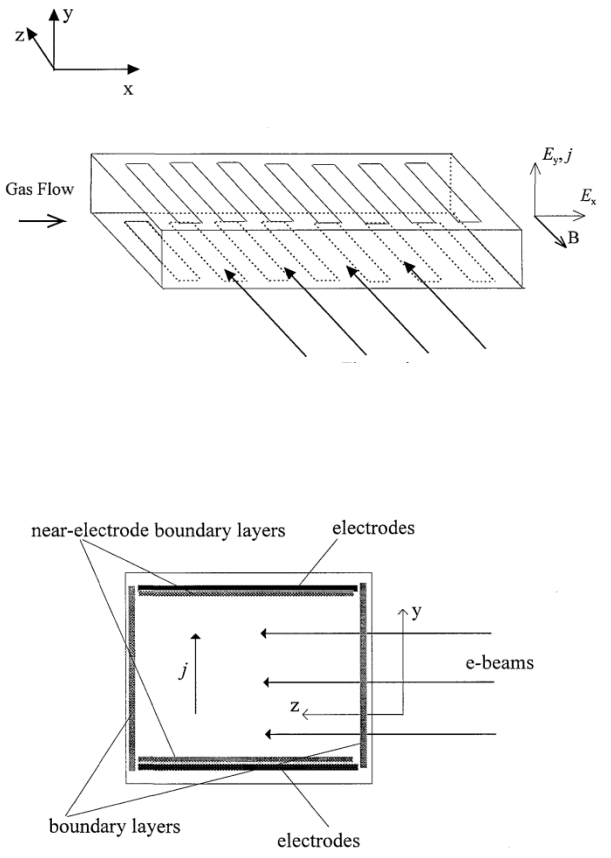


Figure 1.6. Schematic of a MHD channel with ionization control by electron beams [32]

## 1.3 CURRENT CHALLENGES AND LIMITATIONS

As stated in previous sections, due to the outstanding properties and simple configuration of pseudospark discharge and the capability of intense charge particle production, pseudospark discharge has been applied and shows high potential on various research areas. However, the specific operation conditions and parameters of pseudospark also cause challenges and limitations on the research work of pseudospark. Current research challenges associated with pseudosparks are summarized as follows:

**1.3.1 Fundamental Mechanisms in Pseudospark Discharge.** For many of the reported applications of pseudospark discharge, especially the switch applications and laser oscillation, more detailed knowledge of time-dependent characteristics of the discharge formation and development are still required. And the fundamental time-dependent characteristics of pseudospark discharge are not only important for fundamental gas discharge physics, but also closely associated with its applicability in pulse power system. In Section 1.1, the pseudospark discharge has been separated and described as four various phases: predischarge (phase 1), hollow cathode discharge (phase 2), high current main discharge (phase 3), decay and recovery of the discharge plasma (phase 4). In[1, 7, 13], phase 1 is assumed to be more related to the delay time between trigger or the onset of applied potential on discharge devices, and the initiation of breakdown. The research work presented in [9] shows that the high repetition rate of pseudospark device is mainly dependent on decay process of plasma during phase 4. Phase 2 and 3 are more associated with current and charge transfer capability, and high current rising capability ($10^{10}$A/sec~$10^{12}$A/sec), which is closely related with the switching applications. However, compared with the extensively qualitative and quantitative experimental investigations and physical model on the high pressure spark-gap switches in various technological focuses [2, 36-37], investigations of pseudospark discharge as switching devices are still not well determined, including the formation and ignition of plasma, the build-up time to obtain highly conductive phase, which are the fundamentals to evaluate and optimize the device performance.

**1.3.2 Diagnostic of Pulsed Fast Electron Beams.** Accurate detection and versatile monitoring of intense electron beams is one of the most important activities in charge particle physics and applications. The detectors and measuring system show great diversity depending on the requirement and objective of research work. But there are still some general properties among various detector systems as following [38]:

1) On-line measurement;
2) Non-destructive;
3) Radiation resistant absolute measurement;
4) Vacuum compatible;

5) Type of output signal.

Different from dc-beams without time structure, the pulsed electron beams generated from pseudospark discharge must be characterized on the time scale of $10^{-9}$-$10^{-7}$ second. In addition to the common requirements listed above, the time response of pulsed electron beams with a nanosecond time scale is of primary important [39-42]. Since under such time scale, the characteristic physical dimension of transmission system is comparable with the signal wavelength of electron beam pulse, which will cause the reflection and frequency dispersion of detected electron beam pulse signal. Thus special attention is required by the design of the collector and detector of very short intense pulsed beam and more detailed design procedure will be discussed in the following sections in this work. Figure 1.7 shows an example of the electron beam pulse detected by a beam detector with fast response time (bottom) and insufficient response time (top).

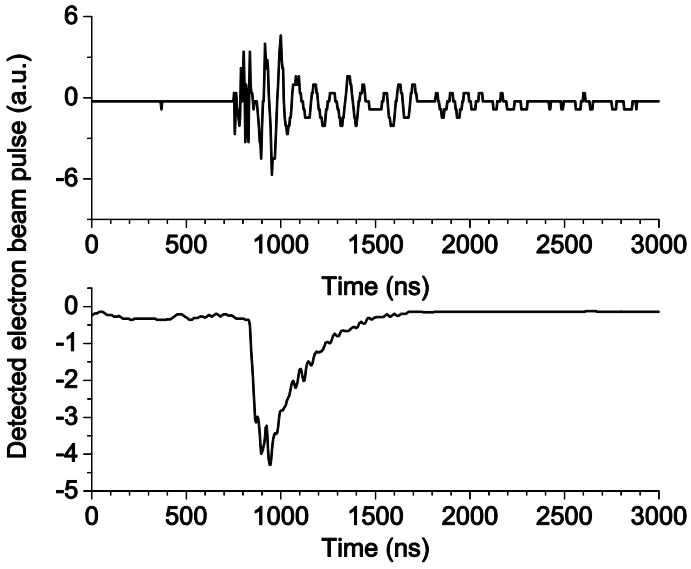


Figure 1.7. Electron beam pulse detected by the detector with fast response time of 8 ns (bottom) and insufficient response time (top)

**1.3.3 Time-resolved Energy Determination of Pulsed Electron Beams.** Determination of beam energy and energy spread is of great importance in evaluating beam quality and optimizing the parameters of electron beam source for various applications. In some previous research work, the average energy of pseudospark produced electron beams were evaluated in various method [3, 43-45], such as x-ray radiation method [3, 43-44] and electron range-energy study method by stopping foil [45]. In addition to the evaluation of mean energy of electron beams, the determination of full energy spectrum and temporal evolution of pulsed electron beam energy distribution over the completed time duration spread of the electron beam pulses is of great interest in many applications [32-36, 46-48]. For example, the detailed temporal evolution of electron energy distribution is essential for understanding or monitoring the beam interaction with a target, either gas or solid [46-48]. Additionally, in MHD related applications, the modeling of high energy electron excited plasma in neutral gas requires more accurate information of electron populations with various energies at various time points [32-36], due to the special attentions on ionization kinetics and the uniformity of beam-generated ionization profiles.

However, only few studies have been focused on the construction of time-resolved electron beam energy distributions which is limited by many factors. The most common method to obtain the time-resolved energy distribution of charge particle (including both ions and electrons) is the retarding potential energy analyzer (RPEA) as shown in Figure 1.8 [49]. In addition to the response time of electron beam detectors which has been discussed previously, gas breakdown threshold in the operational pressure range of pseudospark (tens of mTorr – hundreds of mTorr) is the main limitation to the determination of time-resolved electron energy distributions. Since under this pressure range, the breakdown voltage of gas is located at the bottom of breakdown curve (Paschen curve) which causes unexpected gas breakdown leakage between high retarding potential grid and ground vacuum grid.

In the very limited quantity of previous research work concerning on the electron beam energy analysis [3, 43-45, 50], only [50] presents the time-resolved energy spectrum of pulsed electron beams produced from pseudospark at one given pressure and voltage. There are still more properties to be determined, such as the variations of

electron energy distribution with various operational parameters, the energy transformation efficiency of electron generation by pseudospark device, and the particle populations of electrons with different energy in the pseudospark produced beam.

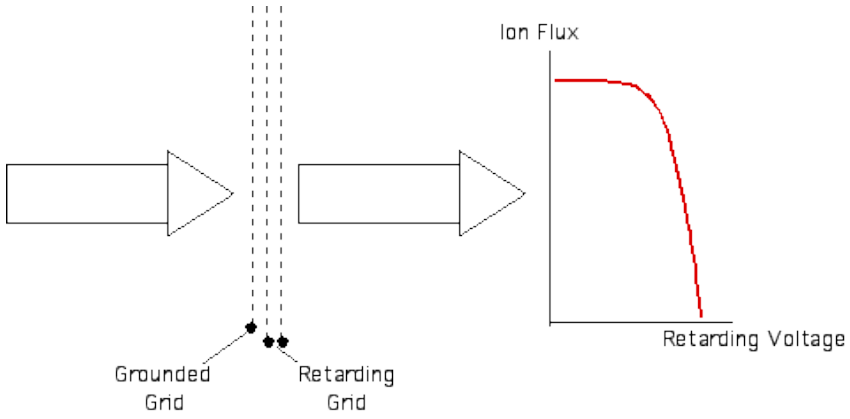


Figure 1.8. A typical retarding potential energy analyzer setup [49]

## 1.4 OBJECTIVES STATEMENT AND OUTLINE OF THE DISSERTATION

Since the pseudospark discharge was discovered in 1970's for the first time, its simple configuration and outstanding properties brought high potential research interest on this high efficiency low cost pulsed discharge device. Although many research progress has been presented in previous work as listed in Section 1.2, there are still a variety of problems and limitations which are not well determined or understood yet, as presented in Section 1.3. The objective of this dissertation is to assess and determine the potential of the pseudospark discharge to serve as an intense electron beam source for ambient plasma creation for aerospace applications. The research work presented in this dissertation is mainly focused on the experimental investigations on various properties of pseudospark device and intense electron beams generated from pseudospark, which are specifically of great importance for the pseudospark discharge as an efficient electron beam source. This dissertation is prepared as three journal articles in the style used by

Missouri University of Science and Technology. Section II in the following part is a general introduction on the construction of current high voltage pseudospark discharge experiment setup in Aerospace Plasma Lab in Missouri S&T, including vacuum system, high voltage charging system, pulsed discharge measurement system, and electron beam drift system. Pictures and test reports on the construction and calibration of the experiment setup are also presented in Section II.

Three journal articles which have been published or under review are presented in this dissertation on various topics of pseudospark discharge. Paper 1 "Experimental investigation of formation time in single-gap pseudospark discharge" has been published in *Journal of Physics D: Applied Physics*, 45(2012) 465023. This paper is focused on experimental investigations of the time-dependent characteristics of single gap pseudospark discharge device in order to understand the initiation of discharge current increase and build-up of highly conductive channel during the high current main discharge phase (phase 3 in Section 1.2), which are the main focus in this work for its importance in the performance as switching device [2, 36-37]. The formation time of discharge starting from initiation to maximum breakdown and its dependence on gas pressures are investigated in single-gap device with varying geometric dimensions of pseudospark device. The main emphasis of this paper is focused on the study of fundamental discharge mechanism in pseudospark discharge device, and the dependence of discharge formation on external parameters, such as geometric factors and gas pressure. The experiment results show that the initiation of a pseudospark discharge is synchronous with the propagation of an ionization detected by a capacitive probe array. And the start of the main high current phase of pseudospark is ignited right after this ionization front stopping at the anode backspace of pseudospark device. The dependence of characteristic time of the propagation of this ionization front under varying external parameters was investigated and presented in Paper 1.

Paper 2 "Faraday cup with nanosecond response and adjustable impedance for fast electron beam characterization" has been published in Review of Scientific Instruments, 82 (7) 073504. In this paper, the main technical points of Faraday cup, a most general beam stopper and collector, was discussed for pulsed electron beam diagnostics with nanosecond spread time structure. The Faraday cup presented in this

paper is specifically designed and applied to determine the time-resolved electron energy distribution function by the self-biased method [46], which requires that the Faraday cup has adjustable impedance. The Faraday cup probe in this work has been validated to have a time response of 8.2 ns.

Paper 3 “Experiment investigation of time-resolved electron beam energy distributions in a transient hollow cathode discharge based electron beam” has been submitted to Journal of Applied Physics and is currently under review. In this paper, a more accurate method to determine time-resolved electron energy spectrum, retarding potential energy analyzer (RPEA) specifically designed for pulsed electron beams at pressure range of tens of mTorr is developed and used to investigate the energy of pseudospark produced electron beams. The main emphasis of this paper is on the time-dependent electron beam energy spectrum generated by multi-gap pseudospark discharge, and the dependence of generated electron energy on external parameters. Experimental investigations under applied potential of 5 kV, 10 kV, 15 kV and 20 kV were carried out and the time-resolved electron energy distributions are constructed. Additionally, the energy efficiency of pseudospark produced electrons is also calculated for energy cost evaluation and compared with the requirement of intense electron beam applications in this work. The energy transformation efficiency increases from 11.4% at 5 kV breakdown voltage to 23.2% at 20 kV breakdown voltage.

Then in the final chapter, the recommendations for future work is discussed and summarized.

## BIBLIOGRAPHY


[1] Gundersen M.A. and Schaerfer G., (eds) 1990 *Physics and Applications of Pseudosparks* (New York, N.Y.: Plenum Press)

[2] Schaefer, G., Kristiansen, M. and Guenther, A. (eds) 1990 *Gas Discharge Closing Switches* (New York, N.Y.: Plenum Press)

[3] Frank, K., Christiansen, J., "Fundamentals of the pseudospark and its applications", (1989) *IEEE Transactions on Plasma Science*, 17 (5), pp. 748-753.

[4] Hartmann, Werner, Lins, Guenter, "Spatial and temporal development of pseudospark switch plasmas", (1993) *IEEE Transactions on Plasma Science*, 21 (5), pp. 506-510.

[5] Stark, Robert, Almen, Ortwin, Christiansen, Jens, Frank, Klaus, Hartmann, Werner, Stetter, Michael, "Investigation of the temporal development of the pseudospark discharge", (1995) *IEEE Transactions on Plasma Science*, 23 (3), pp. 294-299.

[6] Puchkarev, Victor F., Gundersen, Martin A., "Spatial and temporal distribution of potential in the pseudospark switch", (1995) *IEEE Transactions on Plasma Science*, 23 (3), pp. 318-323.

[7] Frank, K., "Scientific and technological progress of pseudospark devices", (1999) *IEEE Transactions on Plasma Science*, 27 (4), pp. 1008-1020.

[8] Korolev, Y.D., Frants, O.B., Geyman, V.G., Landl, N.V., Ivashov, R.V., Shemyakin, I.A., Bischoff, R.E., Frank, K., Petzenhauser, I.J., "Temporal structure of the fast electron beam generated in the pseudospark discharge with external triggering", (2005) *IEEE Transactions on Plasma Science*, 33 (5 I), pp. 1648-1653.

[9] Rosier, O., Apetz, R., Bergmann, K., Jonkers, J., Wester, R., Neff, W., Pankert, J., "Frequency scaling in a hollow-cathode-triggered pinch plasma as radiation source in the extreme ultraviolet", (2004) *IEEE Transactions on Plasma Science*, 32 (1 II), pp. 240-246.

[10] Y. P.Raizer, 1991 *Gas Discharge Physics* (Berlin, Germany: Springer-Verlag)

[11] Goertler, A., Schwandner, A., Christiansen, J., Frank, K., Tkotz, R., "Investigations of two-stage-pseudospark switches for high-current applications", (1995) *IEEE Transactions on Electron Devices*, Vol. 42, No. 11, pp. 2021-2027.

[12] Gaudet, J.A.; Barker, R.J.; Buchenauer, C.J.; Christodoulou, C.; Dickens, J.; Gundersen, M.A.; Joshi, R.P.; Krompholz, H.G.; Kolb, J.F.; Kuthi, A.; Laroussi, M.; Neuber, A.; Nunnally, W.; Schamiloglu, E.; Schoenbach, K.H.; Tyo, J.S.; Vidmar, R.J.; "Research issues in developing compact pulsed power for high peak power applications on mobile platforms", (2004) *Proceedings of the IEEE* , Vol. 92, No. 7, pp. 1144- 1165.

[13] Jiang, C., Kuthi, A., Gundersen, M.A. "Toward ultracompact pseudospark switches", (2005) *Applied Physics Letters*, Vol. 86, No. 2, art. no. 024105, pp. 024105-1-024105-3.

[14] Heo, H., Park, S.S., Nam, S.H., "Experiments with a radial multichannel pseudospark switch for extremely high Coulomb transfer", (2004) *IEEE Transactions on Plasma Science*, 32 (1 II), pp. 196-202.

[15] Liu, C.J., Rhee, M.J., "Experimental study of post-acceleration and transport of a pseudospark-produced electron beam", (1993) *Proceedings of the Particle Accelerator Conference*, Vol. 1, pp. 688- 690.

[16] Jain, K.K., Ding, B.N., Rhee, M.J., "Scaling study of pseudospark produced electron beam", (1991) *Conference Record of the Particle Accelerator Conference, Accelerator Science and Technology., IEEE*, Vol. 3, pp.1972-1974.

[17] Benker, W., Christiansen, J., Frank, K., Gundel, H., Hartmann, W., Redel, T., Stetter, M., "Generation of intense pulsed electron beams by the pseudospark discharge", (1989) *IEEE Transactions on Plasma Science*, Vol. 17, No. 5, pp. 754-757.

[18] Jiang, C., Yao, Q., Eccles, B., Kuthi, A., Gundersen, M.A., "Pseudospark discharge-based extreme-ultraviolet radiation source", (2004) *Power Modulator Symposium, 2004 and 2004 High-Voltage Workshop. Conference Record of the Twenty-Sixth International*, pp.368-370.

[19] Westheide, J., "Investigation on the pseudospark electron beam and its application for the generation of soft X-rays", (1995) *IEEE Transactions on Plasma Science*, Vol. 23, No. 3, pp.254-257.

[20] Christiansen, J., Lieser, N., Rath, W., Steudtner, W., Rózsa, K., Jánossy, M., Apai, P., Mezei, P., "Pulsed laser oscillation at 488.0 nm and 514.5 nm in an Ar-He Pseudospark discharge", (1985) *Optics Communications*, Vol. 56, No. 1, pp. 39-40.

[21] Yin, H., Cross, A.W., He, W., Phelps, A.D.R., Ronald, K., "Pseudospark experiments: Cherenkov interaction and electron beam post-acceleration", (2004) *IEEE Transactions on* Plasma Science, Vol. 32, No. 1, pp. 233- 239.

[22] Yin, H., Cross, A.W., He, W., Phelps, A.D.R., Ronald, K., Bowes, D., and Robertson, C., W., "Millimeter wave generation from a pseudospark-sourced electron beam", (2009) *Physics of Plasmas* Vol. 16, No. 6, art no. 063105.

[23] Benker, W., Christiansen, Jens, Frank, Klaus, Gundel, H., Hartmann, Werner, Redel, T., Stetter, M., "Generation of intense pulsed electron beams by the pseudospark discharge", (1989) *IEEE Transactions on Plasma Science,* 17 (5), pp. 754-757.

[24] Stark, Robert, Christiansen, Jens, Frank, Klaus, Muecke, Friedrich, Stetter, Michael, "Pseudospark produced pulsed electron beam for material processing", (1995) *IEEE Transactions on Plasma Science*, 23 (3), pp. 258-264.

[25] Goertler, Andreas, Schwandner, Alfred, Christiansen, Jens, Frank, Klaus, Granzer, Hermann, "Development of a high current pseudospark switch and measurement of electron density", (1993) *IEEE Transactions on Plasma Science,* 21 (5), pp. 516-521.

[26] Lutfy, F.M., Muntz, E.P., "Initial experimental study of pulsed electron beam fluorescence", (1996) *AIAA Journal*, Vol. 34, No. 3, pp. 478-482.

[27] Honaker, W. C., Hunter Jr., W. W., and Woods, W. C., "Utilization of an Electron Beam for Density Measurements in Hypersonic Helium Flow", (1981) *AIAA Journal*, Vol. 19, No. 4, pp. 458-459.

[28] Muntz, E. P., Kunc, J.A. and Erwin, D. A., "A pulsed electron-photon fluorescence diagnostic technique for temperature and specie concentration measurement at points in relatively dense, unseeded air flow", (1987) *AIAA-87-1526, AIAA Thermophysics Conference*, 22nd, Honolulu, Hawaii.

[29] Muntz, E. P., Lutfy, F. M., and Boyd, I. D., "The study of reacting, high energy flows using pulsed electron-beam fluorescence", (1996) *AIAA-1996-1986, Fluid Dynamics Conference*, 27th, New Orleans, LA.

[30] Muntz, E. P., and Erwin, D. A., "Rapid Pulse Electron Beam Fluorescence for Flow Field Diagnostics", (1993) *New Trends in Instrumentation for Hypersonic Research, edited by A. Boulier, NATO ASI Series, Series E: Applied Sciences*, Vol. 21, Kluwer, Dordrecht, The Netherlands, pp. 265.

[31] Website information: "Optical diagnostics in hypersonic flows and in the upper atmosphere", *the French Aerospace Lab*, http://www.onera.fr/dmph-en/optical-diagnostics/electron-beam-fluorescence.php

[32] Macheret, S. O., Shneider, M. N., Miles, R. B., and Lipinski, R. J., "Electron-Beam-Generated Plasmas in Hypersonic Magnetohydrodynamic Channels", (2001) *AIAA Journal*, 0001-1452, Vol. 39, No. 6, pp 1127-1138.

[33] Macheret, S. O., Miles, . B., Nelson, G. L., "Feasibility study of a hybrid MHD/radiatively driven facility for hypersonic ground testing", (1997) *AIAA-1997-2429, Plasmadynamics and Lasers Conference*, 28th, Atlanta, GA.

[34] Macheret, S. O., Shneider, M. N., Miles, R. B., "Modeling of air plasma generation by electron beams and high-voltage pulses", (2000) *AIAA-2000-2569, AIAA Plasmadynamics and Lasers Conference*, 31st, Denver, CO.

[35] Macheret, S. O., Shneider, M. N., Miles, R. B., "Electron beam generated plasmas in hypersonic MHD channels", (1999) *AIAA-1999-3635, AIAA Thermophysics Conference*, 33rd, Norfolk, VA.

[36] Martin, J. C., *J.C.Martin on pulsed technology*, 1996 (New York : Plenum Press).

[37] Sorensen, T.P., Ristic, V.M., "Rise time and time-dependent spark-gap resistance in nitrogen and helium", (1977) *Journal of Applied Physics*, Vol. 48, No. 1, pp 114-117.

[38] Strehl, P., 2006 *Beam Instrumentation and Diagnostics* (Berlin; New York : Springer)

[39] Iida, T., Taniguchi, R., Fujimoto, T., Sumita, K., "Fast response Faraday cup for low-energy, nanosecond-pulse ion beams" (1982) *Review of Scientific Instruments*, 53 (2), pp. 168-170.

[40] Chuaqui, H., Favre, M., Wyndham, E., Arroyo, L., Choi, P., "Simple Faraday cup with subnanosecond response" (1989) *Review of Scientific Instruments*, 60 (1), pp. 141-142.

[41] Pellinen, D., "A high current, subnanosecond response faraday cup", (1970) *Review of Scientific Instruments*, 41 (9), pp. 1347-1348.

[42] Hu, J., Rovey, J.L., "Faraday cup with nanosecond response and adjustable impedance for fast electron beam characterization", (2011) *Review of Scientific Instruments*, 82 (7), art. no. 073504.

[43] Dewald, E., Frank, K., Hoffmann, D.H.H., Stark, R., Ganciu, M., Mandache, B.N., Nistor, M.G., Pointu, A.-M., Popescu, I.-I., "Pulsed intense electron beams generated in transient hollow cathode discharges: fundamentals and applications" (1997) *IEEE Transactions on Plasma Science*, 25 (2), pp. 272-278.

[44] Dewald, E., Frank, K., Hoffmann, D.H.H., Tauschwitz, A., "Comparative studies on intense electron beams generated in transient hollow-cathode discharges" (2002) *IEEE Transactions on Plasma Science*, 30 (5 I), pp. 1820-1826.

[45] Ramaswamy, K., Destler, W.W., Rodgers, J., "A high-voltage triggered pseudospark discharge experiment", (1996) *Journal of Applied Physics*, 80 (9), pp. 4887-4895.

[46] Modreanu, G., Mandache, N.B., Pointu, A.M., Ganciu, M., Popescu, I.I., "Time-resolved measurement of the energy distribution function of an electron beam created by a transient hollow cathode discharge", (2000) *Journal of Physics D: Applied Physics*, 33 (7), pp. 819-825.

[47] Kowalewicz, Roland, Redel, Thomas, "Interaction of a high current polyenergetic electron beam with metal", (1995) *IEEE Transactions on Plasma Science*, 23 (3), pp. 270-274.

[48] Stark, Robert, Christiansen, Jens, Frank, Klaus, Muecke, Friedrich, Stetter, Michael, "Pseudospark produced pulsed electron beam for material processing", (1995) *IEEE Transactions on Plasma Science*, 23 (3), pp. 258-264.

[49] Website information: *http://cindispace.utdallas.edu/rpa.html*

[50] Ding, B.N., Myers, T.J., Rhee, M.J., "Time-resolved energy spectrum of a pseudospark-produced electron beam" (1993) *Review of Scientific Instruments*, 64 (6), pp. 1442-1444.

# 2. EXPERIMENT SETUP

In this chapter, the pseudospark discharge experiment setup is described in Section 2.1, including the vacuum pumping and control system, high voltage charging and transmission system, and electron beam drift region, which are discussed in the following sections. The design and construction procedure of pseudospark discharge chamber are presented in Section 2.2. Section 2.3 is an introduction to the pumping system and gas flow controller. Main issues in high voltage charging and transmission system are discussed and summarized, and the calibration results of high voltage charging and pulsed high voltage signal transmission system is also presented in Section 2.4. Finally in Section 2.5, the diagnostic system of pseudospark discharge properties and electron beam detectors are described and summarized in this section, and the main performance validation test results are also presented in Section 2.5. In addition, Section 2.6 describes a simplified time domain reflectometer applied for calibration and troubleshooting of fast response probes in the presented experiments. For various research work of given objectives, the more detailed experiment setup will be presented in each article paper in the following chapters.

## 2.1 GENERAL INTRODUCTION OF PSEUDOSPARK DISCHARGE EXPERIMENT

The high voltage pseudospark discharge and electron study experiment setup is shown in Figure 2.1. The presented experiment setup consists of two regions: pseudospark discharge region, and electron beam drift region. The pseudospark discharge chamber, high voltage charging system, and pulsed discharge diagnostics are located in the pseudospark discharge region. A 70 cm long drift tube was connected to discharge chamber as the electron beam drift region. Vacuum pumping and gas flow control system and electron beam detectors are located in the electron drift region to control the ambient neutral gas pressure and investigate the characteristics of electron beams along the propagating path. There was no external applied guide magnetic field in our experiments.

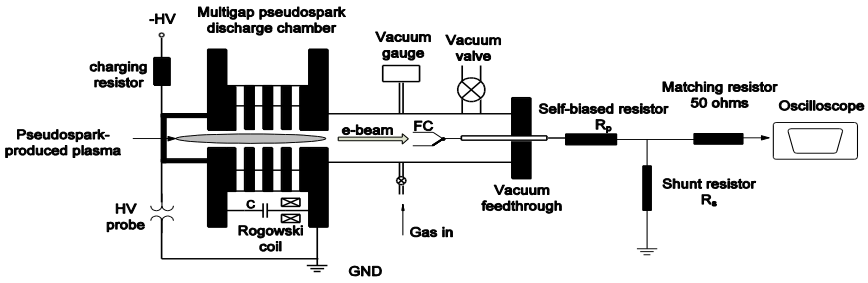


Figure 2.1. Pseudospark discharge and intense electron beam experiment setup

Figure 2.2 presents a photograph picture taken in a 20 kV pseudospark discharge experiment. As shown in Figure 2.2, high density and luminosity plasma is filled in the pseudospark device which is located at the left side on Figure 2.2. Meanwhile an intense electron beam is observed to exit from pseudospark device and propagate in the drift tube region, which is at the right side on Figure 2.2. As the intense electron beam propagating, the luminosity of electron beam become weaken along the downstream direction due to the beam loss by interactions and collisions of the electrons with neutral gas filled in the drift tube [1].

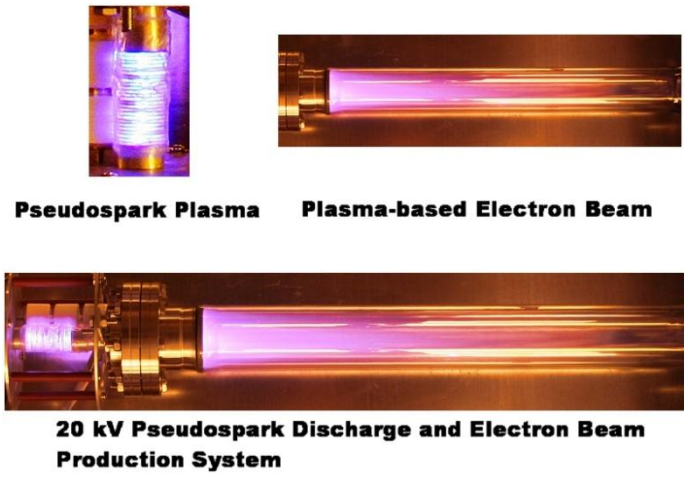


Figure 2.2. Pseudospark discharge and produced intense e-beams obtained in the presented setup

## 2.2 DESIGN AND CONSTRUCTION OF PSEUDOSPARK DISCHARGE CHAMBER

There are two pseudospark discharge chambers under investigation in APLab: single-gap pseudospark configuration, and multi-gap pseudospark configuration. Figure 2.3 (a) and (b) are the schematic drawing and photograph of single-gap pseudospark chamber. Figure 2.4 (a) and (b) are the schematic drawing and photograph of multi-gap pseudospark chamber.

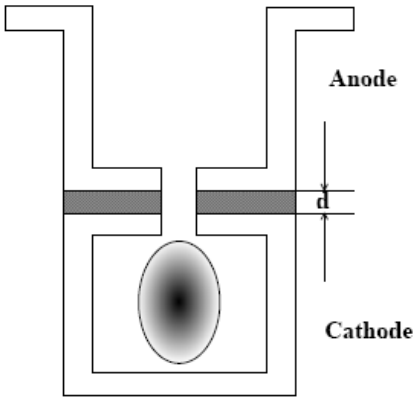


(a) Schematic of single-gap pseudospark device

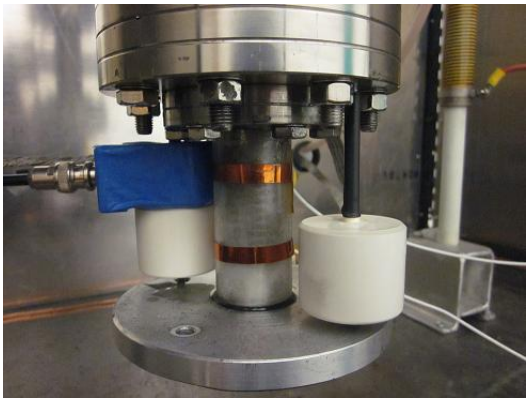

(b) Photo of single-gap pseudospark device

Figure 2.3. Schematic drawing (a) and photograph (b) of single-gap pseudospark chamber

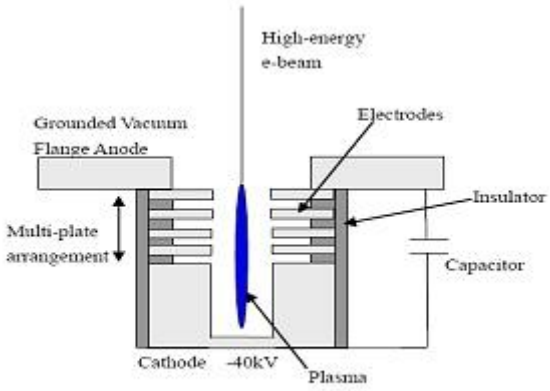


(a) Schematic of multi-gap pseudospark device

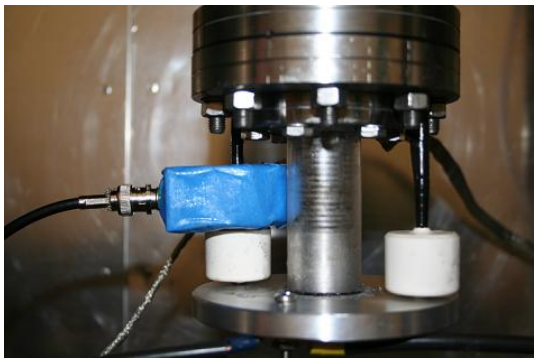

(b) Photo of multi-gap pseudospark device

Figure 2.4. Schematic drawing (a) and photograph (b) of multi-gap pseudospark chamber

As shown in Figure 2.3 and Figure 2.4, the pseudospark discharge chambers, both in single and multiple gap configurations consist of a cylindrical hollow cathode, grounded anode, electrodes and insulator disks between anode and cathode. In single-gap pseudospark configuration, the insulator thickness between anode and cathode can be varied by the stack of insulator disks (d in Figure 2.3). In multi-gap configuration, the gap numbers can be varied from 1 to 20 gaps. Each electrode and the hollow cathode have an

on-axis hole for the electron beam extraction. Other main configuration parameters of the pseudospark chamber are presented in Table 2.1.

Table 2.1. Main configuration parameters of the pseudospark chamber

| **Geometric dimensions of the PS chamber** | |
|---|---|
| **Gap distance** | 2 mm |
| **Number of gaps** | 1~16 |
| **Electrode thickness** | 1.5 mm |
| **Central hole of the electron path** | 1 mm |
| **External diameter of insulator** | 22 mm |
| **Internal diameter of the insulator** | 12 mm |
| **External diameter of the electrodes** | 22 mm |
| **External diameter of hollow cathode** | 22 mm |
| **Length of hollow cathode** | 25 mm |
| **Materials of the quartz insulator** | Acrylic |
| **Materials of the electrodes** | Stainless steel |

## 2.3 VACUUM PUMPING SYSTEM AND GAS FLOW CONTROLLER

As shown in Figure 2.1, in the electron beam drift region, a 70 cm transparent long drift tube was connected to discharge chamber for beam propagation study. The pseudospark discharge experiment is operated under the vacuum level of $10^{-2}$ Torr. The whole experimental system was evacuated down to $10^{-5}$ Torr initially by a two-stage mechanical pump and turbo pump located in the electron beam region. The operating gas was argon. A two-stage pumping system is applied to obtain the vacuum: the Edwards mechanical pump can vacuum the system down to $10^{-2}$ Torr within 15 minutes and the Varian V-70 turbo pump continues to vacuum the system to $10^{-5}$ Torr. It takes 30-40 minutes for the whole process.

Argon gas enters into the vacuum system through a mass flow controller. The mass flow rate of argon can be adjusted accurately to control the operation pressure in

vacuum system. With this Alicat Scientific 44072 gas flow controller, the gas pressure of the chamber can be controlled at a very slow rate, dp/dt = 1 mTorr/sec. A calibrated linear positioner is installed in the vacuum system to study the electron beam characteristics in the longitudinal direction of drift region.

## 2.4 HIGH VOLTAGE CHARGING AND TRANSMISSION SYSTEM FOR PSEUDOSPARK DISCHARGE AND MEASUREMENT

As mentioned in above sections, pseudospark discharge and the produced electron beam are conducted under high voltage (1 kV~10s kV), high current (100s A~10s kA) and fast time (ns), which cause the generation, detection and transmission of high voltage signal become very challenging. The most important issue in such high voltage system is the electric insulation, in discharge chamber, detectors and signal transmission system. Without proper insulation, no high voltage can be obtained or maintained and no stable signal can be detected. In the presented experiment setup, debugging and elimination of leakage current flowing through the system is the main objective of high voltage generation and transmission.

The simplified electric symbol schematic of the charging/discharge setup is shown in Figure 2.5. The presented system is designed to work under 100 kV of negative polarity. Due to the power level, most commercial high voltage power supplies have comparatively low current limit (usually 1~5 mA) and are usually sensitive to the current flow through the main circuit (I1 in Figure 2.5). The high voltage power supply currently used in the presented experiment has an upper limiting current of 1mA, and the current limiting resistor has comparatively high resistance of 20 MΩ. All of these conditions make even very low leakage current flow (< 1mA) be a trouble to the experiment operations since it can cause several kV or 10s kV voltage drop loss on charging resistor.

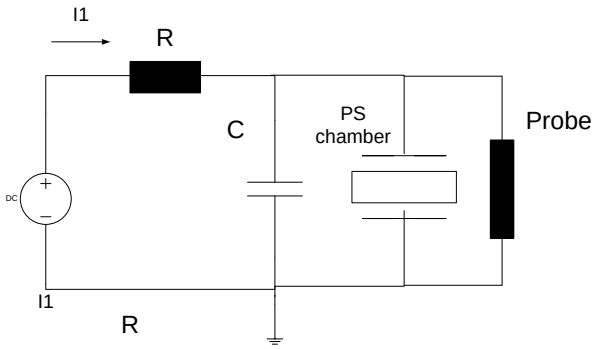


Figure 2.5. Simplified electric symbol of high voltage charging and discharge setup

The possible factors which may cause the leakage current of the pseudospark charging system can be the high voltage probe channel, the leakage current flow through the charging/discharge capacitors, and the dielectric strength of the pseudospark chamber. In order to eliminate the leakage current, a series of debugging tests was conducted. The final conclusions are summarized as following.

**2.4.1 Leakage Current by Residue Charge Effect.** A main cause of the leakage current in the presented system is the "residue charge" produced in the vacuum system after gas breakdown, instead of the commonly assumed leakage current through high voltage probe. Such an effect can produce a leakage current 5 - 10 times greater than the leakage current introduced by high voltage probe, which was expected to be the most leakage current source in the former work. However, it was found during APLab's experimental research that such a residue charge effect can be eliminated by thorough cleaning of the discharge chamber by acetone in ultrasonic cleaner. Figure 2.6 is the comparison results on leakage currents between the pseudospark chamber with and without residue charge effect. As shown in Figure 2.6, the leakage current without high voltage probe connected become zero after eliminating the residue charge effect.

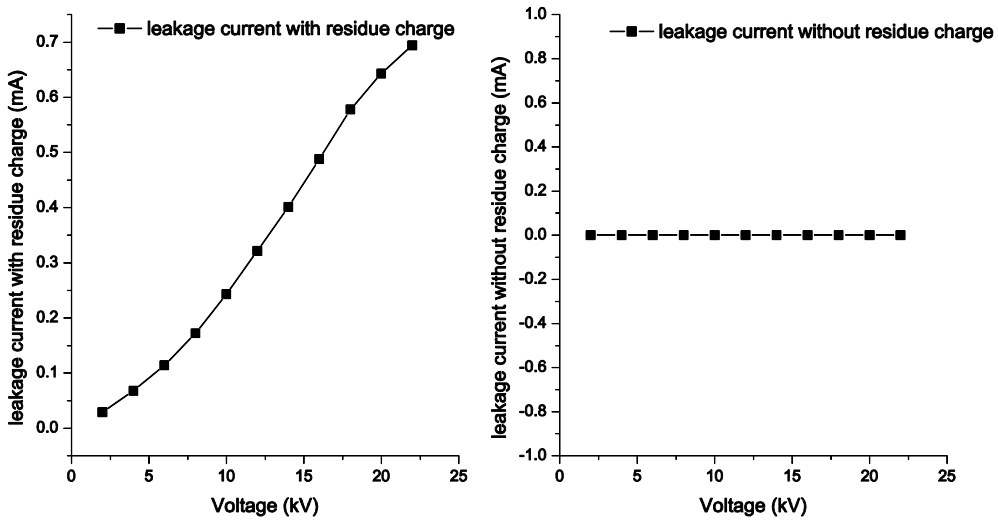


Figure 2.6. Leakage current through pseudospark discharge chamber with residue charge (left side) and without residue charge (right side)

**2.4.2 Leakage Current by High Voltage Detection Probe.** After the elimination of residue charge effect, the leakage current produced by high voltage probe cannot be neglected either. Meanwhile, the higher time resolution rate of the high voltage probe is also an important issue in our work. Thus a North Star custom high voltage probe PVM-5 with 400 MΩ equal impedance, which is 4 times higher than the Tek 6015B high voltage probe, and 80 MHz operation frequency is used in all in all experiments. Figure 2.7 is the comparison results between the leakage current induced by Tek 6015B and North Star PVM-5, it shows that the North Star PVM-5 can decrease the leakage current by 75% of the leakage current induced by Tek 6015B.

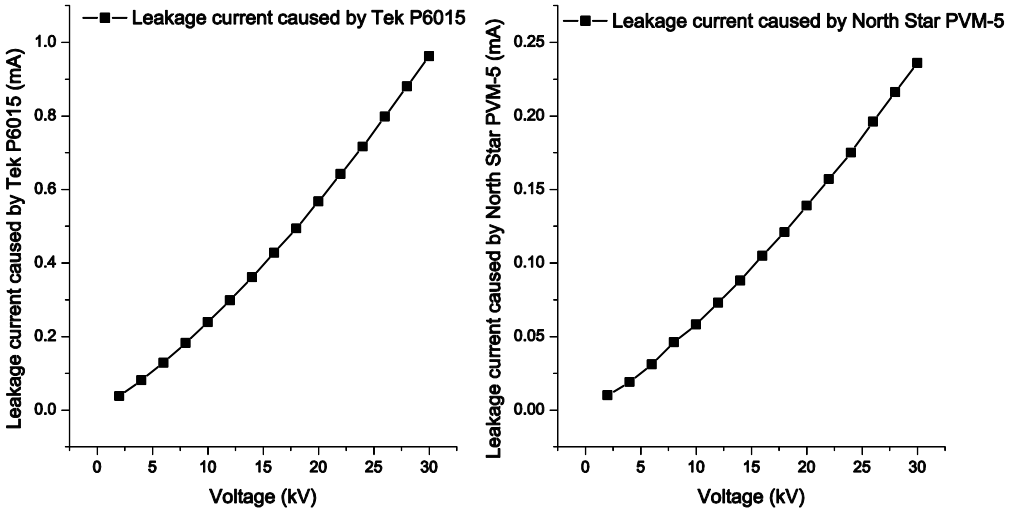


Figure 2.7. Leakage current flowing through high voltage probe Tek 6015 (left side) and North Star PVM-5 (right side)

**2.4.3 Leakage Current and Instability of Pseudospark Discharge Configuration.** The instability of the electric signals when operating at high voltage is another problem. Through serial debugging work, it was found that in pseudospark chamber, there was partial discharge (spark) because of the sharp edge of metal electrodes and central bore holes under high voltage. Thus all the edges of metal electrodes are machined to round shape with a 45° angle. Additionally, when the energetic electrons passing through the central path of pseudospark device, the interaction of electrons with metal electrode will leave a deposition film on the metal surface of electrode leading to contamination of electrode.

The contamination of electrode by interaction of energetic electrons passing through the electron beam path is an important factor leading to instability of discharge properties after given discharge shot counts. Figure 2.8 shows three electrodes after various operational time. The left one displays most contamination in the center of electrode around the central hole of electron beam path after approximately 105 discharge shots. The middle one also shows contamination on electrode after 104 shots. And the

right one is the polished electrode without contamination film. Then in Figure 2.9, the leakage current caused by electrode contamination under various applied voltages on a 12-gap pseudospark device is presented with polished electrodes and contaminated electrodes (middle of Figure 2.8) are compared under applied voltages varying from 0-10 kV. As illustrated in Figure 2.9, the leakage current through the pseudospark device with polished electrodes maintains zero under all investigated voltage values, while the leakage current through contaminated electrodes keeps increased with increasing voltage. Thus all the experiments presented in this dissertation were operated in pseudospark device with polished electrodes. And all the electrodes used in experiments will be polished after $10^3$ discharge shots.

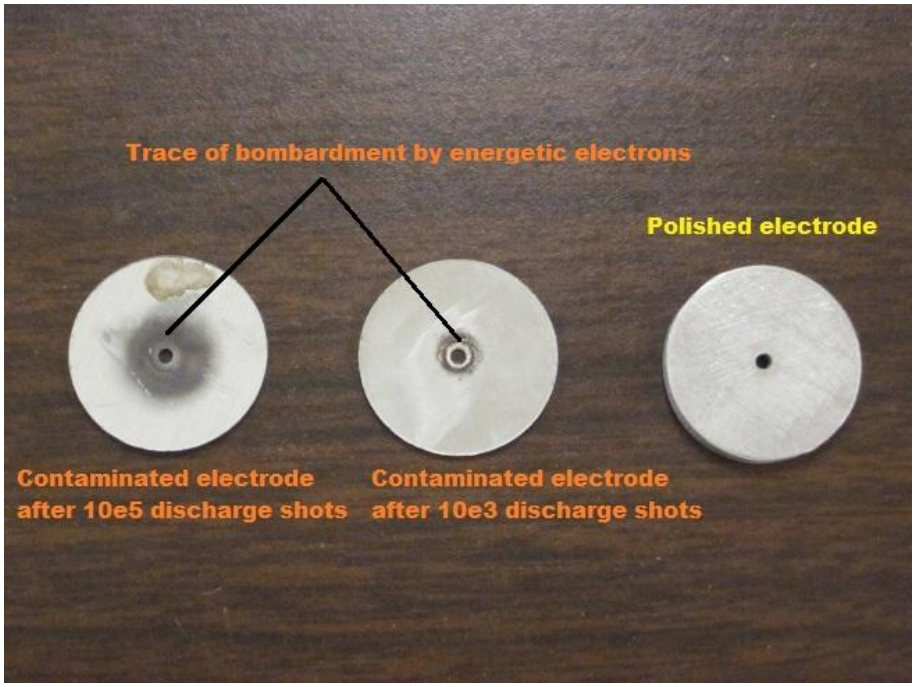


Figure 2.8. Three electrodes after various operational time

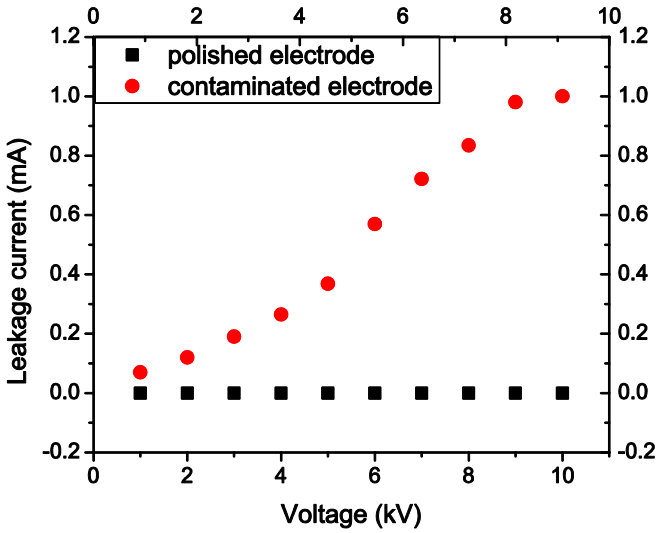


Figure 2.9. Leakage current in pseudospark device with polished electrodes and contaminated electrodes

**2.4.4 Transmission of High Voltage Pulse Signal.** The coaxial cable with a characteristic impedance of 50 ohms is usually applied to transmit the nanosecond signal and the typical structure of a RG 58U coaxial cable is shown in Figure 2.10. However, in pseudospark discharge experiment, different from the fast pulse signal of low amplitude value, the high voltage pulse signal requires high dielectric strength of transmission line, in addition to the time response limit of transmission system. The breakdown of coaxial cable under high voltage peak between copper wire and external grounding copper mesh will lead to corona discharge inside the coaxial cable. In addition, insufficient grounding layer of coaxial cable will cause the leakage of external noise into the transmission line. All of those will generate inaccuracy of measurements of pseudospark properties.

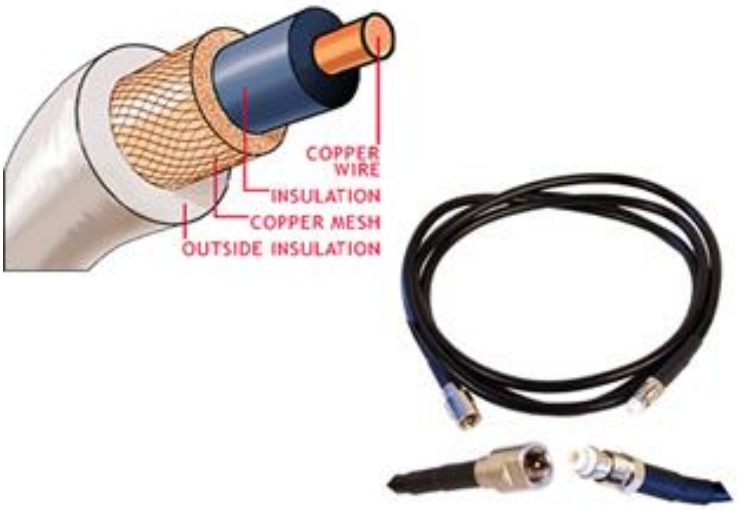


Figure 2.10 Structure of a regular RG 58U coaxial cable [2]

Figure 2.11 and Figure 2.12 shows the 10 continuous shot of pseudospark breakdown properties (voltage and discharge current) using two different coaxial cables from the same pseudospark device under the same applied voltage 14 kV. Discharge properties in Figure 2.11 were obtained using general RG 58U coaxial cable, which has a single layer grounding mesh and with a voltage rating of 1400 V root-mean-square (RMS) value. As shown in Figure 2.11, the instability ratio between 10 continuous shots defined as the difference ratio of the maximum amplitude to the minimum amplitude of discharge current is 33.8%. Discharge properties in Figure 2.12 were obtained using RG 223 coaxial cable, which has double layer grounding mesh and with voltage rating of 5 kV RMS value. As illustrated in Figure 2.12, the instability ratio decreases to 3.55% which is a great performance improvement compared with the performance of RG58 U. All the experiment results presented in this dissertation work are obtained by RG 223 coaxial cable.

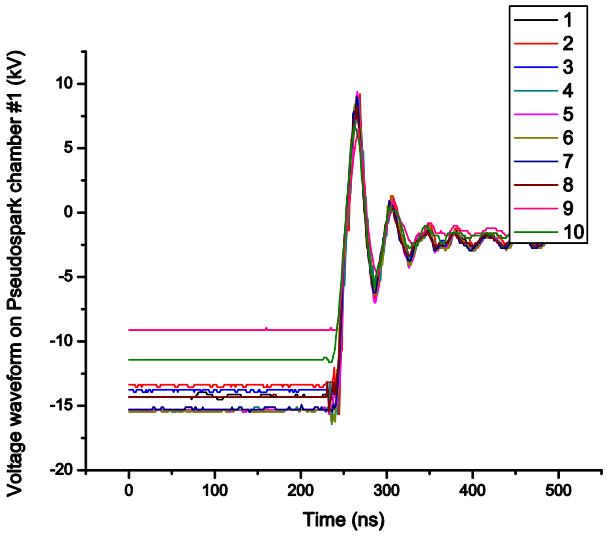


(a) Breakdown voltage waveforms

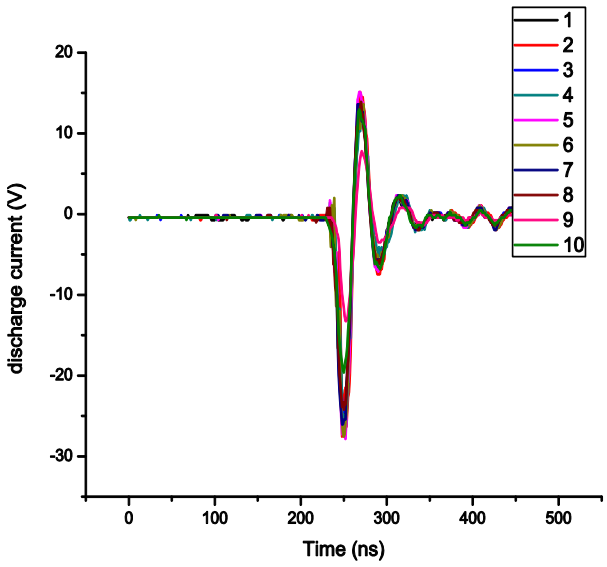


(b) Discharge current waveforms

Figure 2.11. Discharge properties measured by RG 58U coaxial cable

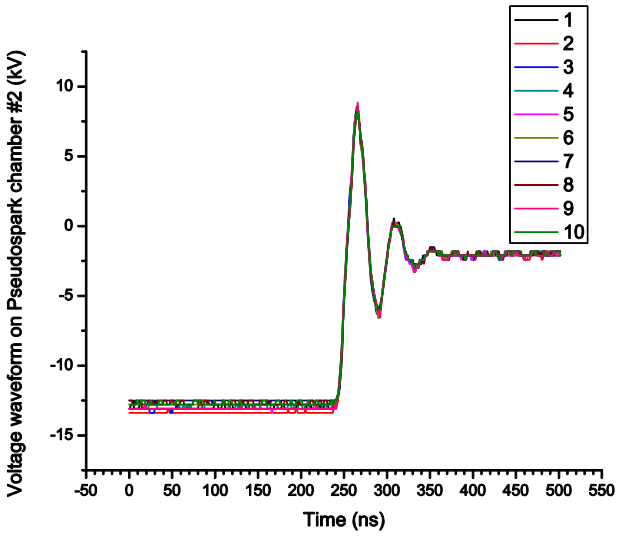


(a) Breakdown voltage waveforms

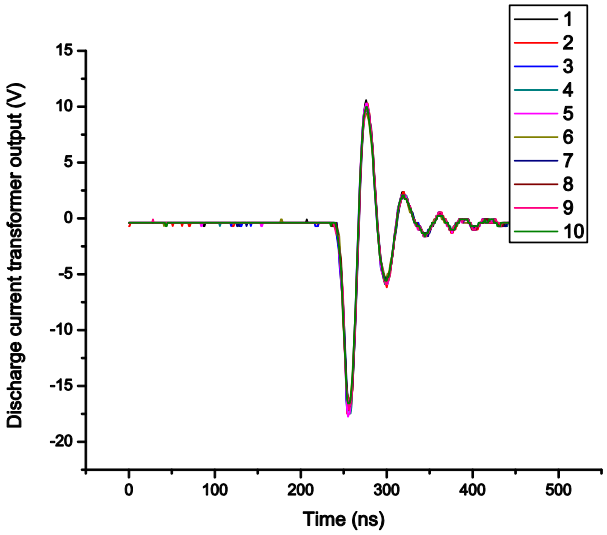


(b) Discharge current waveforms

Figure 2.12. Discharge properties measured by RG 223 coaxial cable

## 2.5 DIAGNOSTICS OF PSEUDOSPARK DISCHARG PROPERTIES AND ELECTRON BEAM CHARACTERISTICS

**2.5.1 Discharge Properties Diagnostics.** As stated in the above section, pseudospark discharge is a pulse discharge with a time range of 10s ns to 100s ns pulse width, and several ns rising edge. Thus the response time of the electric measurement methods and tools are of great importance in such pulse discharge experiments. The electric measurement system in APLab's pseudospark experiment consists of the discharge characteristic measurements and electron beam detectors. The breakdown voltage of pseudospark discharge is measured by the wide-bandwidth high voltage probe PVM-5 with a 80 MHz maximum frequency by North Star High Voltage connected to the hollow cathode directly. A Rogowski coil with 20 MHz rated bandwidth is located in the discharge loop to measure the discharge current flowing through the energy storage capacitors.

Figure 2.13 and Figure 2.14 are quantitative results of the response time of the voltage probe and discharge current transformer presented as the rise time percent difference for multiple times. The rise time percent difference is defined as the magnitude of the difference between output signal rise time and input signal rise time divided by the input signal fall time. A value close to zero is desirable. The test results show that the error difference ratio of fast rise time varied from 8 ns to 80 ns is below 5% for high voltage probe and below 10% for Rogowski coil.

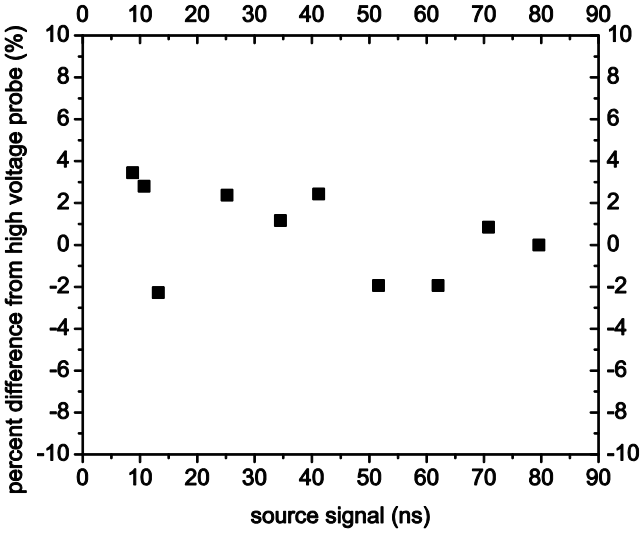


Figure 2.13. Test results of response time from high voltage probe PVM-5

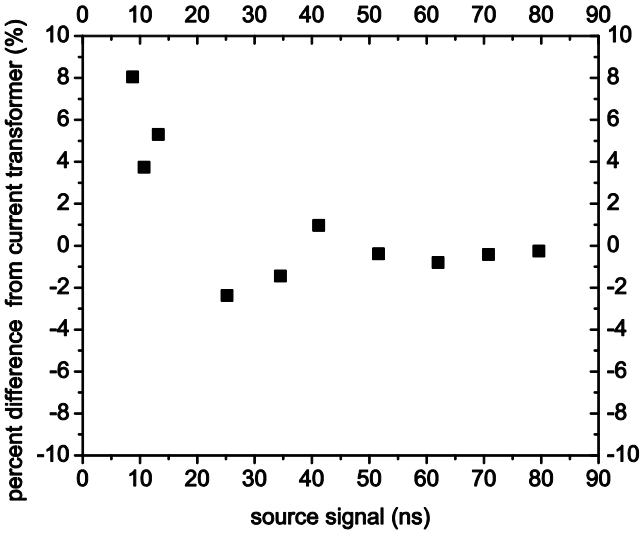


Figure 2.14. Test results of response time from current transformer

The data acquisition is realized by high speed oscilloscope with 500 MHz bandwidth, 1 G/s sampling rate. The control of oscilloscope readout and data storage is acquired by a Labview software workbench. Table 2.2 presents the main technical information of facilities and equipments located in discharge region.

Table 2.2 Main technical specifications of facilities and equipments

| **Facility and equipment** | **Technical information** |
|---|---|
| **High voltage power supply** | -100kV maximum output, 1mA current limit |
| **High voltage probe** | High voltage probe-1: Tek P-6015B, 1:1000 attenuation, 3 pF input capacitance, 20kV DC, 40 kV peak, 4 ns usable rise time<br><br>High voltage probe-2: North Star PVM-5, 1:1000 attenuation, 12 pF input capacitance, 60kV DC, 100 kV peak, 2.5 ns usable rise time |
| **High speed oscilloscope** | High speed oscilloscope-1: Tek TDS 2014B, 100 MHz, 1Gs/s<br><br>High speed oscilloscope-2: Agilent 54815A, 500 MHz, 1Gs/s |
| **Rogowski current transformer_1** | 20 MHz, 20 ns usable rise time,5 kA maximum input current |
| **Rogowski current transformer_2** | 100 MHz, 10 ns usable rise time, 350 A maximum input DC current, 100 A maximum input pulse current |

**2.5.2 Intense Pulsed Electron Beam Diagnostics.** Pseudospark discharge with proper configuration is capable of generating intense charge particles, including ion beam and electron beam. The electron beam produced by pseudospark discharge is a fast pulsed discharge with time duration of 10s ns ~ 100s ns. In APLab's pseudospark experiment, three various types of pulsed electron beam detectors are constructed and calibrated: Faraday cup with adjustable impedance, Faraday cup with low impedance, and Rogowski coil. Figure 2.15 shows the Faraday cup and Rogowski coil in the electron drift region. The technical specifications of Rogowski coil has been presented in Table 2.2 in previous section as "Rogowski current transformer_2". And the Faraday cup with adjustable impedance will be presented in Paper 2 in this dissertation. Only the design procedure and performance validation of low resistance Faraday cup is presented in this section.


Figure 2.15. Faraday cup and Rogowski coil for electron beam detection

A fast response Faraday cup (FC) with nanosecond response and low resistance of 0.08 ohms is developed to measure the intense electron beam produced by pseudospark discharge as shown in Figure 2.16. This Faraday cup consists of a collector cup to capture

the electron beams, the grounding plate and a low resistance carbon resistor with 0.08 ohms resistance connected between collector cup and grounding plate. This Faraday cup is constructed based on a semi-rigid coaxial cable with 50 ohms impedance. The inner conductor of this coaxial cable is joined with the copper collector cup. The coaxial cable insulated with Teflon coating is passed through the center of carbon resistor, and the outer grounding mesh of this coaxial cable is connected to the grounding plate. The other side of this semi-rigid coaxial cable is connected to the N type coaxial connector. Then a low shunt resistance can be formed between collector and grounding plate as a compact configuration with minimum stray inductance and reflection of pulse signal.

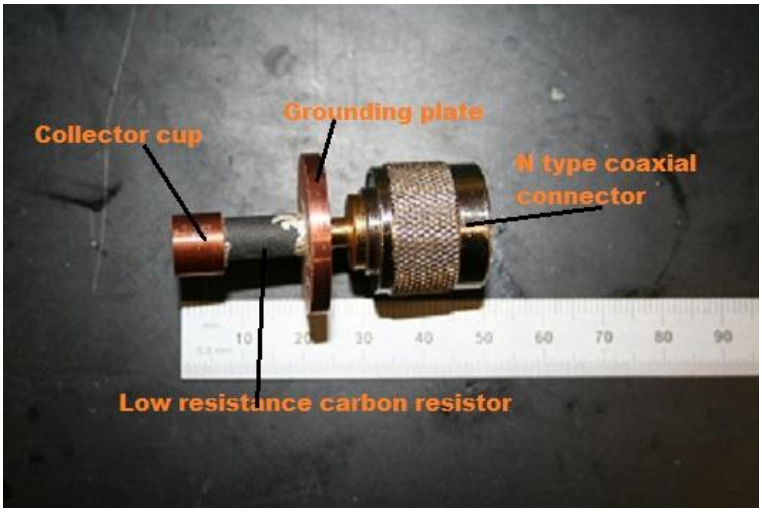


Figure 2.16. Low resistance Faraday cup electron beam collector

The quantitative results of the response time of the FC are presented as the attenuation ratio and fall time percent difference for multiple input signal values are shown in Figure 2.17, Figure 2.18 and Figure 2.19. Figure 2.17 is the output signal from low resistance Faraday cup probe and input signal from pulse generator. The shunt resistance can be determined from the attenuation ratio of Faraday cup, defined as ratio of amplitude of output signal from Faraday cup to the amplitude of pulse generator signal,

which is calculated to be 0.086 ohms. Figure 2.18 shows the falling edge of pulse generator input signal, and the output signal from the presented low resistance Faraday cup. As illustrated in Figure 2.18, the input signal on the bottom of Figure 2.18 has a 10.7 ns falling edge, while the output signal on top of Figure 2.18 displays a 13.8 ns falling edge. Then the difference percent of falling edge of output signal from low resistance Faraday cup and input signal from pulse generator, defined as the magnitude of the difference between FC signal fall time and input signal fall time divided by the input signal fall time under various pulse falling time values is shown in Figure 2.19. A value close to zero is desirable. In Figure 2.19, data are presented for source signal fall times from 8.6 to 79.6 ns. Within the tested range, the fall time percent difference has a maximum of 21.8% at the fastest source fall time, 8.6 ns. As source fall time increases, fall time ratio decreases to below 10% and has a value of 2.26% at 70.8 ns.

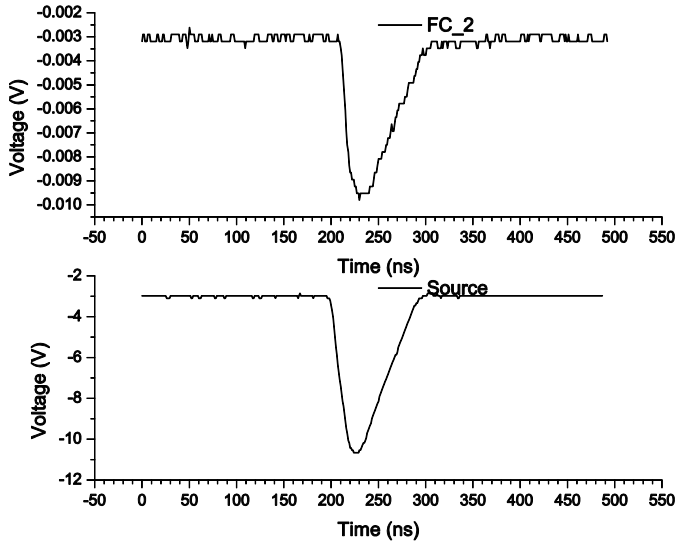


Figure 2.17. Output signal of low resistance of Faraday cup (top) and input signal from pulse generator (bottom)

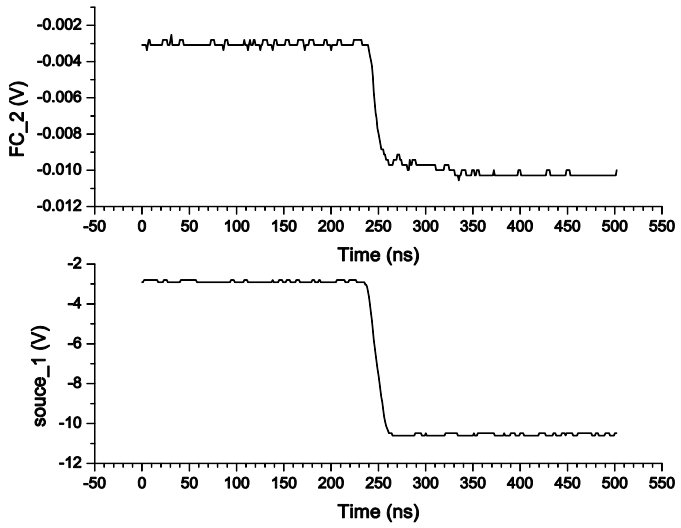


Figure 2.18. Signal falling edge of output signal from Faraday cup (top) and input signal from pulse generator (bottom)

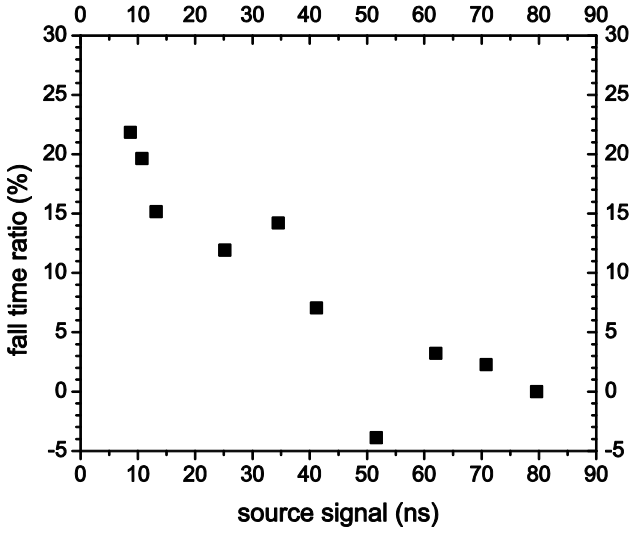


Figure 2.19. Difference ratio of fall time of output signal from low resistance Faraday cup and input signal from pulse generator

## 2.6 A SIMPLIFIED TIME DOMAIN REFLECTOMETER SETUP FOR CALIBRATION OF FAST RESPONSE PROBES

Different types of probes with fast response time below 10 ns lowest limit is described in previous sections, including Rogowski coils and Faraday cup probes. Generally, the probes like Rogowski coil current transformer for fast signal measurements are designed to obtain a 50 ohms standard impedance to match the impedance of transmission system, in order to minimize the possible reflection and frequency dispersion of fast signals. However, the characteristic impedance of Rogowski coil probe will have greater offset due to the variation of permeability of the magnetic core in Rogowski coil probe. Furthermore, in fast signal measurements, the long coaxial cable may have discontinuity and damage located at the unknown points. Thus in pulse signal diagnostics, a simple and efficient tool for troubleshooting and calibration of fast response probes is very useful in experiments. In industrial applications, a time domain reflectometer (TDR) is the most efficient method for calibration of probes with 50 ohms characteristic impedance.

A standard time-domain reflectometer (TDR), as shown in Figure 2.20, is an electronic instrument used to characterize and locate faults in metallic cables (coaxial cable or any other electrical path). The basic mechanism of TDR is based on the transmission line theory illustrated in Figure 2.21. If the characteristic impedances of source ($Z_s$), load ($Z_L$) and transmission line ($Z_c$) are not matched, only part of the signal will be transmitted, and the rest will be reflected back. And the reflection coefficient as presented in [3]:

$$\Gamma = \frac{Z_L - Z_c}{Z_L + Z_c} \tag{1}$$

Then discontinuity on the electric path can be determined from the time difference between the source pulse, which is the pulse signal on the left side of Figure 2.20 (b), and the reflected pulse on the right side of Figure 2.20 (b).The location of discontinuity can be determine by

$$\Delta d = vop\ (velocity\ of\ propagation\ in\ given\ cable) \times \Delta t \qquad (2)$$

Where $\Delta d$ is the difference between source signal and discontinuity location, and $\Delta t$ is the time difference on oscilloscope between source signal and reflection signal.

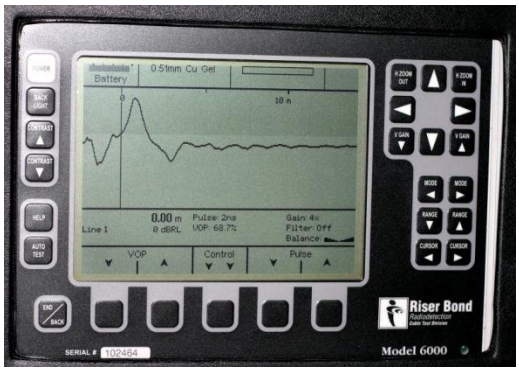


(a) Photograph of a commercial TDR

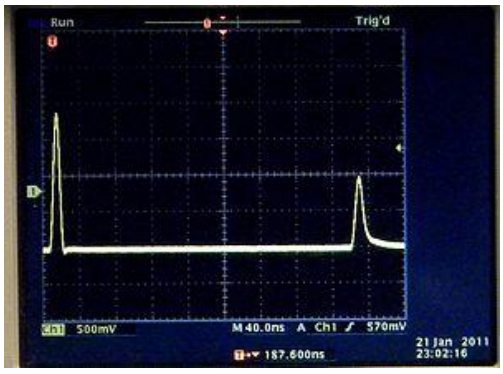


(b) Source signals generated by TDR (left) and the detected reflecting pulse signal (right)

Figure 2.20. A typical commercial TDR and the detected signals

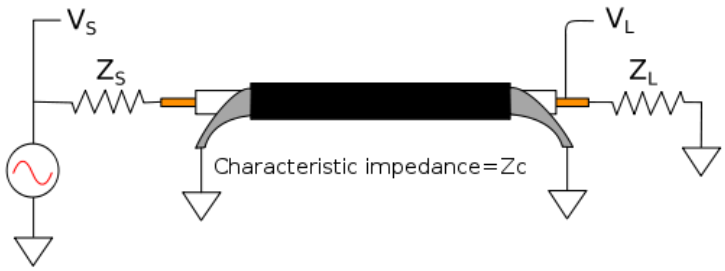


Figure 2.21. Illustration of transmission line with source (Zs) and load (ZL)

Although TDR is convenient for calibration of impedance discontinuity on signal transmission line, a commercial TDR is usually expensive (thousands dollars). Thus in our experiments, a simplified TDR setup by oscilloscope, pulse generator and RG 58U coaxial cable is constructed to realize the basic functions of TDR. The schematic and photograph of this simplified TDR setup are illustrated in Figure 2.22 (a) and (b).

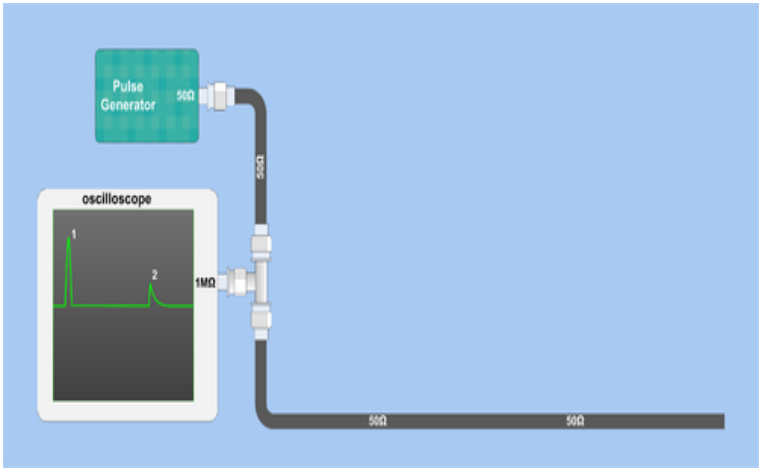


(a) Schematic of TDR setup

Figure 2.22. Schematic (a) and photograph (b) of the simplified TDR setup

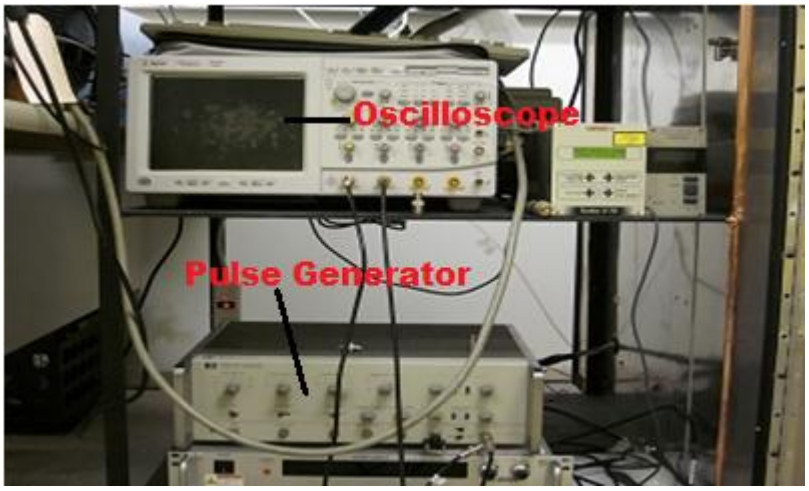


(b) Photo of simplified TDR setup

Figure 2.22. Schematic (a) and photograph (b) of the simplified TDR setup (cont.)

The performance validation test results are shown in Figure 2.23. The tests are operated by a 4.5 m RG 58U coaxial cable with standard 50 ohms terminal (Figure 2.23 (a)), 25 ohms terminal (Figure 2.23 (b)) and open end terminal (Figure 2.23 (c)). Based on the data in Figure 2.23, the discontinuity location is determined by

$$Distance = VOP \times \Delta t = 0.66 \times c \times 45\ ns/2 = 4.5m$$

which is exactly the length of test coaxial cable. $c$ is the velocity of light in vacuum $3 \times 10^8$ m/sec.

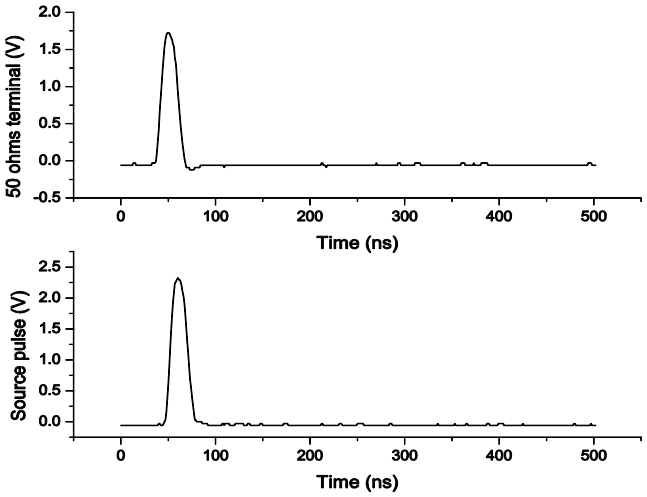


(a) Standard 50 ohms terminal

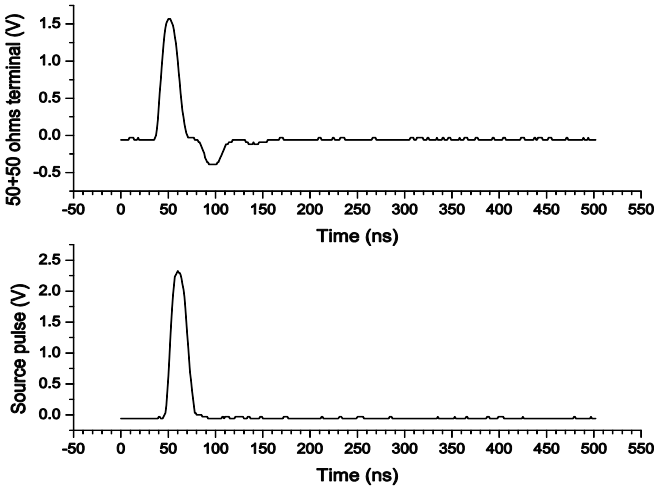


(b) 25 ohms terminal

Figure 2.23 Performance validation of simplified TDR setup

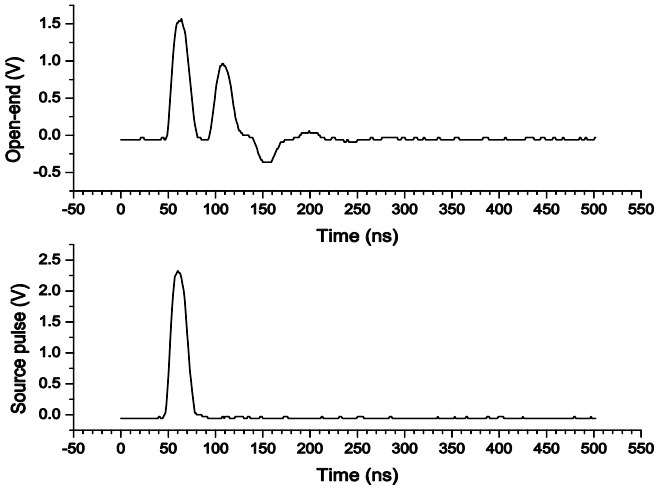


(c) Open-end terminal

Figure 2.23. Performance validation of simplified TDR setup (cont.)

This simplified TDR setup has been applied in the calibration of fast response probes used in pseudospark discharge experiments and the results are shown in Figure 2.24. Figure 2.24 (a) on the top is the test results of Rogowski coil probe NO.1 for discharge current measurement. Figure 2.24 (b) on the bottom shows the test results of Faraday cup probe with 50 ohms terminal. Both results show that there are some impedance mismatching on two probes, but the mismatching amplitude is less than 15%.

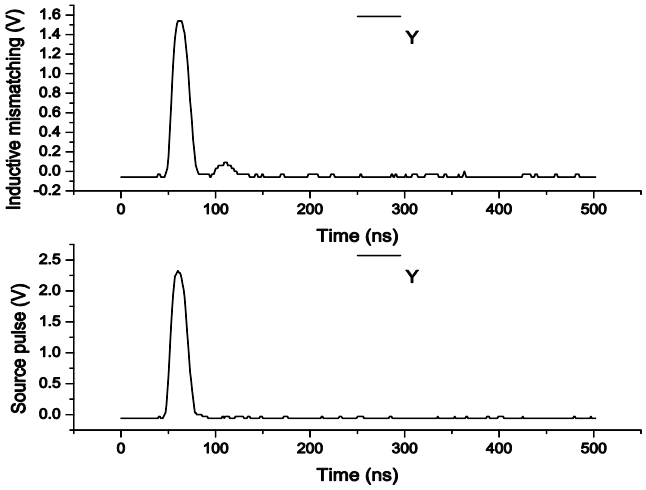


(a) TDR test results of Rogowski coil probe

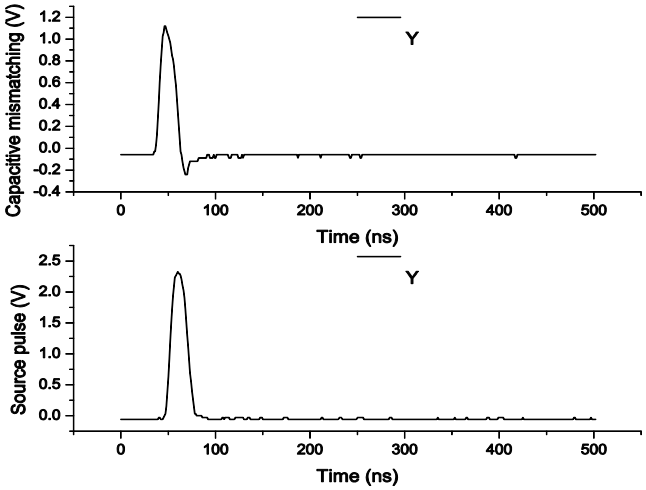


(b) TDR test results of Faraday cup probe

Figure 2.24. Test results of Rogowski coil probe and Faraday cup probe by this TDR setup

## BIBLIOGRAPHY

[1] Miller, R.B., 1982 An introduction to the physics of intense charged particle beams (New York, N.Y.: Plenum Press)

[2] Website information: *http://www.webdesigningwebertizers.com/finalproject2/cabling.html*

[3] D. M. Pozar, *Microwave Engineering,* 3rd ed. (John Wiley and Sons, Inc., 2005).

## PAPER

# I. EXPERIMENTAL INVESTIGATION OF FORMATION TIME IN SINGLE-GAP PSEUDOSPARK DISCHARGE

Hu, Jing and Joshua L. Rovey

## ABSTRACT

Experiment results on the formation of pseudospark discharge in single-gap device are presented. The formation process is investigated by capacitive probes and shows two phases: a slow initiation phase and a fast current increasing phase. The initiation of the discharge is found to be synchronous with a high speed ionization wave propagating from cathode to anode. Transition to the high current phase is initiated when the ionization front reaches the anode side. The experimental results on four different gap widths are presented under different pressures. The characteristic time of the initiation phase of the discharge is decreased with increasing pressure in all four gap widths. The mean velocity of the observed ionization front is varied from $5.4 \times 10\, cm/\mu s$ to $1.7 \times 10^3\, cm/\mu s$ under the investigated pressures. In four gap widths, the velocity of the ionization front can be fitted by one given curve as an exponential decline function of E/P.

## 1. INTRODUCTION

The pseudospark discharge was first discovered in the late 1970's, as an axially symmetric, high voltage gas discharge operating at low pressure regime located on the left hand side of the Paschen curve, which is usually initiated from a hollow cathode discharge (HCD) [1-5]. The fundamental discharge configuration consists of planar anode and hollow cathode, or multi-gap electrodes, with a central hole located in the electrodes. The central hole in the electrodes makes the effective distance of the

discharge path a maximum in the region of the bore hole on the axial center of the electrodes and cathode cavity.

Pseudospark discharge has many unique properties. It is a pulsed gas discharge that can obtain tens to hundreds of kV voltage hold-off capability and kA discharge current during total time of discharge of tens to hundreds ns, and several ns rise time. Physical volume of pseudospark device, including discharge gap and hollow cathode, is tens of $cm^3$. These characteristics make it suitable for a variety of applications, including high power switches [1-6], high energy e-beam sources [2,5,7,8], and in Ref [2,9], pulsed laser oscillations were observed in an Ar-He pseudospark discharge. Most of the reported applications, especially the switch applications and laser oscillation, require knowledge of time-dependent characteristics of the discharge formation and development, which reveals a number of complex phenomena to be explained.

The temporal development of a pseudospark discharge can be separated into four different phases [5-6]:

1) Predischarge (ignition of the pseudospark);
2) Hollow cathode discharge;
3) High current main discharge;
4) Decay of the discharge plasma.

The voltage-current characteristic and build-up of the highly conductive plasma of the discharge are of great interest because that part of the discharge is most closely associated with its applicability in a pulsed power system. In Ref [3-5], it is stated that phase 1 is related to the delay time between trigger and the onset of applied potential on discharge devices. And the repetition rate of the pseudospark device is mainly dependent on the decay process of plasma during phase 4 [7]. Comparatively, the exact mechanism of the hollow cathode phase (phase 2) and superdense high current main discharge phase (phase 3) is not fully understood yet. However, phase 2 and 3 have been considered to comprise multiple complex processes by a great number of previous studies [5,10,12]. For example, in [5], a physical model of prebreakdown in the hollow cathode discharge is established based on numerical simulation results. In this work, it was put forward that the prebreakdown phase of the pseudospark is related to the buildup of a positive space charge in the hollow cathode mainly due to ionization by electron impact. In [10], the

simulations based on a hybrid fluid-particle model were developed to describe the evolution of the initiation phase of pseudospark discharges. The simulation results presented in [10] shows that the pseudospark discharge is initiated by the rapid multiplication of electrons in hollow cathode region, and the current rise is characterized by the expansion of plasma from the hollow cathode and the enhance electron emission from the cathode.

Besides the research studies on the fundamental physical mechanisms of discharge evolution, the industrial applications requires more concerns on device performances in the current and charge transfer capability, and high current rising capability ($10^{10}$A/sec~$10^{11}$A/sec) of pseudospark. However, compared with the extensively qualitative and quantitative experimental investigations and physical model on the high pressure spark-gap switches in various technological focuses [1,11,13]. investigations of pseudospark discharge as switching devices are still not well determined, including the formation and initiation of plasma, build-up time to obtain highly conductive phase, total rise time to maximum peak current, time-varied oscillation period and frequency, modeling and determination of plasma resistivity and inductance, which are of great importance in order to verify discharge formation models and optimize the performance of this discharge device [1,5,11,13].

This paper presents the detailed experimental investigations of the time-dependent characteristics of single gap pseudospark discharge device. The formation time of the initiation of discharge current increase and build-up of highly conductive channel during the high current main discharge phase (phase 3) are the main focus in this work for its importance in the performance as switching device [1,3,11]. The formation time of discharge starting from initiation to maximum breakdown and its dependence on gas pressures are investigated in single-gap device with four various width of gap region. And the discharge development is temporally correlated with movement of a space charge front detected by two capacitive probes. The main emphasis of this paper is on the problem of discharge mechanism in pseudospark discharge device, and the dependence of discharge formation on external parameters, such as geometric factors and gas pressure. Additionally, a discussion of an ionization front model is proposed to explain the initial

formation and time evolution of the plasma column and ionization wave inside the device.

This work is organized into the following sections: a detailed introduction to the current pseudospark experiment setup and measurement methods is presented in Sec II. The experiment investigation results of discharge properties on gap space and neutral gas pressure are presented and summarized in Sec III. Finally, discussions and conclusions based on the experimental results and comparison with the results in related references are summarized in the last section.

## 2. EXPERIMENT SETUP

The single-gap pseudospark discharge chamber is shown in Figure 1. It consists of a cylindrical hollow cathode and grounded anode insulated by a pyrex disk. Anode, cathode and insulator have 22 mm outer diameter and 2 mm on-axis hole for electron beam extraction. The length of cathode cavity is 25 mm and the thickness of hollow cathode cavity and anode electrode is 1 mm. The gap distance between a pair of electrodes can be varied from 2 mm to 14 mm. Two 390 pF resin-dipped ceramic capacitors were connected between the anode and cathode symmetrically for energy storage. The material of all electrodes is stainless steel.

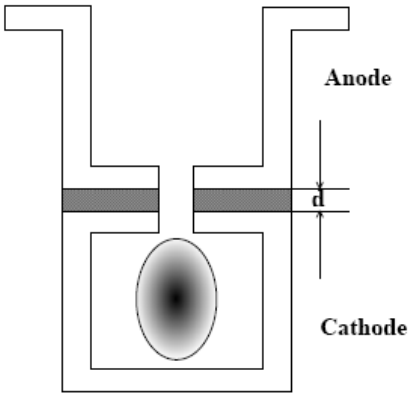


Figure 1. Single-gap pseudospark discharge configuration

The pseudospark discharge experimental setup is shown in Figure 2 (a), (b) and (c). The hollow cathode was connected to the high voltage dc power supply (100kV, 1mA) through a 20 MΩ charging resistor. A custom North Star high voltage probe PVM-5 is connected to the cathode to measure the voltage breakdown waveform. The discharge current evolution during the pseudospark breakdown is measured by a fast response Rogowski coil with rising time limit of 4 ns. Two capacitive probes as presented in Ref [14-16] are located in the inter-gap space at anode end (PA) and cathode end (PC) to detect the movement of plasma formation propagating along the gap space between anode and cathode.

The whole experimental system was evacuated to $10^{-5}$ Torr initially by a two-stage mechanical pump and turbo pump located at anode side. The operating gas was argon. Argon gas enters into the vacuum system through a mass flow controller. The mass flow rate of argon can be adjusted accurately to control the operation pressure in vacuum system. There was no external applied guide magnetic field in our experiments.

Data are acquired by a high speed oscilloscope with 500 MHz bandwidth, 1 Gs/s sampling rate. The control of oscilloscope readout and data storage is acquired by a Labview software workbench. All the presented experiment results in the following sections represent the mean value over twenty repeated cycles.


(a) Capacitive probes constructed on flexible PCB film

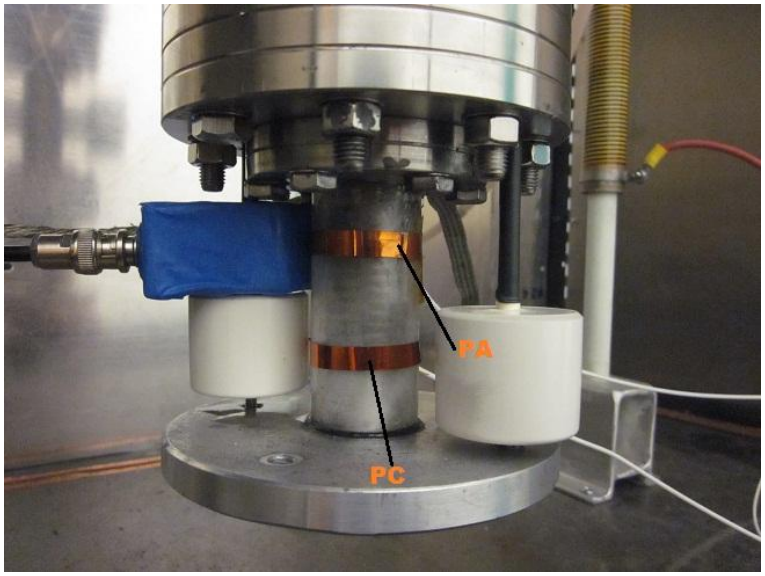


(b) Pseudospark chamber with two capacitive probes

Figure 2. Capacitive probes and experiment setup of single-gap pseudospark discharge experiment

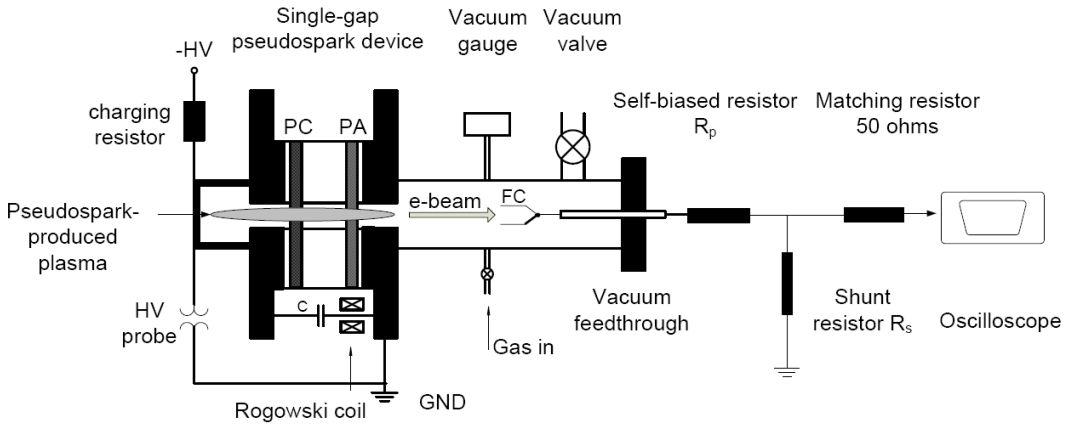


(c) Experiment setup of pseudospark discharge experiment

Figure 2. Capacitive probes and experiment setup of single-gap pseudospark discharge experiment (cont.)

## 3. EXPERIMENT RESULTS

### 3.1 TEMPORAL EVOLUTION OF DISCHARGE IN SINGLE-GAP PSEUDOSPARK DEVICE

Figure 3 shows the self-breakdown voltage and discharge current obtained from a single-gap pseudospark device with a gap thickness of 10 mm at 35 mTorr. As shown in Figure 3, during the increase of voltage applied on the pseudospark device (before 150 ns in Figure 3 and Figure 4), the high voltage capacitor is charging continuously charged until the electric field strength between anode and cathode is high enough to reach the "breakdown" value at the given pressure, then the conducting plasma discharge forms between anode and cathode. Charge is carried through the plasma until the energy storage by the capacitors is drained, at which point the plasma discharge is extinguished and the capacitor is recharged for the next shot (after 300 ns in Figure 3). Thus the pseudospark discharge in this experiment can operate under single mode or repetitive mode. All the data presented in this work is obtained in single mode.

The time duration between 150 ns and 300 ns is the main discharge starting from increase of discharge current. After the voltage breakdown, the current and the voltage signals show damped oscillations, which is the typical characteristic for self-sustained pulsed gas discharges initiated from a hollow cathode discharge (HCD) [6,17]. In Ref [17], fast shutter camera photos showed that the development of the plasma column is closely related to the first half-wave of the discharge current, while the damped current oscillations after the voltage breakdown are related to the external circuit parameters [17]. Thus in this work, the rise time and oscillation period to obtain the maximum discharge current in the first half-wave was our main focus.

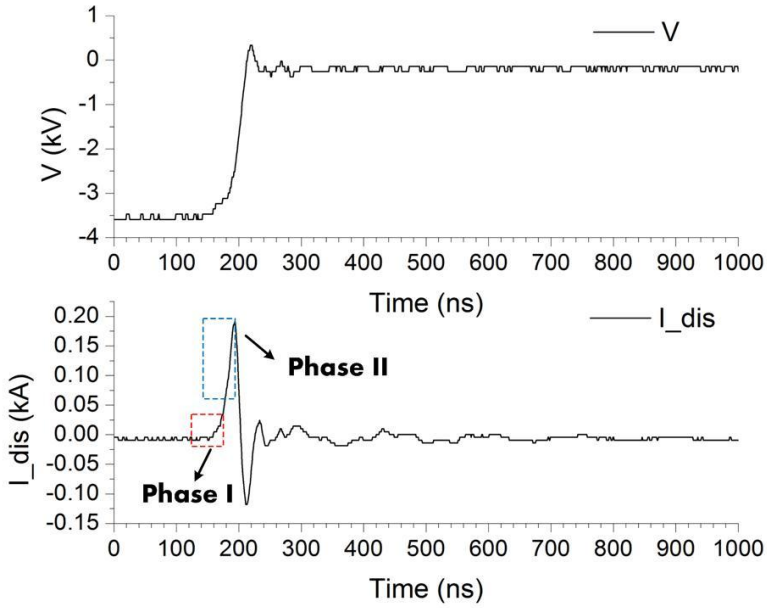


Figure 3. Breakdown voltage (top) and current (bottom) waveform traces

In addition to the subsequent damped oscillations, Figure 3 also shows two different phases in the “rising” edge on the first half-wave of the discharge current starting from the initiation of the discharge. Phase I is a slow current increasing phase and

phase II is the fast high current build-up phase. These two different phases can be more clearly presented by time-dependent dI(t)/dt illustrated in Figure 4. As shown in Figure 4, starting from 150 ns, the dI(t)/dt has a comparatively slow and flat current rising rate until 170 ns, from $1.05 \times 10^9$A/sec to $1.74 \times 10^9$A/sec within 20 ns. After that the temporal current rising rate keeps a fast increasing trend on the rising edge of the discharge current until reaching a maximum, increasing from $2.03 \times 10^9$A/sec to $1.17 \times 10^{10}$A/sec in 13 ns.

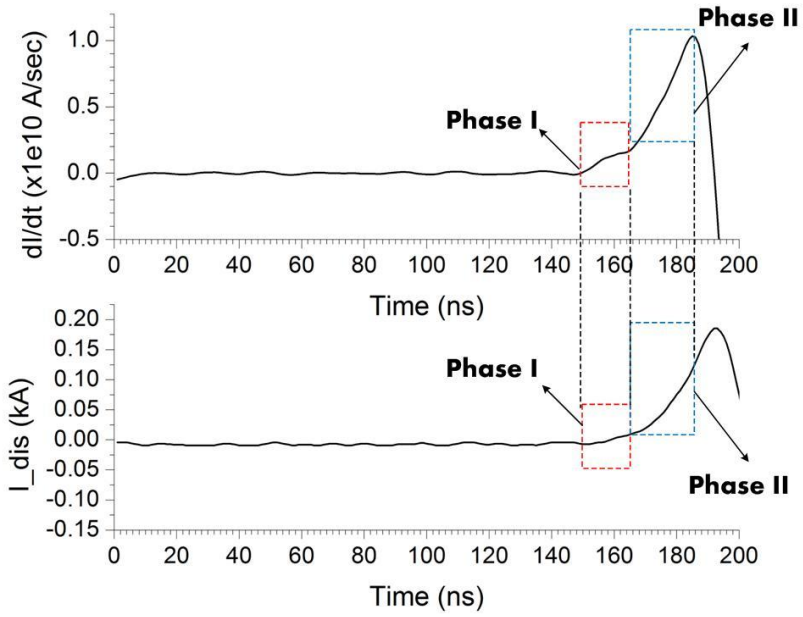


Figure 4. Discharge current and time-dependent dI(t)/d(t) corresponding to Figure 3

Similarly, in Ref [6,17], the two phases on the rising edge of discharge waveform were also presented and temporally related with fast shutter camera photographs in a similar type of HCD like the pseudospark. In Ref [6], it was shown that the phase I, slow current increasing phase was synchronous with the movement of an ionization wave front from the cathode to the anode, followed by a sudden increase of discharge current. And

the fast ionization wave was observed to propagate from cathode to anode with a velocity of $10^6$ m/s. In order to investigate the presence of a fast ionization wave propagation mode in a single-gap pseudospark discharge device, and its correlation with initiation of discharge, two capacitive probes were located on the inter-gap space to detect the formation and movement of plasma and the ionization wave.

The construction of capacitive probes in our work has the same configuration as the capacitive probe array used in Ref [14-16]. The mechanism and physical interpretation of capacitive probes have been discussed in detail in Ref [14-16]. Simply speaking, the rise of the capacitive probe signal shows that a plasma has formed at the location of the corresponding probe. The capacitive probe signals for the same shot as Figure 3 and Figure 4 are shown in Figure 5, with the rising edge of discharge current, signals of capacitive probe located near cathode (PC), and capacitive probe located near anode (PA).

As illustrated in Figure 5, the capacitive probe signals show that there is a negative polarity signal moving from cathode to anode side in the discharge gap space. Furthermore, comparing the starting time of phase I and phase II with the peak time of the two cathode probe signals, it shows that phase I corresponds with the time difference between the two probe signal peaks. This observation is identical with the experiment results presented in Ref [6] and the qualitative model of electric breakdown assisted by ionization wave propagation [18]. In Ref [6], based on the presented results (Figure 4 and Figure 5 in Ref [6]), the initiation phase (phase I in our work) starts synchronously with an ionization front moving from cathode to anode with slowly increasing discharge current. The propagation velocity of this front was estimated as $10^6$ m/s. The ionization front stops in front of the anode end then the fast discharge current increasing starts at the same time [6]. These observations indicate that the initiation of the pseudospark discharge is assisted by the propagation of a moving space-charge-creating front, and when this front stops at anode backside, the fast high current phase is initiated.

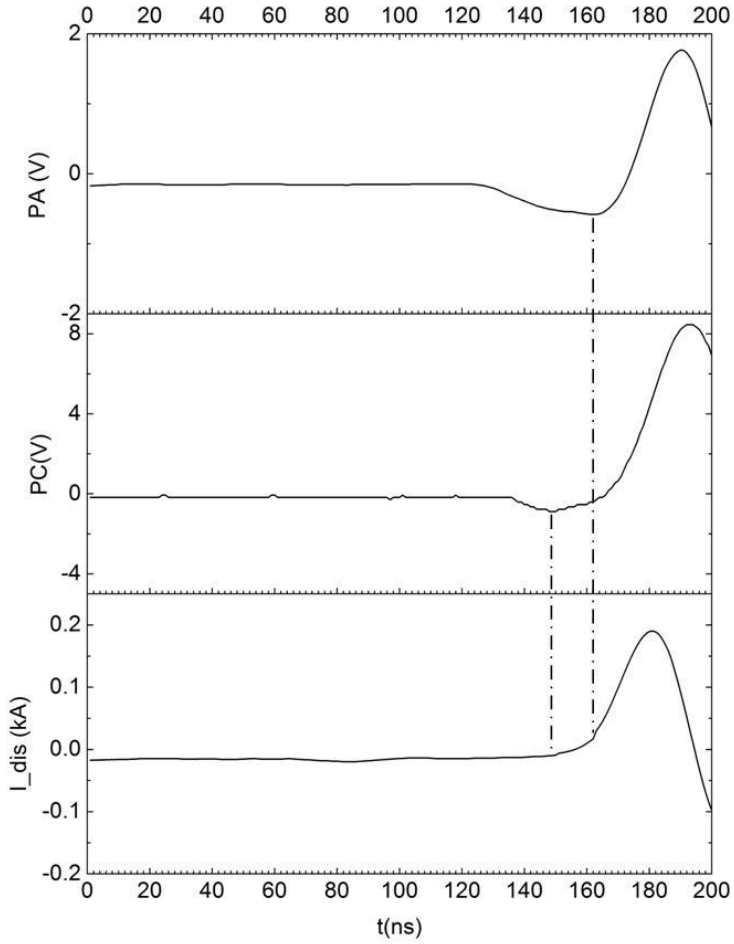


Figure 5. Time-related signal of discharge current, capacitive probe on cathode side (PC) and capacitive probe on anode side (PA)

## 3.2 CHARACTERISTIC TIMES IN SINGLE-GAP PSEUDOSPARK DEVICES WITH VARIOUS GAP SPACE

The single-gap pseudospark device as illustrated in Figure 1 consists of grounded anode and hollow cathode of given length. The external capacitance, length of cathode cavity, and radial diameter of the device remain constant among all the experiments presented.

**3.2.1 Total Rise Time from Initiation of Breakdown to Maximum Current.** Figure 6 shows the time duration of the rising edge of the discharge current in a single-gap pseudospark device with different gap width. For the same pressure, the rise increases with wider gap width, equivalent to a “slower” build up process of the highly conductive plasma channel on the pseudospark axis. Meanwhile, the variation of discharge current magnitude in the devices with various gap width is most related with the applied voltage on the discharge gap, corresponding to the given gap width and operation pressure, which will be discussed in the following Section 3.2.3.

The total rise time for different ambient pressures obtained in single-gap pseudospark device with gap width d = 2mm, 4mm, 6mm and 14mm is presented in Figure 7. The rise time starting from breakdown front to the maximum current peak decreases with ambient pressure in a single gap device. Furthermore, the effect of pressure on rise time becomes more obvious in a device with wider gap. In pseudospark device with 14mm gap width, the rise time in 15 mTorr argon is 83.4 ns, 514.8% higher than the rise time in 110 mTorr, the maximum pressure under which the pseudospark can operate with a 14 mm gap. But in a pseudospark device with 2mm gap width, the rise time in 15 mTorr is 208% higher than the rise time in the maximum operation pressure of 240 mTorr.

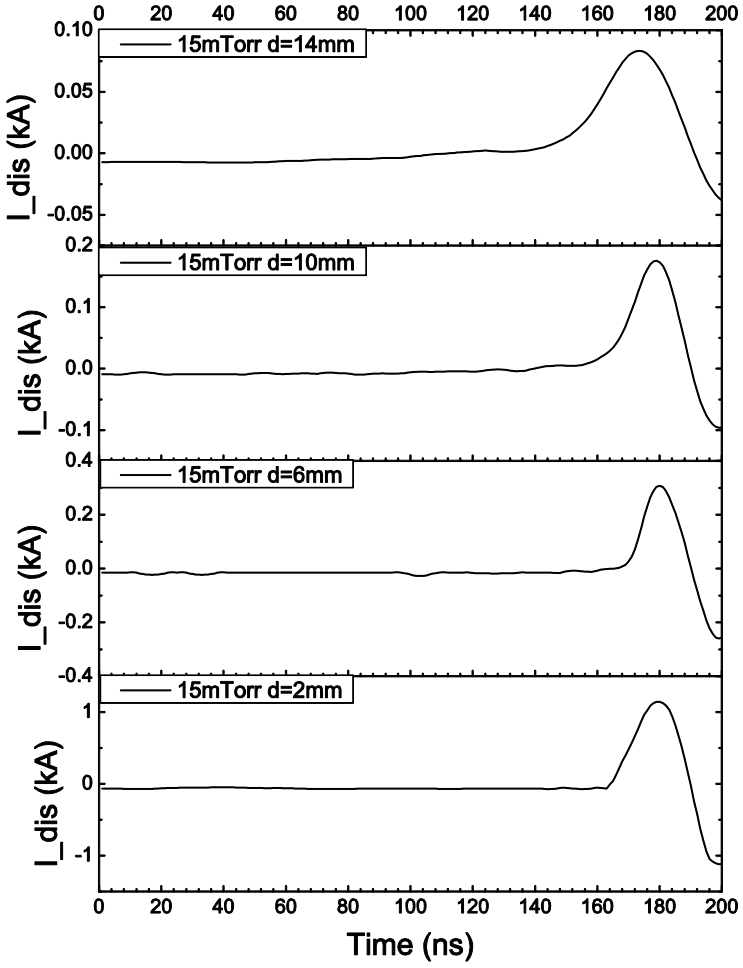


Figure 6. First half-wave discharge current in various single-gap pseudospark devices

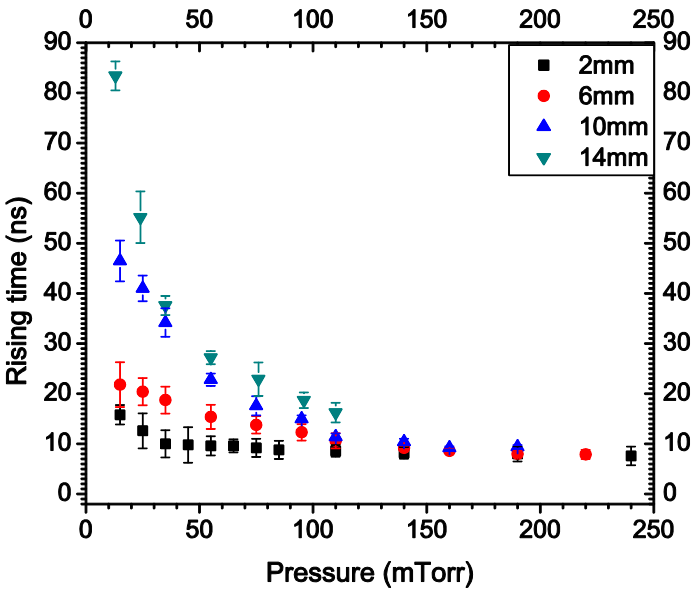


Figure 7. Rise time in various single-gap pseudospark devices

**3.2.2. Characteristic Time of Slower Initiation Phase and Fast Highly Conductive Phase.** As stated in previous sections, there are two different phases on the rising edge of discharge waveform starting from the initiation of main discharge: a slow current rising phase (phase I) and the following fast high current build-up phase (phase II), as marked in Figure 3 and Figure 4. In Figure 5, the starting point of phase I and phase II are synchronous with the propagation of a moving space-charge-creating front from cathode to the anode backspace. And Figure 6 shows that under the same ambient pressure, the time duration of phase I is increased in the wider discharge gap. Thus in this section, the characteristic time duration of phase I and II are presented in single-gap pseudospark devices of various gap space widths.

Figure 8 is the characteristic time of phase I versus pressures in various gap width and Figure 9 shows the time duration of phase II. In order to illustrate the proportion of phase I and phase II compared with total time of rising edge, data in Figure 8 and Figure 9 are presented on the same axis scale as Figure 7.

As illustrated in Figure 8, the time duration of phase I shows a similar variation trend as total rise time with ambient pressure. For a discharge gap of 14 mm space width, time duration of phase I decreases from 71.8 ns at 15 mTorr to 6.4 ns at 110 mTorr. In discharge gap of 2 mm width, time duration of phase I decreases from 9.7 ns at 15 mTorr to 1.5 ns at 220 mTorr. In the higher pressure region, the time difference of phase I becomes lower for various gap space widths.

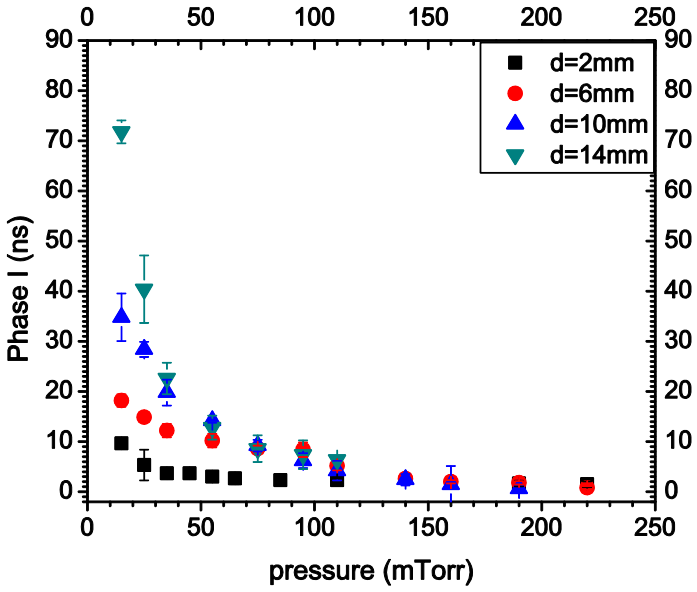


Figure 8. Characteristic time of phase I under various pressures

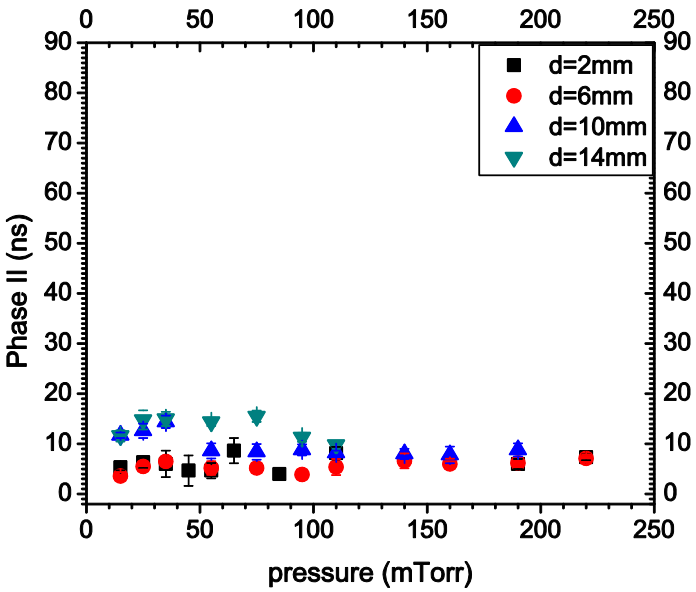


Figure 9. Characteristic time of phase II under various pressures

Compared with phase I, the time duration of phase II does not vary as much as phase I in a single gap device as pressure increases. The time duration of phase II is assumed to be most related with the impedance of external circuit, including ohmic resistance, stray inductance and dynamic inductance of the discharge loop, and the capacitance [1,11-13]. The stray inductance of the presented discharge loop in this work can be measured by a RLC meter and calculated from geometric dimensions by the formula [19].

$$L_{loop} = N^2 \frac{2\mu_0\mu_r w}{\pi}\left[\ln\left(\frac{w}{a}\right) - 0.774\right] \quad (1)$$

Where N is the number of loop, w is the length of inductance loop, $a$ is the wire radius and $\mu_r$ is the relative permeability of the medium. And the results show the stray inductance of the circuit is approximately 40~50 nH. With the 780 pF external capacitance, the generated quarter damping oscillation period is estimated to $3.4\sqrt{1/LC}$ which equals to 18~20 ns. This result is close to the time duration of phase II in our work,

which suggests that the time duration of phase II is mainly determined by the R, L, C parameters of the external circuit and discharge loop. Although the variation of time duration of phase II is not so great as phase I, it still can be seen in Figure 9 that the time of phase II is longer in 14 mm gap than shorter gap width, which is mainly caused by higher resistance and inductance of plasma column in longer discharge gap [1,11,13,17]. The exact values of ohmic resistance, dynamic inductance of discharge loop, including the plasma column, must be determined by dynamic measurement and analysis methods as shown in [13,20], etc., which are beyond the topic of this work.

**3.2.3 Propagation Speed of Ionization Front in Single-gap Device.** The time evolution of initiation phase I, as presented in Figure 8, shows the propagation of an ionization front, which varies with ambient pressure [14-15,18,21], electric field, and propagation path. The characteristic mean speed of the ionization front is determined by the gap space width and the time duration of initiation phase in this section. The propagation speed of the ionization front in single-gap device with various gap widths under ambient pressures is presented in Figure 10. This propagation velocity is calculated as:

$$V_{propagation} = \frac{d}{t} \tag{2}$$

where d is the gap space width and t is the time duration of phase I presented in Figure 9.

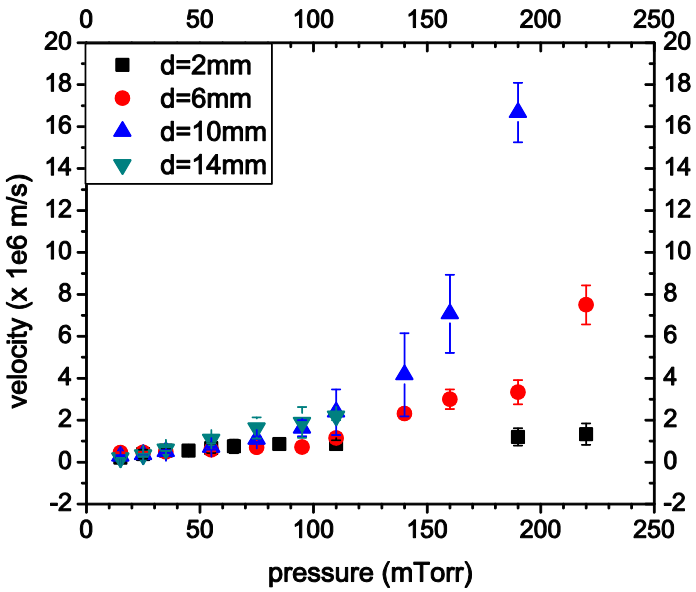


Figure 10. Propagation speed of ionization front

According to the results in Figure 10 in a given gap device with given gap space width, the velocity is increased with pressure, since the velocity of the ionization front is promoted by the effective ionization frequency [18,21], which increases with ambient pressure on the left side of Paschen curve. Considering the comparison of this velocity of the ionization front in pseudospark device with various gap widths, the dependency of the velocity of ionization front on the applied potential in the gap region and the generated electric field is another important parameter. Figure 11 shows the breakdown voltage of the single-gap pseudospark devices with four gap widths presented in this work. As illustrated in Figure 11 and some other work [22-24], in the low pressure region on left side of Paschen curve, the breakdown voltage of pseudospark is decreased with increase pressure in a single device. And in the device with different geometric configurations, the stable operational pressure region of the pseudospark discharge gap is also affected by the gap width (d in Figure 1) [22-24], which also directly determines the magnitude of electric field inside the gap region.

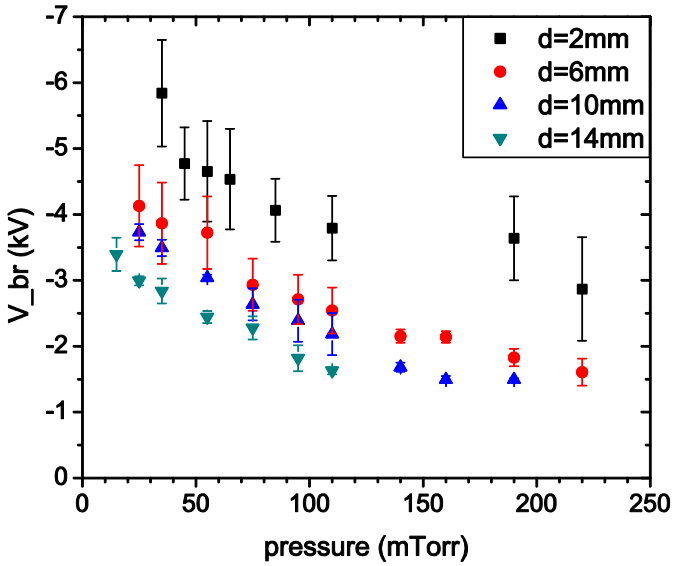


Figure 11. Breakdown voltage versus pressure in four devices

The breakdown voltage versus pressure in pseudospark device with different geometric factors can not be described by a general scaling law like Paschen's law yet due to the geometry complexity in pseudospark device, including hollow cathode structure and common central hole in electrode side [1,5,23-24]. However, it should be noted that the dependence of ionization frequency on reduced field value E/P can be considered instead of the dependence on electric field or pressure [1]. Considering the effect of various gap widths, the evolution of the speed of ionization front can be represented best by the dependence on the value of E/P, where E is the static electric field expressed in V/cm and P is the neutral gas pressure expressed in Torr as shown in Figure 10 and Figure 11. Based on the data presented in Figure 10 and Figure 11, the velocity of the ionization front obtained with all four gap widths can be fitted by a function of E/P with the following form:

$$V = A1 \times \exp\left(-B1 \times \frac{E}{P}\right) + A2 \times \exp\left(-B2 \times \frac{E}{P}\right) \quad (3)$$

Where $A1 = 4.3, B1 = 2 \times 10^4, A2 = 87.0, B2 = 1.6 \times 10^3$, with the V in the unit of $10^6$ m/s, E/p in the unit of V/[Torr•cm]. Fitting results are illustrated in Figure 12.

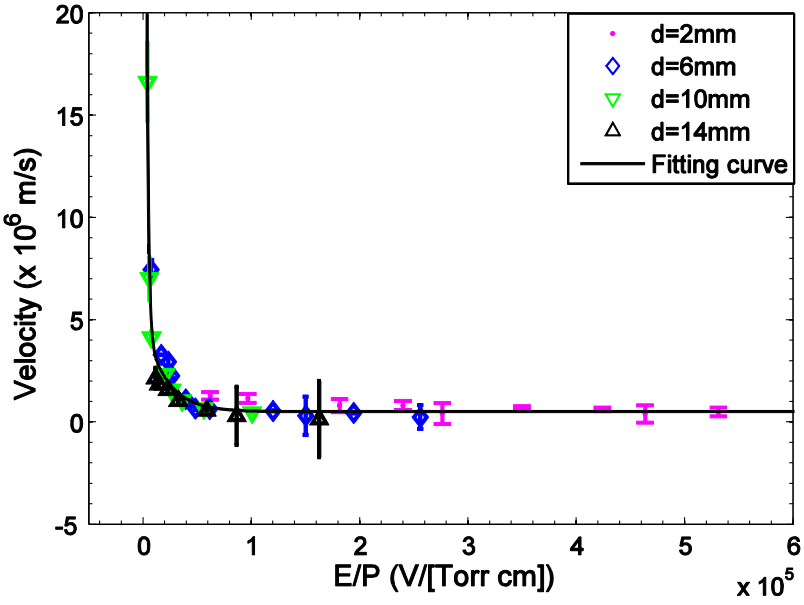


Figure 12. Dependence of calculated velocity of ionization front on E/P

## 4. DISCUSSION AND CONCLUSION

The transient hollow cathode discharge (THCD), such as single-gap or multi-gap pseudospark, channel spark, works under left branch of the Paschen curve and can obtain high voltage of kV to tens of kV. In such a high voltage low pressure region, the reduced field value of E/P, or equally E/N, is extremely high to $10^6$ V/[Torr•cm]. In such a high E/N value, the mean free path is relatively large at cm level, which means that a very high proportion of the free electrons produced in the inter gap space are lost to the anode without sufficient bulk ionization by electron impact collisions. Then there must be other

charge multiplication and ionization processes causing the initiation of the high current discharge.

Based on our experiment results, the propagation of an ionization front is synchronous with the initiation of a pseudospark discharge. When this front stops at anode backspace, the discharge transits to the high current phase. Such an ionization front is considered to be stimulated by the electron beam injected through the anode-cathode gap space, which is initiated from the hollow cathode region [5,6,10,14-15,17]. The characteristic time of the propagation of this ionization front was investigated under ambient pressures and in various inter gap space width in our work. Results show that the characteristic time of the initiation phase and velocity of the ionization front are affected directly by the pressure of gas and reduced electric field. Furthermore, the calculated propagating velocity in four different gap widths can be fitted in the same exponential decay function of E/P, which presents a steep decrease of velocity of ionization front with lower neutral gas density, and higher E/P value. Qualitatively, this trend is consistent with the variation of ionization frequency on the left side of the Paschen curve [18,21], which increases with gas pressure and decreases with E/P.

Furthermore, in many applications, such as pulse technology, laser drive, etc., the fast total rising time obtained by the discharge device is a very important technical focus. Our experiment results show that the total time for a single-gap discharge device to reach high current consists of a slow initiation phase and a fast current rising phase. The former phase has been investigated by capacitive probe experiments. The latter phase is considered to be related to the equivalent inductance and resistance of the plasma column formed during the main discharge phase [1,6,11,17]. Our results also shows that the characteristic time of phase II is identical with the falling time of the first half wave of discharge current. The exact and time-resolved determination of the effects of ohmic resistance, time-varied inductance of plasma column and capacitance of the discharge configuration should be determined by other dynamic measurement methods, such as transmission line method as presented in [13,20].

Meanwhile, it should be clarified that the discussion of hollow cathode effect is not taken into discussion in this work. Based on the previous work performed by Mittag in [5], Boeuf and Pitchford [10], the hollow cathode effect plays an important role in the

phase prior to the high current main discharge (described as phase 2 in the Introduction). In this phase, the expansion of plasma in the hollow cathode region, the large multiplication of electrons due to the pendulum movement in the hollow cathode and the buildup of sheath in this region have been discussed in [5,10]. The limit of the capacitive probe method implies that it may be not appropriate to determine the plasma formation or ionization events in the hollow cathode region because of the rapid plasma expansion in radial direction [25]. So in our work the hollow cathode configuration remains the same in all the presented work and only the propagation of ionization front in the internal gap region are under investigation. The hollow cathode effect on the time-dependent discharge parameters should be determined by other methods, such as optical and spectral measurements as performed in [26].

## REFERENCES

[1] Schaefer G, Kristiansen M and Guenther A (eds) 1990 *Gas Discharge Closing Switches* (New York, N.Y.: Plenum Press)

[2] Frank K and Christiansen J 1989 IEEE Trans. Plasma Sci. **17** 748

[3] Tkotz R, Gortler A, Christiansen J, Dollinger S, Frank K, Heine F, Herleb U, Insam S, Kowalewicz R, Mehr T, Poister A, Prucker U, Schlaug M and Schwandner A 1995 *IEEE Trans. Plasma Sci.* **23** 309

[4] Jiang C, Kuthi A and Gundersen M A 2005 *Appl. Phys. Lett.* **86** 024105

[5] Gundersen M A and Schaerfer G (eds) 1990 *Physics and Applications of Pseudosparks* (New York, N.Y.: Plenum Press)

[6] Frank K, Stark R, Christiansen J, Felsner P, Gortler A, Hoffmann D, Prucker U, Schwandner A, Stetter M, Tkotz R and Urban J 1997 *IEEE Trans. Plasma Sci.* **25** 740

[7] Rosier O, Apetz R, Bergmann K, Jonkers J, Wester R, Neff W and Pankert J 2004 *IEEE Trans. Plasma Sci.* **32** 240

[8] Gastel M, Hillmann H, Muller F and Westheide J 1995 *IEEE Trans. Plasma Sci.* **23** 248

[9] Christiansen J, Lieser N, Rath W, Steudtner W, Rozsa K, Janossy M, Apai P and Mezei P 1985 *Optics Comm.* **56** 39

[10] Boeuf, Jean-Pierre, Pitchford, Leanne C 1991 *IEEE Trans. Plasma Sci.* **19** 286

[11] Martin J C 1996 *J.C.Martin on Pulsed Technology*, (New York, N.Y.: Plenum Press)

[12] Larigaldie, Serge 1995 *IEEE Trans. Plasma Sci.* **23** 362

[13] Sorensen T P and Ristic V M 1977 *J. appl. Phys.* **48** 114

[14] Favre M, Wyndham E, Lenero A M, Suzuki F, Valenzuela J, Avaria G, Ruiz M, Bhuyan H, Chuaqui H and Choi P 2008 *Plasma Sources Sci. Technol.* **17** 024011

[15] Favre M, Choi P, Chuaqui H, Mitchell I, Wyndham E and Lenero A M 2003 *Plasma Sources Sci. Technol.* **12** 78

[16] Favre M, Chuaqui H, Lenero A M, Wyndham E and Choi P 2001 *Rev. Sci. Instrum.* **72** 2186

[17] Dewald E, Frank K, Hoffmann D H H and Tauschwitz A 2002 *IEEE Trans. Plasma Sci.* **30** 363

[18] Lagarkov A N and Rutkevich I M 1994 *Ionization Waves in Electric Breakdown of Gases* (New York : Springer-Verlag)

[19] Walker C S 1990 *Capacitance, Inductance, and Crosstalk Analysis* (Norwood, MA : Artech House)

[20] VanDevender J.P 1978 *J. Phys, D: Appl. Phys.* **49** 2616

[21] Sinkevich O A and Gerasimov D N 2000 J. *Phys, D: Appl. Phys.* **33** 54

[22] Rhee M J, Liu C J 1994 *Appl. Phys. Lett.* **65** 3314

[23] Rhee M J, Ding B N 1992 *Phys. Flu. B.* **4** 764

[24] Yin H, He W, Cross A W , Phelps A D R , Ronald K 2001 *J. appl. Phys.* **90** 3212

[25] Choi P, Favre M 1994 *Rev. Sci. Instrum.* **65** 2281

[26] Stetter M, Felsner P, Christiansen J, Frank K, Goertler A, Hintz G, Mehr T, Stark R, Tkotz R 1995 *IEEE Trans. Plasma Sci.* **23** 283

# II. FARADAY CUP WITH NANOSECOND RESPONSE AND ADJUSTABLE IMPEDANCE FOR FAST ELECTRON BEAM CHARACTERIZATION

Hu, Jing and Joshua L. Rovey

## ABSTRACT

A movable Faraday cup design with simple structure and adjustable impedance is described in this work. This Faraday cup has external adjustable shunt resistance for self-biased measurement setup and 50Ω characteristic impedance to match with 50 Ω standard BNC coaxial cable and vacuum feedthroughs for nanosecond-level pulse signal measurements. Adjustable shunt resistance allows self-biased measurements to be quickly acquired to determine the electron energy distribution function. The performance of the Faraday cup is validated by tests of response time and amplitude of output signal. When compared with a reference source, the percent difference of the Faraday cup signal fall time is less than 10% for fall times greater than 10 ns. The percent difference of the Faraday cup signal pulse width is below 6.7% for pulse widths greater than 10 ns. A pseudospark-generated electron beam is used to compare the amplitude of the Faraday cup signal with a calibrated F-70 commercial current transformer. The error of the Faraday cup output amplitude is below 10% for the 4 to 14 kV tested pseudospark voltages. The main benefit of this Faraday cup is demonstrated by adjusting the external shunt resistance and performing the self-biased method for obtaining the electron energy distribution function. Results from a 4 kV pseudospark discharge indicate a "double-humped" energy distribution.

## 1. INTRODUCTION

A Faraday cup (FC) is a beamline diagnostic that is used to measure the electric parameters of electron beams, such as beam current. The structure and parameters of a

FC can be optimized for the characteristics of various electron beam types. In addition to the traditional design considerations of FCs, such as electron emission, electron stopping range, and particle back-scattering, the development of high voltage pulsed power sources places new requirements on effective passive probes. For instance, fast response time and movable configurations to study the characteristics and evolution of electron beams at various locations. In this work, a FC with sub-nanosecond response time and adjustable resistance for self-biased measurement is presented.

The FC described in this paper is used to measure the intense electron beam produced by a pseudospark discharge, which is a type of high voltage pulsed discharge with rise time on the order of nanoseconds and currents in the range of amps to hundreds of amps. This FC is also used to determine the time-resolved electron energy distribution function by the self-biased method [1-2], which requires that the FC have adjustable impedance. Although there are various passive probes for pulsed electron beam diagnostics that have been published formerly [3-5], in these designs for pulse applications, in order to minimize the stray inductance, which is important for nanosecond-level pulse signal, the outer conductor of the transmission line is connected with the inner conductor by a fixed shunt resistor to form a compact assembly. Thus, the impedance of the FC is not adjustable and the self-biased resistance cannot be changed to capture electrons of different energy level. The design presented here provides a new contribution in the fabrication of FCs with subnanosecond response time, and the adjustable shunt resistor configuration for self-biased electron energy measurement [1-2]. In our design, the grounding conductor is not connected with the inner conductor by a fixed resistor, so the FC can be setup as a movable detector to measure electron loss and energy spread along the drift path of the electron beam.

## 2. DESIGN PROCEDURE

The FC is designed to measure an electron beam pulse signal with duration on the order of 50 nanoseconds and rise time shorter than 10 nanoseconds. For such a short pulse, the maximum signal frequency can be up to 0.1~1 GHz [6], thus the characteristic

impedance and the impedance matching between the FC and test network are important design considerations. A schematic of the design is shown in Figure 1 and the corresponding transmission line model is illustrated in Figure 2. The cup core is formed by a changeable carbon collector. The bottom of the FC is machined with a small step junction structure to permit a short center line of the coaxial cable passing through. The carbon collector is well-insulated from the external grounding conductor by a 7.6 mm thickness insulating layer, and the resistance of the FC is adjusted external to the vacuum system. The FC is modeled as a short transmission line terminated by standard RG-58U BNC 50Ω coaxial cable. The signal source is the pulsed current of the electron beam. Based on basic transmission line theory [7], the FC can be considered a parallel planar waveguide configuration with characteristic impedance given by Equation (1). By selecting appropriate values for the radial dimension (w) and the distance between the carbon collector and grounding layer (d), the FC can be designed to have a matched characteristic impedance and minimum reflection and dispersion of high frequency signals.

$$Z_0 = \frac{\mu}{\epsilon}\sqrt{\frac{d}{w}} \tag{1}$$

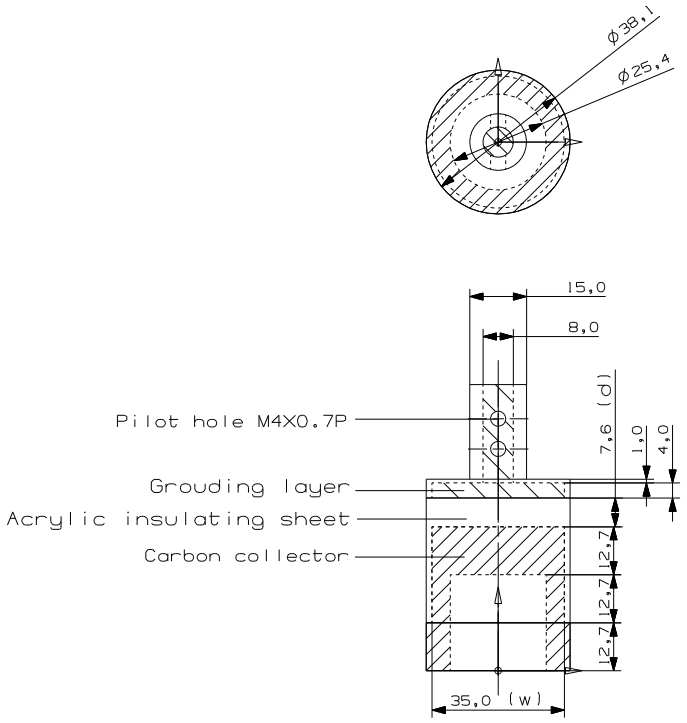


Figure 1. Schematic drawing of the FC (all units are in mm)

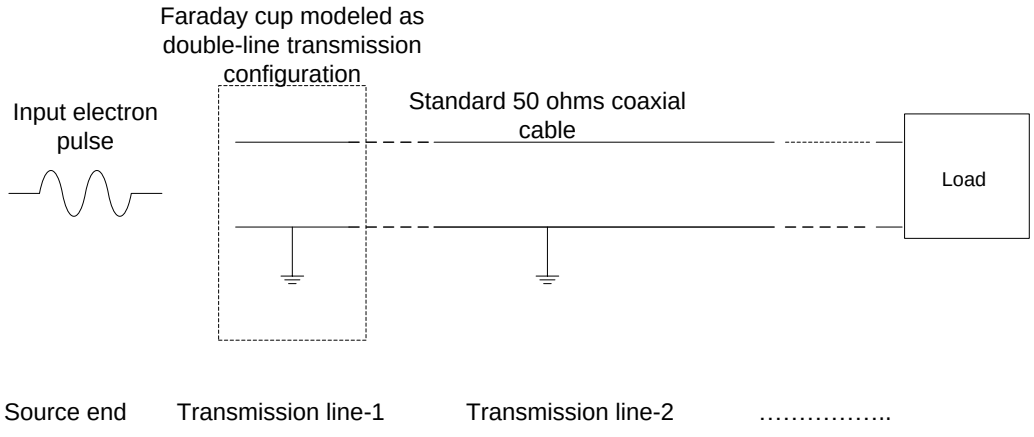


Figure 2. The transmission line model of the FC configuration

Furthermore, in the self-biased FC design, the dielectric strength between carbon conductor and grounding layer is another important consideration because there could be a high self-biased voltage pulse up to 1-10 kV between them during operation. Under such a high voltage pulse, partial discharge and spark may take place between carbon conductor and grounding, and at the air gap between their edges. The radial dimension of the carbon cup w is limited by the geometric dimensions of the experiment system, such as vacuum port, drift tube, etc. The dielectric strength is then set to yield a $50\Omega$ impedance match and hold enough high potential difference between carbon conductor and grounding.

Based on all above design considerations, in our FC structure, the insulator layer is acrylic sheet with a relative permittivity of 2.7 ($\epsilon_r \approx 2.7\ at\ 20℃$) instead of the more commonly used Teflon ($\epsilon_r \approx 1.9\sim2.1\ at\ 20℃$), in order to meet the requirements from dielectric strength and vacuum tube and port limit. Thus the ratio of *w/d* should be 4.6 to achieve a $50\Omega$ impedance match. In our design, the optimum d is 7.6 mm and w is 35 mm.

The grounding conductor of the $50\Omega$ BNC cable is connected with both the external grounding conductor of the FC (insulating layer) and the linear motion arm to minimize stray inductance. A short $50\Omega$ coaxial cable carries the signal out through the $50\Omega$ vacuum feedthrough and connects with an external self-biased test circuit consisting of self-biasing resistor $R_p$ and current view shunt resistor $R_s$ [1-2]. The whole system is designed to obtain the $50\Omega$ impedance matching at both the source terminal and load terminal through the FC. And since the impedance matches at each terminal, the internal conductor does not have to be connected with the grounding conductor through any low inductance shunt resistor to minimize the pulse signal dispersion and reflection. Then the external self-biased resistor can be changed externally to obtain the electron beam current with different energy [2]. In the experiments presented in this work, there is no negative biased metallic shielding grid located in front of the cup front face since the calculated displacement current in our experiment operations is lower than 3% of the total electron beam current. A schematic of this self-biased method and the experiment setup including the discharge chamber are illustrated in Figure 3.

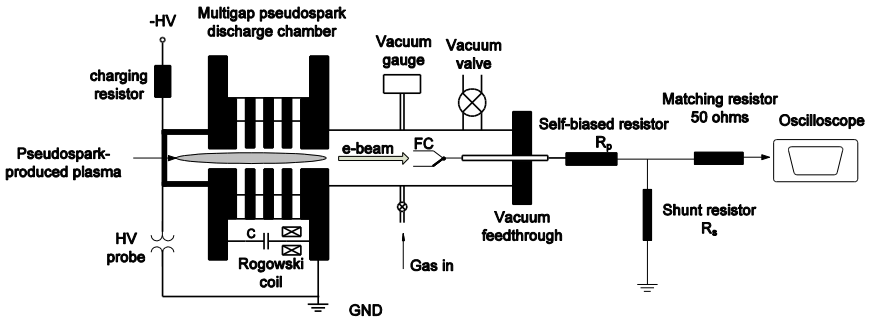


Figure 3. The schematic of self-biased FC set-up (not to scale)

## 3. EXPERIMENT RESULTS

Three main experiments are conducted. First, the response time of the FC is validated by comparing with a known test signal. Second, the current amplitude is validated by comparing with a calibrated current transducer. Finally, the main benefit of the FC is demonstrated through external adjustment of the shunt resistance to acquire the electron energy distribution function using the self-biased method.

### 3.1 RESPONSE TIME

To test the response time of the FC circuit, the front surface of the FC collector is connected to a pulse generator with $50\Omega$ internal load. The FC is terminated by a $50\Omega$ non-inductive resistor and the voltage drop on the FC is recorded by an oscilloscope. The typical waveforms of input and output signals are shown in Figure 4. The input signal (bottom trace) has a measured 10%-90% fall time of 10 ns, and rise time of 36.6 ns, which are similar to the pseudospark-produced electron beam pulse. The FC output signal (top trace) has a measured fall time of 11 ns, and rise time of 44.6 ns.

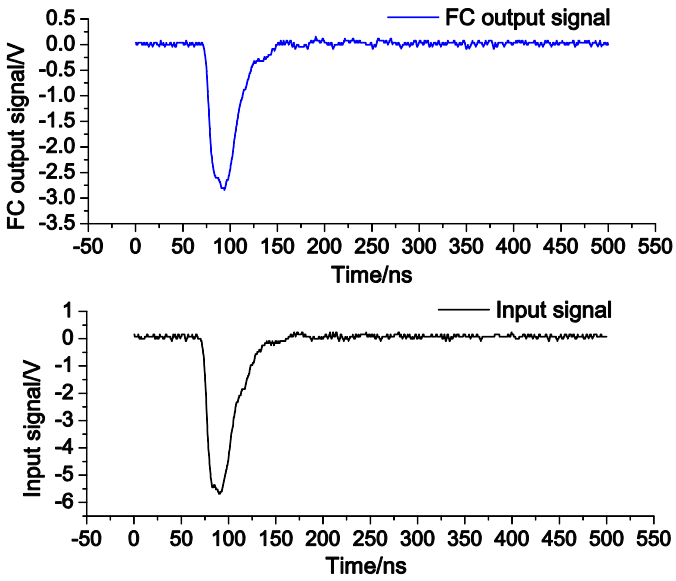


Figure 4. Response of FC: bottom- input signal; top- FC output signal

In Figure 5 and Figure 6, quantitative results of the response time of the FC are presented as the fall time percent difference and pulse width percent difference for multiple times. The fall time percent difference is defined as the magnitude of the difference between FC signal fall time and input signal fall time divided by the input signal fall time. A value close to zero is desirable. In Figure 5, data are presented for source signal fall times from 8.7 to 79.6 ns. Within the tested range, the fall time percent difference has a maximum of 33.3% at the fastest source fall time, 8.7 ns. As source fall time increases, fall time ratio decreases to below 10% and has a value of -1.9% at 62 ns.

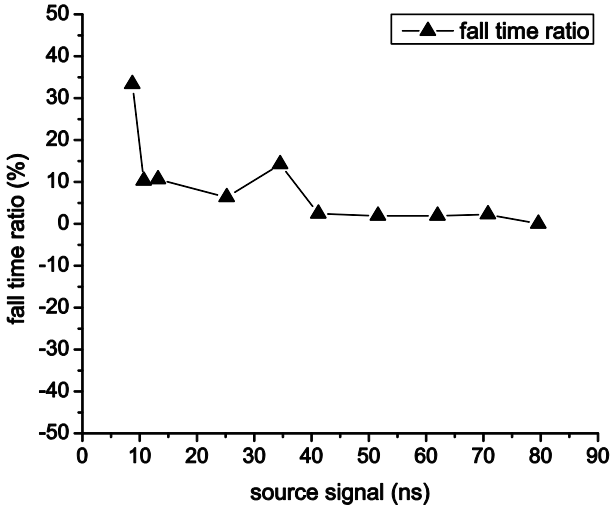


Figure 5. Fall time percent difference

Pulse width percent difference is an indicator of the signal dispersion, and is defined as the magnitude of the difference between FC output pulse width and input signal pulse width divided by input signal pulse width. Pulse width data are presented in Figure 6 for source signal pulse widths from 11.9 to 182.8 ns. Within the range tested, the pulse width percent difference has a maximum value of 6.7% at 11.9 ns. For source pulse width times greater than 30 ns the pulse width ratio remains relatively constant at approximately 0.2%.

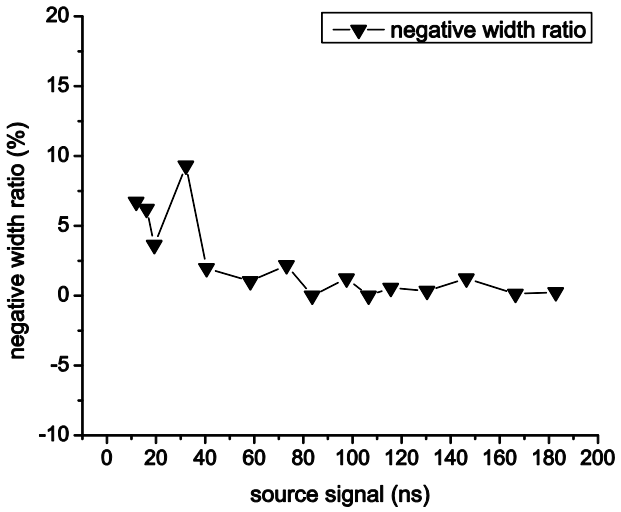


Figure 6. Pulse width percent difference

### 3.2 CURRENT MEASUREMENT

FC electron beam current measurements are compared with measurements from a calibrated F-70 RF commercial current transformer, which has a usable frequency range of 1 kHz to 100 MHz. The pseudospark is operated at a pressure of 82 mTorr on Argon at a discharge voltage of 4 kV. Figure 7 shows the electron beam current pulse measured by both the FC terminated by $25\Omega$, and the F-70 RF commercial current transformer. The FC records an electron beam peak current of 36.6 A and full width at half maximum (FWHM) of 40 ns. The F-70 RF current transformer obtains a peak current of 37 A and FWHM of 36 ns.

Measurements similar to those presented in Figure 7 are obtained for pseudospark operating voltages from 4 to 14 kV. The peak current measured by the FC is presented in Figure 8. As discharge voltage increases from 4 to 14 kV, the electron beam current collected by the FC increases from 36.6 A to 132.2 A.

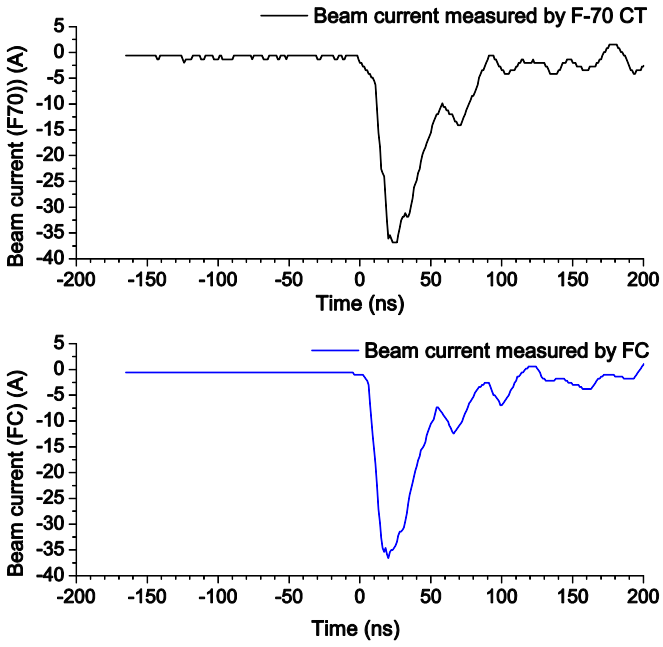


Figure 7. Electron beam current pulse measured by the calibrated F-70 RF current transformer (CT) and the FC (FC)

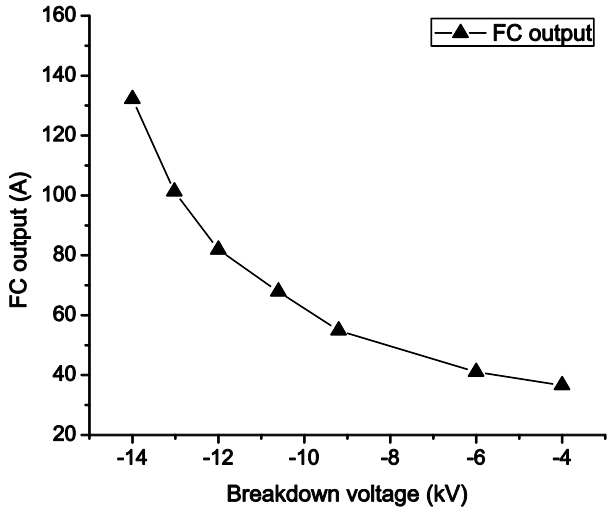


Figure 8. FC peak current for multiple voltages

FC peak current is compared with peak current measured by the CT. These results are presented in Figure 9 as the amplitude percent difference. The amplitude percent difference is the magnitude of the difference between the FC amplitude and CT amplitude divided by the CT amplitude. Amplitude percent difference is less than 10% for all investigated pseudospark discharge voltages.

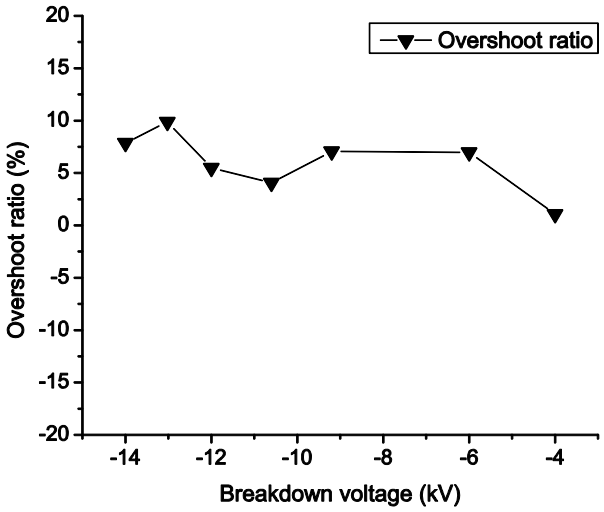


Figure 9. Amplitude percent difference for multiple discharge voltages

### 3.3 ELECTRON BEAM ENERGY DISTRIBUTION FUNCTION (EEDF)

The previous two experiments evaluated the FC response time and current measurement. From Figure 5, for signal times on the order of 10 ns or greater, the FC has a percent difference of 10% or less. From Figure 9, the FC has an amplitude percent difference of 10% or less. Next, the FC is used to measure the electron energy distribution function of the pseudospark discharge. The shunt resistor and self-biased resistor are adjusted externally to the vacuum system. This is an advantage of this design.

As shown in Figure 10, the electron beam current is measured using different self-biased resistors ($R_p$ in Figure 3) from 51 to 550Ω.

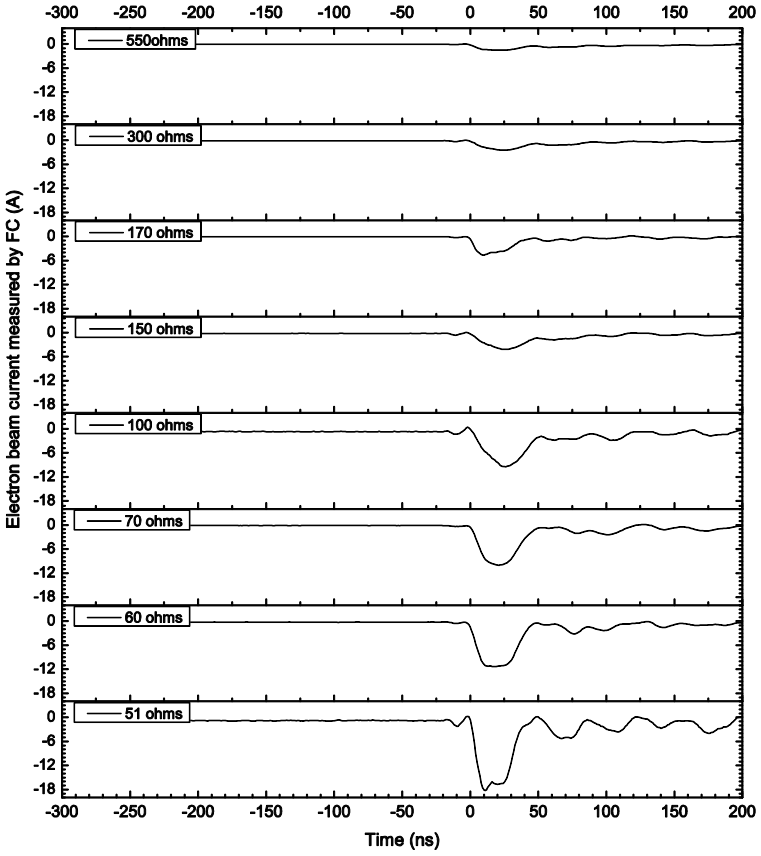


Figure 10. Measured electron beam current with different self-biased resistor (Rp in Figure 3)

The measured electron beam current traces show that the number of electrons collected by the FC and self-biased circuit vary depending on the value of the self-biased resistor $R_p$. Using these measurements, the electron energy distribution function can be

calculated using the relation between the measured electron beam current $I_b$ and self-biased voltage $V_{sb}$ [1-2],

$$cg(V_{sb}) = -\frac{dI_b/d(V_{sb})}{\sqrt{V_{sb}}} \quad (2)$$

The calculated beam EEDF at different times during the discharge are shown in Figure 11. Only times greater than 10 ns are shown because this is the fastest response time for which the percent difference is less than 10% (Figure 5). At t = 10 ns the electron energy distribution is Maxwellian with a temperature of 150 eV. By t = 19 ns the EEDF has shifted to a double-hump with low-energy peak at 300 eV and high-energy peak at 800 eV. This double-hump distribution remains for all times investigated and the lower energy peak always has a larger magnitude. At t =22 ns and 28 ns, the electron energy distribution show a double hump shape: one peak is centered at the low energy region and the second peak is at higher energy. At t = 22ns, the low energy electron peak is at 415 eV and the high energy peak is centered at 920 eV. At t =28 ns the low energy peak is at 560 eV. The high energy peak is still at 900 eV, but its magnitude has decreased 63% from 0.16 (a.u.) to 0.06 (a.u.). Furthermore, FWHM of the higher energy peak has increased from 200 eV at t = 22 ns to 300 eV at t = 28 ns. The EEDFs at t = 38 ns and t = 58 ns show both energy peaks shifting to lower energy. At t = 38 ns, the peaks are centered at 200 eV and 460 eV. The FWHM of high energy electrons increases from 300 eV at t = 28 ns to > 500 eV at t = 38 ns. At these time intervals the low energy FWHM remains constant at 200 eV.

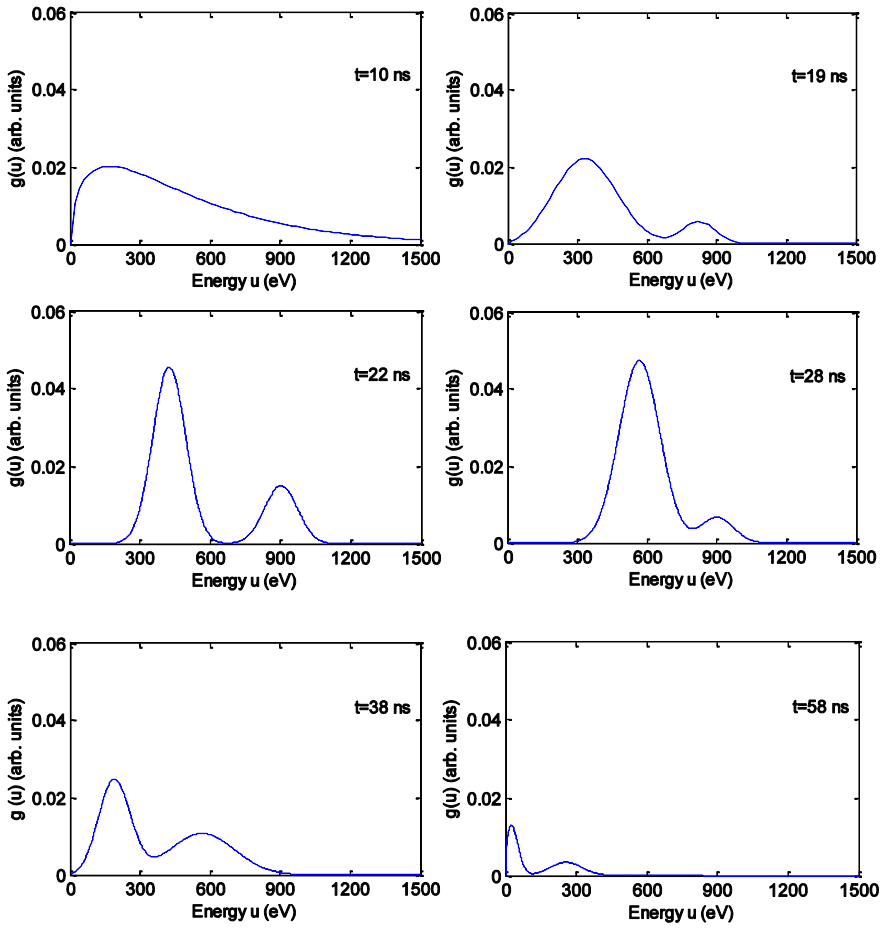


Figure 11. Temporal evolution of the EEDF corresponding to Figure 10

## 4. CONCLUSIONS

A simple, easily fabricated, fast response FC design for time-resolved electron energy distribution function (EEDF) measurement is presented in this work. The performance of FC is validated by comparison of response time and current amplitude of the output signal with known reference signals. Based on comparison with known test signals, the FC has a percent difference less than 10% for a fastest response time of 10 ns. For peak currents between 30 to 130 A, the FC also has a percent difference of less than 10%. The FC can be used to capture the pulsed electron beam generated by the pseudospark plasma discharge operating between 4 to 14 kV discharge voltage. It may

also be applicable to other fast-discharge plasma physics experiments. External adjustment of shunt resistance makes this Faraday probe capable of capturing self-biased measurements of beam current for deconvolution into the electron energy distribution function. Application of this technique indicates a double-humped pseudospark beam electron energy distribution function that reaches a peak energy of 900 eV at 22 ns after initiation of the discharge.

## REFERENCES

[1] M. Nistor and N. B. Mandache, *Journal of Optoelectronics and Advanced Materials* **7**, 1619 – 1622 (2005).

[2] G. Modreanu, N. B. Mandache, A. M. Pointu, M. Ganciu, and I. I. Popescu, *Journal of Physics D: Applied Physics* **33**, 819 – 825 (2000).

[3] H. Chuaqui, M. Favre, E. Wyndham, L. Arroyo, and P. Choi, *Review of Scientific Instruments* **60**, 141 – 142 (1989).

[4] A. Luches, V. Nassisi, and M. R. Perrone, *Review of Scientific Instruments* **56**, 758 – 759 (1985).

[5] D. Pellinen, *Review of Scientific Instruments* **41**, 1347 – 1348 (1970).

[6] H. Bluhm, *Pulsed Power Systems: Principles and Applications,* 1st ed. (Springer, 2006).

[7] D. M. Pozar, *Microwave Engineering,* 3rd ed. (John Wiley and Sons, Inc., 2005).

# III. EXPERIMENTAL INVESTIGATION OF TIME-RESOLVED ELECTRON BEAM ENERGY DISTRIBUTIONS GENERATED IN A TRANSIENT HOLLOW CATHODE DISCHARGE

Hu, Jing and Joshua L. Rovey

## ABSTRACT

In this paper, a retarding potential energy analyzer (RPEA) specific for pulsed electron beams at pressure range of tens of mTorr is developed and used to investigate the energy of transient hollow cathode discharge produced electron beams. This RPEA has been applied in a pseudospark-based electron beam source at applied potential up to 20 kV. Experimental investigations under applied potential of 5 kV, 10 kV, 15 kV and 20 kV were carried out and the time-resolved electron energy distributions are constructed. The numbers of electrons within various energy groups are calculated from the time-resolved electron energy spectrum. Results show that the maximum number of electrons is emitted with 40% - 60% of the full applied potential on pseudospark device, and varies from 22.5% to 38.9% of the total number of emitted electrons. Additionally, the energy transformation efficiency of stored electrical energy to electron beam energy is calculated from presented data. The energy transformation efficiency increases from 11.4% at 5 kV breakdown voltage to 23.2% at 20 kV breakdown voltage.

## 1. INTRODUCTION

Transient hollow cathode discharge (THCD), known as a low pressure pulsed discharge, is characterized by a hollow cathode structure of considerable physical volume compared with the whole device and initiation of THCD originated from the hollow cathode region. Based on the specific configurations, THCD has a variety of forms such as pseudospark [1-3], channel spark [4-6], capillary spark [7-8], etc. Although the

discharge properties among those forms of THCD show different specific characteristics [9]-[10], there are some common characteristics in various THCD types:

1) THCD operated in low pressure of tens to hundreds of mTorr, high voltage of kV to tens of kV, where the reduced electric field (E/N) is of the order of $10^{11}$ V-cm$^2$ [1, 3].
2) THCD can obtain high current main discharge up to tens of kA within very fast time of $10^{-9}$ s due to the rapid formation of potential gradient and plasma inside the hollow cathode region [1-10]. Thus the THCD can obtain very high current rise rate of $10^{11}$-$10^{12}$ A/sec;
3) The low pressure of THCD is promising to obtain high repetition rate of discharge, which requires a fast decay and recombination time of the discharge plasma [11];
4) The THCD is capable of producing intense electron beams with excellent properties due to the high current (A-kA), high power density (up to $10^9$ W/cm$^2$), small parameters (0.2-2 mm) and low emittance (10s of mm mrad) [1-4, 6, 9-13].

In the past decades, considerable research work has demonstrated that THCD of various forms was suitable and promising for a variety of applications due to its characteristics. In [1, 14-17], the pseudospark device has been successfully developed as pulse power switches and shows potential to be a better substitute for traditional thyratron [1]. Besides the switch applications, another promising application for THCD is the intense electron beam source with remarkable parameters. In [18-20], electron beams produced from a multi-gap pseudospark device have been applied for millimeter wave generation. In [6] and [17], the electron beams produced from pseudospark discharge and capillary discharge were investigated for ultraviolet (EUV) radiation. In [2,5,9,11], the electron beams produced by THCD were successfully tested in applications such as material processing, thin film technologies and intense soft x-ray sources. In [21-22], a new technique called the pulsed-electron-beam fluorescence (PEBF) technique was developed for the determination of gas number densities and vibrational population distributions using the pulsed electron beams generated from pseudospark device. In PEBF technique, the characteristic of short pulse duration of electron beams generated

from pseudospark ($10^{-9}$ s) is of special interest since the background light problem of fluorescence can be minimized by the short signal integration time.

Besides multiple applications of pulsed electron beams produced by THCD, plasma generation by high energy electron beams is another application for THCD device [23-26]. For example, magnetohydrodynamic (MHD) channel requires highly efficient neutral gas ionization by high energy intense electron beams. In [23, 25-26], the feasibility of electron beam generated plasmas in hypersonic MHD channel control was discussed. The MHD control of hypersonic flow and scramjet inlets by electron beam ionization was developed and validated. In these previous efforts, electron beams are assumed to be the most efficient way of ionizing cold gases. Ref [26] shows that compared to low-energy (1-3 eV) electrons in conventional discharges that dissipate most of their energy in nonionizing inelastic collisions, the ionizing electrons with comparatively high energy from tens of eV to thousand of eV minimize the power required to sustain weakly ionized plasmas, which can be easily achieved by THCD discharge.

Although the characteristics of pulsed electron beams generated by THCD, such as high energy, high current, short pulse duration, moderate operation pressure, are favorable for multiple applications, they also lead to challenges in the investigation and determination of electron beam properties. Electron beam energy is a quite important parameter to evaluate the electron beam quality. In some previous studies, the average energy values of THCD produced electron beams were determined and evaluated in [2,4,9,27]. However, the full energy spectrum and temporal evolution of pulsed electron beam energy distribution is of great importance and interest for thin film deposition [2,5,28], radiation generation [9-10,29], and plasma generation [23, 25-26], which has not been well determined. Specifically, the modeling of high energy electron excited plasma in neutral gas requires more accurate information of electron populations with various energies at various time points [23, 25-26]. However, only few studies have been focused on the construction of time-resolved electron beam energy distributions which is limited by many factors, such as response time of diagnostics and gas breakdown threshold in the operational pressure range of THCD. In [30-31], the time-resolved energy spectrum of pulsed electron beams produced from pseudospark was constructed at a given pressure

and voltage. Besides previous work concerning the energy measurements, there are still more properties to be determined, such as the variations of electron energy distribution with various operational parameters, the energy transformation efficiency of electron generation by THCD, and the particle populations of electrons with different energy in the THCD produced beam. Thus the main emphasis of this paper is on the time-dependent electron beam energy distribution produced by a pseudospark, and the dependence of generated electron energy on external parameters. Additionally, the energy efficiency of pseudospark produced electrons is calculated for energy cost evaluation and compared with the requirement of intense electron beam applications.

This paper presents detailed experimental investigations and discussions of the time-resolved electron beam energy distributions from a multigap pseudospark device. This work is organized into the following sections: a detailed introduction to the pseudospark-based electron beam source and time-resolved electron energy distribution measurement setup is presented in Sec II. The experiment investigation results of time-resolved electron beam distribution and the comparative studies under various operation conditions are presented in Sec III. Finally, conclusions on the experimental investigations and comparisons between the time-resolved electron energy results in our work and previous related studies are summarized in the last section.

## 2. EXPERIMENTAL METHOD AND SETUP

The general method to determine the time-resolved electron energy distribution function is the retarding potential energy analysis (RPEA) as illustrated in Figure 1. A retarding potential, *V*, is applied to the retarding grid to decelerate the moving electrons exiting from the electron beam source. Only the electrons with energy higher than value of *eV*, where e is the single electron charge, can pass through the retarding potential and be collected by the electron beam collector in the downstream direction of retarding grid. When varying retarding potential to different values of $V_i$, a series of electron beam current pulses are collected as $\mathrm{I}(\epsilon_\mathrm{i}, \mathrm{t})$, where $\epsilon_\mathrm{i} = \mathrm{eV_i}$ represents the electron energy. More details of data analysis and deduction procedure by linear approximation have been

presented in [30] and the summarized method for determining energy distribution from RPEA measurements is as follows:

$$\left.\frac{d^2N}{dtd\epsilon}\right|_{\epsilon_i+\frac{1}{2}\Delta\epsilon_i} = \frac{I(\epsilon_i,t) - I(\epsilon_i+\Delta\epsilon_i,t)}{e\Delta\epsilon_i} \tag{1}$$

Where $\left.\frac{\mathrm{d}^2\mathrm{N}}{\mathrm{dtd}\epsilon}\right|_{\epsilon_\mathrm{i}+\frac{1}{2}\Delta\epsilon_\mathrm{i}}$ is the energy distribution at energy $\epsilon_\mathrm{i}+\frac{1}{2}\Delta\epsilon_\mathrm{i}$, and $\mathrm{I}(\epsilon_\mathrm{i},\mathrm{t})$ and $\mathrm{I}(\epsilon_\mathrm{i}+\Delta\epsilon_\mathrm{i},\mathrm{t})$ are the electron beam current collected at retarding potential of $\mathrm{V_i}$ and $\mathrm{V_i}+\Delta\mathrm{V_i}$.

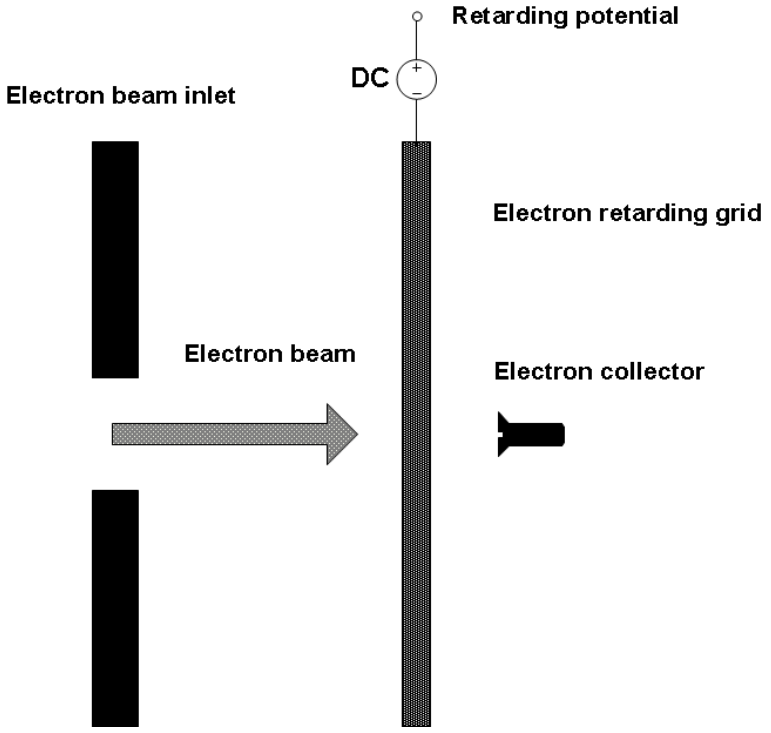


Figure 1. Fundamental configuration of retarding potential energy analyzer (RPEA)

RPEA is usually applied in low energy at several eV to 10s eV and DC electron beam energy analysis. For THCD based electron beam, there are mainly two factors to limit the application of general setup of RPEA. First is the response time of electron detector for electron pulse with $10^{-9}$ second rising edge. Secondly, the threshold value of retarding potential is difficult to maintain at several kV to tens kV without causing gas breakdown between retarding grid and ground in the pressure range of tens of mTorr to hundreds of mTorr, which is located at the bottom part of Paschen curve and has very low breakdown voltage. In our work, the improved RPEA for THCD-based electron beams and the multi-gap pseudospark discharge device as electron source are shown in Figure 2.

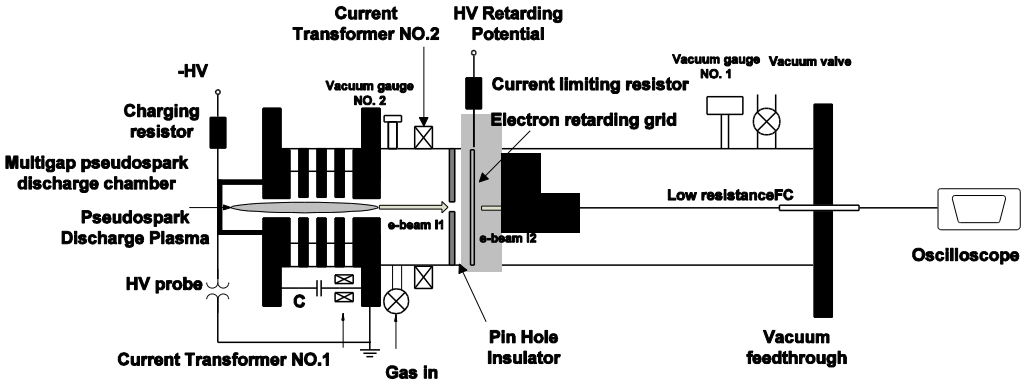


Figure 2. Experiment setup of time-resolved energy analyzer of pseudospark-based electron beams

The experiment setup consists of two sections: The left side is the multigap pseudospark discharge section, including a 16-gap pseudospark discharge device. The hollow cathode was connected to the high voltage dc power supply (100kV, 1mA) through a 20 MΩ charging resistor. A custom North Star high voltage probe PVM-5 is connected to the cathode to measure the voltage breakdown waveform. And the discharge

current is measured by a fast response Rogowski coil (current transformer NO.1 in Figure 2) with rising time limit of 4 ns. Two 700 pF resin-dipped ceramic capacitors were connected between the anode and cathode symmetrically for energy storage.

The improved RPEA for THCD-based electron beams is located on the right side in Figure 2, including electron beam detectors and high voltage retarding grid. The electron beam detectors include Rogoswki coil with a response time of 4 ns (current transformer NO.2 in Figure 2) and a low resistance of $0.08\,\Omega$ Faraday cup. Current transformer NO.2 is located right behind the electron beam exit and in front of the pin hole to determine the full value of pseduspark produced electron beam current I1. Faraday cup of $0.08\,\Omega$ is located behind the pinhole to determine the electron beam current I2 passing through the pinhole without retarding potential. Thus when various retarding potential is applied on the grid and detected by the Faraday cup, the total particle number directly generated from pseudospark device can be calibrated by the ratio of I1/I2 [30]. This Faraday cup has been validated to have a fast response time of 8.3 ns by a pulse generator. Compared with the Faraday cup terminated by 50 ohms high resistance in [30-31] which has been validated to reject the low energy by the self-biasing potential on the Faraday cup [9-10, 32-33], the low resistance Faraday cup and Rogoswki coil can collect all the electrons in the beam pulse, including high energy and low energy components.

The electron beam drift region and pseudospark electron beam source are insulated by a pin hole with a 1 mm diameter right behind the electron outlet at anode of pseudospark device. By this pin hole, a pressure gradient is formed between the RPEA region and pseudospark-based electron source region. When the pressure of pseudospark-based electron source is increased to $10^{-2}$ Torr, the pressure of RPEA region can be maintained at $10^{-5}$ Torr. In such a very low pressure region, the applied voltage on retarding grid can go up to 20 kV without any gas breakdown in all the operation pressures presented in this work as the test results shown in Figure 3.

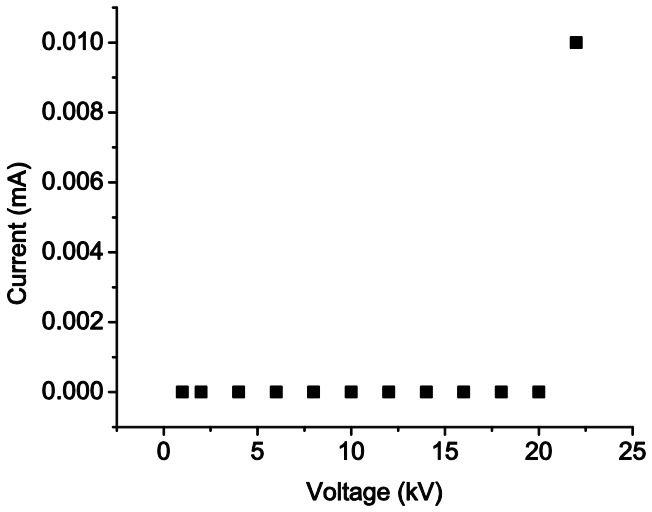


Figure 3. Applied retarding grid potential versus leakage current due to gas breakdown

The vacuum and gas control system is also located in this section. The whole experimental system was evacuated to $10^{-5}$ Torr initially by a two-stage mechanical pump and turbo pump located at anode side. The operating gas was argon. Argon gas enters into the vacuum system through a mass flow controller. The mass flow rate of argon can be adjusted accurately to control the operation pressure in vacuum system. All the experimental data are acquired by a high speed oscilloscope with 500 MHz bandwidth, 1 GS sampling rate. The control of oscilloscope readout and data storage is accomplished by a Labview software workbench. All the presented experimental results in the following sections represent the mean value over five repeated cycles.

## 3. EXPERIMENT RESULTS

In this section, the electron beam current results passing through retarding potential grid collected by the Faraday cup will be presented. The time-resolved electron beam energy spectrum is constructed from the differential electron beam pulses with

varying retarding potentials. Additionally, based on the time-resolved electron beam energy distribution results, the total populations of electrons within various energy ranges and the total energy carried by the electrons are calculated and presented in this section. Finally, the energy transformation efficiency by pseudospark-based electron beam source is compared under various pseudospark breakdown voltages.

## 3.1 TEMPORAL EVOLUTION OF COLLECTED ELECTRON BEAM CURRENT BY VARYING RETARDING POTENTIAL

As stated in Sec II, by varying the voltage on the electron retarding grid, only electrons with energy higher than the retarding potential can pass through the retarding grid. Figure 4 presents the electron beam pulses collected with retarding potential of 1kV, 3kV, 5kV, 7kV, 9kV and 11kV, and the waveform of breakdown voltage of 10kV applied on the pseudospark device. As shown in Figure 4, the electron beam current pulse starts synchronously with the start of breakdown of gas in pseudospark device. Under the low retarding potential, the collected electron beam pulse shows a fast rising edge and a slow and long tail. With the increase of retarding potential, the peak value of collected electron current decreases because more electrons are stopped by the retarding grid. Compared with the sharp rising edge, the long tail of the electron beam current decreases rapidly with increasing retarding potential. At the highest retarding potential 11 kV, all the electrons within 600 ns ~ 1500 ns have been stopped by the retarding grid, while the peak current of the rising edge of beam pulse under 11 kV retarding potential still remains 28% of the peak value under 1 kV retarding potential. Such variations suggest that the high energy electrons are mainly formed during the early phase on the rising edge of the emitted electron beam pulse starting from the ignition of gas breakdown in pseudospark device at approximately 350 ns as illustrated in Figure 4. Meanwhile, the low energy electrons have a wide energy spread. The early phase of electron beam pulse consists of both high energy electrons and low energy electrons. And the long decreasing tail of the electron beam pulse mainly consists of low energy electrons, which is identical with the prediction in [9-10, 29].

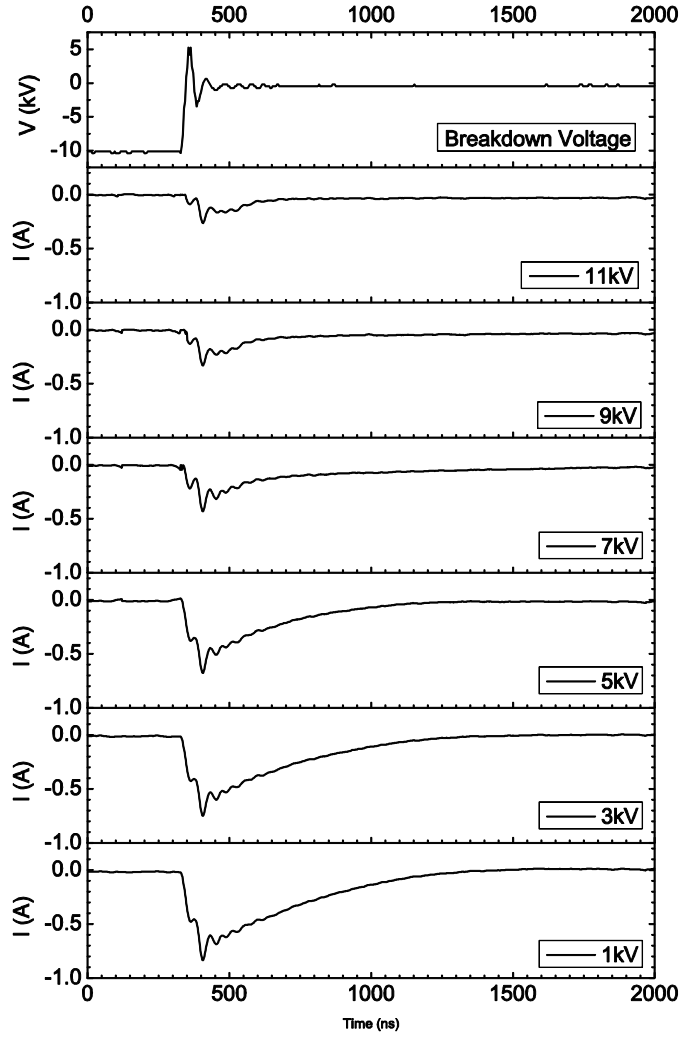


Figure 4. Collected electron beam current with varying retarding potential at 10kV breakdown voltage

Meanwhile, the space charge effect in RPEA can affect the construction of electron beam energy spectrum due to the formation of virtual cathode [34]. The virtual cathode by space charge effect in field of RPEA is formed only when the electron beam

current inside the energy analyzer is larger than the limiting value given by the Child-Langmuir law:

$$I_{lim=}J_{lim} \times S = \frac{4\varepsilon_0}{9}\sqrt{\frac{2e}{m_e}}\frac{U^{3/2}}{d^2} \times S \quad (2)$$

which is equal to 1.86 A for the limiting current value at 10 kV. The electron beam current injected into the RPEA is 1.1 A which is less than this calculated limiting current. Thus the space charge effect in RPEA in our experiment will not affect results of the electron beam energy spectrum.

### 3.2 TIME-RESOLVED ELECTRON ENERGY DISTRIBUTION SPECTRUM

The detailed method for constructing the time-resolved energy spectrum from collected electron beam pulses has been presented in Ref [30]. Figure 5 presents the normalized particle numbers (a.u.) with energy of 2keV, 4keV, 6keV, 8keV and 10keV emitted at given time, which is constructed from the waveforms presented in Figure 4. It should be stated that in Figure 5, the electron density are represented as the groups with uniform energy at given times are mainly for the convenience of particle modeling in our current work. Based on the temporal evolution of electron density with different energies shown in Figure 5, the electrons can be divided into groups at various energy ranges: low energy group with energy below 20% of full breakdown voltage (10 kV in the presented experiment), medium energy group with energy within 20% ~ 60% of full breakdown voltage, high energy group with energy higher than 60% of full breakdown voltage. As shown in Figure 5, the high energy electrons (8 keV and 10 keV) are emitted at the earliest time, starting from the beginning of electron beam pulse to the peak energy value at 450 ns, which is identical with the peak of electron beam current. At later times in the electron beam pulse, high energy electrons stop to be emitted, while more medium energy electrons exit from the discharge gap. The electrons with lowest energy are emitted as the slow long tail of the electron beam pulse. Additionally, the energy spread ranges are also varied for low energy, medium energy and high energy electrons. As

illustrated in Figure 5, the low energy electrons have a wider temporal distribution compared with higher energy electrons. Based on the results shown in Figure 5, the full width at half maximum (FWHM) of electron distribution with energy of 2 keV is 800 ns, while the FWHM of electron distribution with energy of 10 keV is 200 ns.

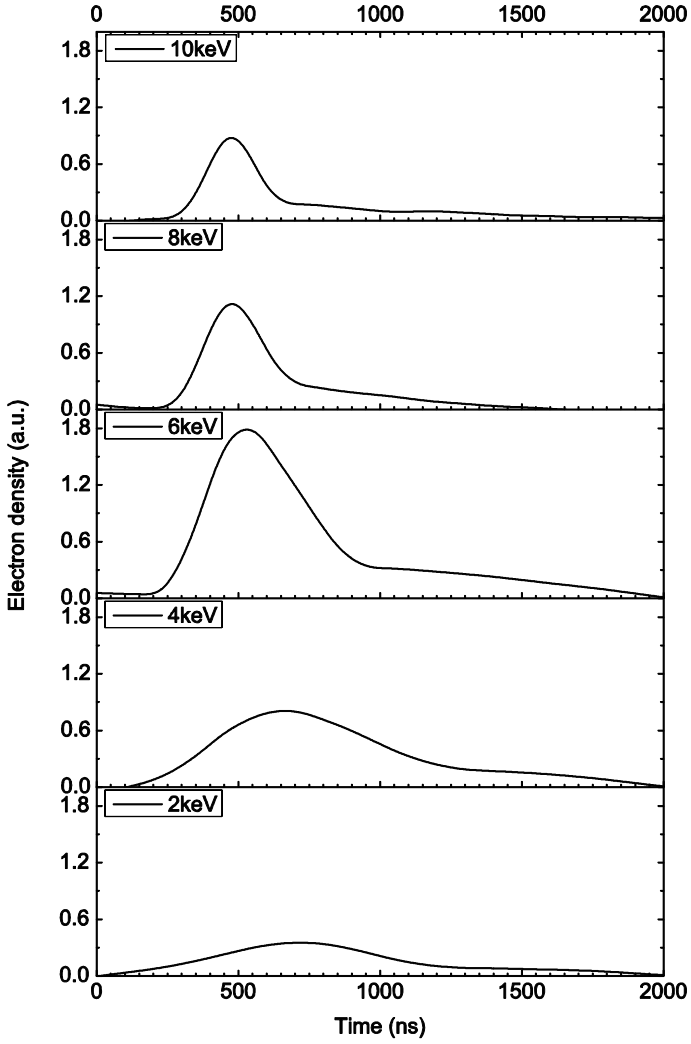


Figure 5. Time-resolved distributions of electrons within various energy groups at 10 kV breakdown voltage

In order to show the evolution of electron emission process more clearly, the three dimensional electron energy distributions of various energy groups corresponding to Figure 5 are illustrated in Figure 6. According to the results shown in Figure 5 and Figure 6, the medium energy electrons construct the maximum population of electrons emitted from the electron source. The high energy component of electron beam pulse has a higher number of electrons than lowest energy component. In order to quantify the numbers of emitted electrons in various groups, the time integrated electron numbers in various energy range will be presented in the following section.

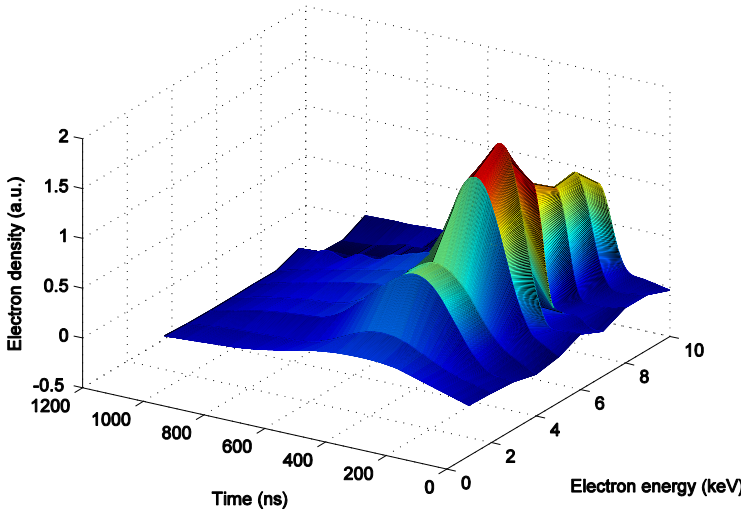


Figure 6. 3-D time-resolved electron energy distributions at 10kV breakdown voltage

### 3.3 POPULATIONS OF ELECTRONS WITH VARIOUS ENERGY

As presented in Ref [30] and Sec II in this paper, the time-resolved energy spectrum at energy $\epsilon_b + \frac{1}{2}\Delta\epsilon_b$ as a function of time can be constructed in terms of the experimentally obtained differential current waveform as Equation (1). Thus the total number of electrons at energy of $\epsilon_b + \frac{1}{2}\Delta\epsilon_b$ can be determined by

$$N|_{\epsilon_b+\frac{1}{2}\Delta\epsilon_b} = \int_0^{\infty} \frac{I(\epsilon_b, t) - I(\epsilon_b + \Delta\epsilon_b, t)}{e} dt \quad (3)$$

where e is the charge of single electron. Then the electrons at various energy groups of 2 keV, 4 keV, 6 keV, 8 keV and 10 keV corresponding to the data presented in Figure 2 and Figure 3 are determined by Equation (3). Furthermore, as stated in Sec II and [30], it should be noted that all the electron beam current values to determine the total generated particle numbers $N|_{\epsilon_b+\frac{1}{2}\Delta\epsilon_b}$ should be calibrated by the scaling factor of I1/I2, which is the electron beam current directly exiting from electron beam source (I1) to sampled electron beam current passing through pinhole without retarding potential (I2). Figure 7 shows these two electron beam current values I1 and I2 at 10 kV breakdown voltage.

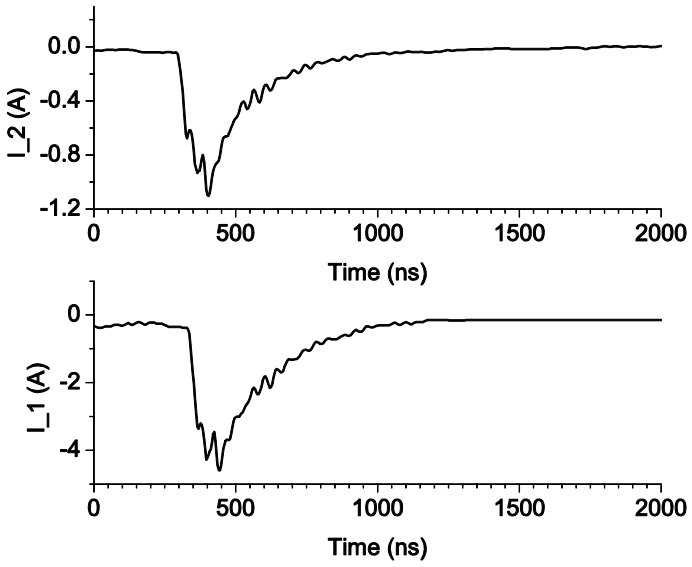


Figure 7. Electron beam current before passing through the pin hole (Bottom) and after passing through the pin hole (Top) at 10 kV breakdown voltage

The calculated results are illustrated in Figure 8 as follows. It was shown that electrons with maximum particle numbers are at the energy of 6 keV, which is within the

medium energy compared with the full breakdown voltage of pseudospark device. Pseudospark has been known for its capability to produce high energy electrons with energy close or equal to full applied voltage [2-3,11]. Based on our results, the electrons at high energy groups (80%~100% of full breakdown voltage) has the lowest particle numbers compared with medium energy electrons and low energy electrons.

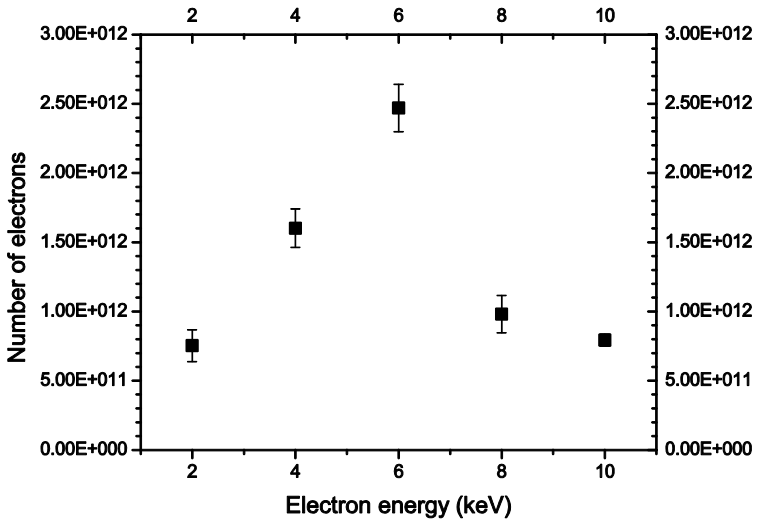


Figure 8. Particle numbers of electrons at various energy groups at 10 kV breakdown voltage

In order to evaluate the weight of electrons at various energy groups in the total generated electrons from pseudospark device, the ratio values of electrons with energy internal of 1 keV to the total particle number of generated electrons are presented in Figure 9. The results illustrated in Figure 9 show that the generated electrons have highest intensity at energy between 5 keV~6 keV, which is located at the medium energy range compared with full breakdown voltage of pseudospark device. 32.7% of the total generated electrons are at energy of 5 keV and 6 keV. The least number of electrons have

the lowest energy range below 2 keV and highest energy range above 8 keV. As illustrated in Figure 9, the calculated particle numbers of electrons at 1 keV and 2 keV are 4.7% and 5.0% to total generated electrons. The high energy electrons at energy above 80% of full breakdown voltage (8 keV in this case) is 11.0% of the total electron numbers. The electrons with energy above 2 keV but below 5 keV are 21.2% of the total electrons.

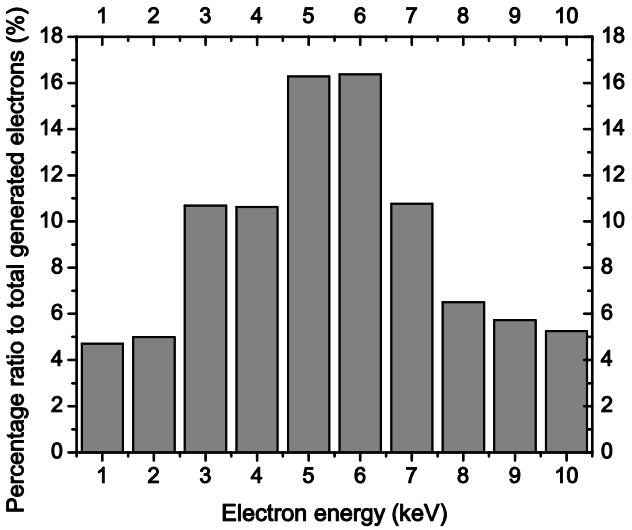


Figure 9. Ratio percentage of electrons at various energy groups to the total generated electrons at 10kV breakdown voltage

## 3.4 ENERGY TRANSFORMATION EFFICIENCY OF PSEUDOSPARK DEVICE AS ELECTRON BEAM SOURCE

The energy transformation efficiency to generate the electron beam is an important parameter to be considered, especially for a pulsed electron beam source with a short time duration like THCD device. With the time-resolved electron beam energy

distributions presented in this work, the total energy carried by electron beam can be calculated by:

$$E_{total} = \sum_{1}^{i} N_i \epsilon_i \tag{4}$$

Where $\epsilon_i$ is the electron energy of ith group, and $N_i$ is number of electrons at an energy of $\epsilon_i$.

In our work, the energy transformation efficiency is defined as the ratio of total energy carried by beam electrons to the total energy stored in capacitors which can be determined by:

$$\eta = \frac{E_{total}}{E_{stored}} = \frac{\sum_1^i N_i \epsilon_i}{\frac{1}{2} C_{ext} V_{breakdown}{}^2} \tag{5}$$

Based on the data presented in previous section, the energy transformation efficiency is calculated to be 17.4% for 10 kV discharge.

## 3.5 ELECTRON ENERGY DISTRIBUTIONS AT VARIOUS APPLIED VOLTAGES ON PSEUDOSPARK DEVICE

The time-resolved electron energy distributions, electron numbers at various energy groups, their percentage on the total generated electrons, and the energy transformation efficiency of electron generation at 10 kV breakdown voltage on pseudospark device are presented in the previous sections. The same experiments and data analysis were carried out under breakdown voltage on pseudospark device of 5 kV, 10 kV, 15 kV and 20 kV. In order to quantify and compare the electron energy distribution results among various voltages on pseudospark device, the generated electrons at each breakdown voltage are divided into groups at energy of 0-20%, 20%-40%, 40%-60%, 60%-80%, 80%-100% of full breakdown voltage on discharge device. Firstly, particle numbers of total generated electrons from pseudospark device

under breakdown voltage of 5 kV, 10 kV, 15 kV and 20 kV are presented in Figure 10. As shown in Figure 10, the number of electrons increases from $6.0 \times 10^{12}$ at 5 kV to $4.3 \times 10^{13}$ at 20 kV.

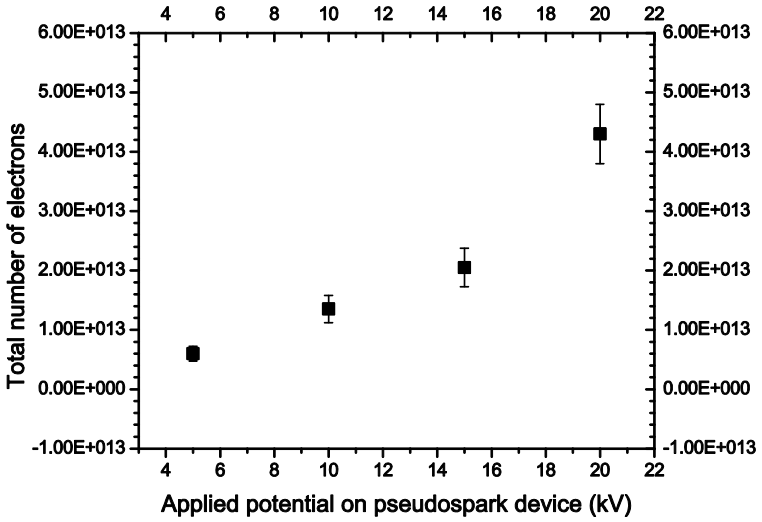


Figure 10. Total particle numbers of generated electrons under various applied voltages

The fraction of electrons within the various energy groups under breakdown voltage of 5 kV, 10 kV, 15 kV and 20 kV (Ranked from left to right as shown in Figure) are illustrated in Figure 11. Based on the results presented in Figure 11, for most of the applied voltages investigated, the electrons with maximum particle numbers are located at the medium energy range, 40%~60% of full breakdown voltage on the electron beam source. Additionally, the fraction of electrons within 40%-60% energy group decreases as breakdown voltage on pseudospark device increases. At the minimum breakdown voltage on pseudospark device 5 kV, the electrons within energy group of 40%-60% of full potential constitute 38.9% of the total generated electrons. Under 10 kV voltage on pseudospark device, the electrons at energy of 40%-60% of full applied decreased to 22.5%

of the total generated electrons. For lowest energy group below 20% of full breakdown voltage, the electron fraction increases with the increasing breakdown voltage on pseudospark device, from 6.9% at 5 kV breakdown voltage to 13.6% at 20 kV breakdown voltage. The highest energy group above 80% of full potential also displays an increasing trend with breakdown voltage on pseudospark device. As illustrated in Figure 11, the electrons above 80% of full potential constitute 16.4% of total electrons under 20 kV device breakdown voltage, while the number percentage of this energy group is only 7.2% at 5 kV device breakdown voltage.

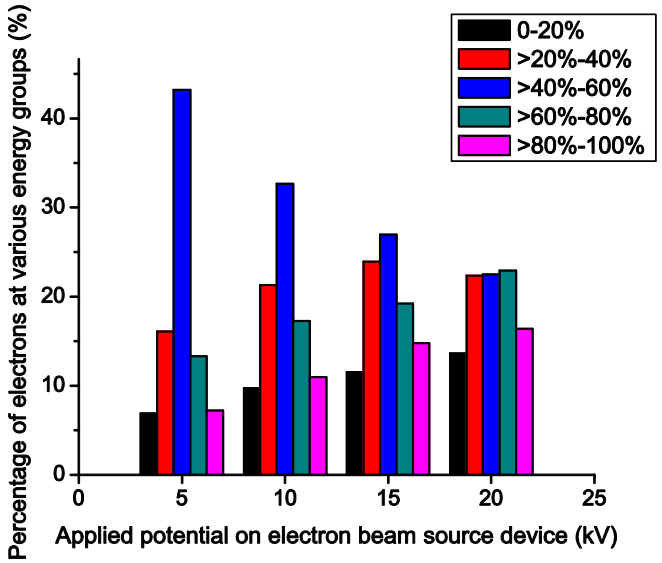


Figure 11. The ratio percentage of electrons at various energy groups under different breakdown voltage on pseudospark device

Based on the particle numbers of electrons at various energy groups, the total energy carried by the electrons under various breakdown voltage on pseudospark device is calculated by Equation (3) and the results are illustrated in Figure 12, and the energy transformation efficiency is calculated with Equation (4) and the results are shown in

Figure 13. The total energy of generated electrons increases with increasing breakdown voltage on pseudospark device. At 5 kV breakdown voltage, the electron energy is 2 mJ, while the total electron energy increases to 65 mJ at 20 kV breakdown voltage, which is a 32.5 times increase in energy. The energy transformation efficiency from capacitance stored energy also increases with breakdown voltage on pseudospark device. As illustrated in Figure 13, the energy transformation efficiency increases from 11.4% at 5 kV to 23.2% at 20 kV, which is a factor of 2 increase.

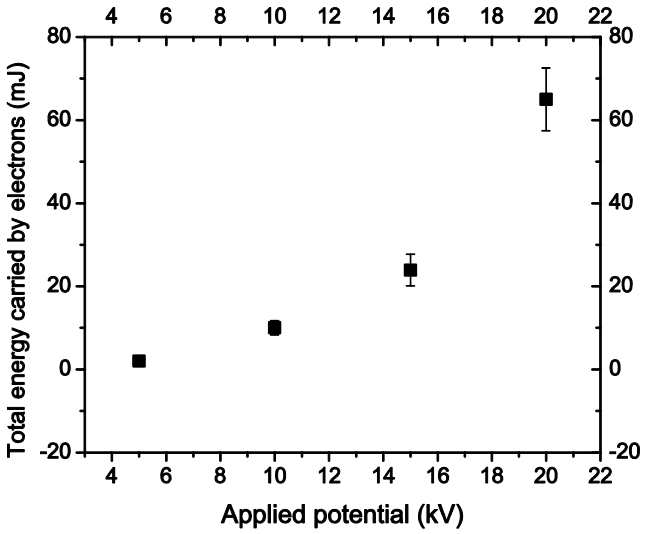


Figure 12. Total energy carried by generated electrons under various applied potential on pseudospark device

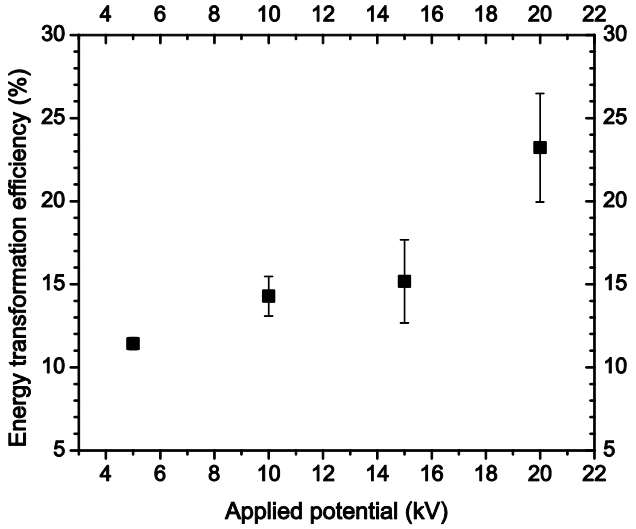


Figure 13. Energy transformation efficiency under various applied potential on pseudospark device

## 4. DISCUSSION AND CONCLUSION

In this paper, an improved RPEA is used to analyze pulsed electron beam energy from a multi-gap pseudospark discharge device. The presented RPEA is capable of operating under tens of mTorr and holding 20 kV retarding potential without any leakage breakdown on the RPEA. The time response of the presented RPEA setup is 8.3 ns. And the low-resistance of the electron beam detector permits the collection of electron energy at both high energy and low energy ranges. Experimental results on time-resolved electron energy distributions by this RPEA setup under various breakdown voltage on pseudospark device as electron beam source are presented in this work. Time-resolved energy spectrum and particle numbers of electrons at various energy groups are constructed through the differential electron beam pulses obtained at different retarding potential. The evaluation of electron beam energy transformation efficiency is defined and calculated compared to the input energy stored in the capacitors in pseudospark device. Based on the results presented in previous sections, main conclusions are summarized as follows:

1) The time-resolved electron energy spectrum shows that compared with the high energy electrons which are emitted at the earliest phase of electron beam pulse within approximately 300 ns after the ignition of gas breakdown in pseudospark device, the low energy electrons are distributed more uniformly at the total time duration of the beam pulse. For example, under 10 kV breakdown voltage on pseudospark device, the FWHM of electrons temporal distribution spread for electrons at 2 keV is 800 ns, which is 4 times the FWHM of electrons temporal distribution spread for electrons at 10 keV. Meanwhile, the long "tail" of the electron beam pulse consists of mainly the low energy electrons. Such observations and results are consistent with the results and simulations presented in [9-10, 35]. In [9-10], the high energy and low energy electrons are distinguished by a 'low-resistance' Faraday cup and a 'high-resistance' Faraday cup. The electron beam pulse collected by the high-resistance Faraday cup shows a narrow peak without the long tail collected by the low-resistance Faraday cup. This difference illustrates that the low energy electrons, rejected by the self-biased potential on high-resistance Faraday cup, is mainly focused on the tail of electron beam pulse. In [35], the simulation results based on a hybrid fluid-particle model show that the electrons accelerated to the full potential in the cathode fall are emitted at the earliest phase of the beam pulse. The collision rate and energy loss of electrons at high energy and low energy in vacuum and neutral gas is also an important factor of the time-resolved electron distribution spread formation [36]. The higher cross sections of low energy electrons cause a more dispersive distribution on the full time duration of the electron beam pulse, while the lower cross section and collision rate of high energy electrons result in a more concentrated distribution and propagation in the neutral gas and vacuum.

2) All the generated electrons from pseudospark device are divided into separate energy groups of 0-20%, 20%-40%, 40%-60%, 60%-80%, 80%-100% of full applied breakdown potential under all the investigated breakdown voltages and the percentage of electron numbers within individual energy groups is compared to the total generated electrons for different breakdown voltages. The results show that under all the investigated breakdown voltages, the electrons with maximum particle numbers are located in the medium energy range, 40-60% of full applied potential. Furthermore, the electron numbers at highest energy group are decreased with the breakdown voltage on

pseudospark discharge. Compared with the simulation results presented in [35], this observation in our work suggests that under higher breakdown voltage, the electron multiplication in the hollow cathode region is enhanced by higher cathode fall, causing more high energy electrons generated at the earliest phase of electron emission process. The electron particle numbers at lowest energy group below 20% of full applied potential is also decreased with lower breakdown voltage. The formation of those low energy electrons are still not well understood yet. Based on the statement suggested by Hartmann and Gundersen [3,37], when the cathode sheath thickness is smaller than 100μm, field-emission or field-enhance thermionic emission becomes the dominating process for the final discharge enhancement and electron multiplication and emission from cathode in pseudospark device. Thus under higher breakdown voltage on pseudospark device, the higher electric field strength compresses the cathode sheath thickness in the final process of discharge and electron generation, which enhances more low energy electrons emitted from pseudospark device. However, based on our results, the percentage of medium energy electrons within 40%-60% is increased with lower breakdown voltage. The formation of electrons within this energy range is still not well determined.

3) The energy transformation efficiency of electron generation is an important performance indicator for an electron beam source. In our work, the energy transformation efficiency of electron generation is defined as the ratio of total energy carried by the electrons calculated from time-resolved energy spectrum, to the total input energy, defined as the energy stored in the capacitors for pseudospark discharge. Previous work on this topic is limited and only [38] presents a method to estimate the electron beam generation efficiency. The total energy carried by electrons calculated from time-resolved energy spectrum is increased from 2 mJ at 5 kV breakdown voltage to 65 mJ at 20 kV breakdown voltage. Compared with the results presented in [38] (20% of efficiency of electron-beam generation by the pseudospark with external capacitor of 380 pF ), the energy transformation efficiency of electron generation by the pseudospark device presented in this work is varied from 11.4%-23.2%, which is found to be increased with breakdown voltage applied on pseudospark device with 1.4 nF external capacitors.

## REFERENCES


[1] Schaefer, G., Kristiansen, M. and Guenther, A. (eds) 1990 *Gas Discharge Closing Switches* (New York, N.Y.: Plenum Press)

[2] Frank, K., Christiansen, J., "Fundamentals of the pseudospark and its applications", (1989) *IEEE Transactions on Plasma Science*, 17 (5), pp. 748-753.

[3] Gundersen M.A. and Schaerfer G., (eds) 1990 *Physics and Applications of Pseudosparks* (New York, N.Y.: Plenum Press)

[4] Krasik, Ya.E., Gleizer, S., Chirko, K., Gleizer, J.Z., Felsteiner, J., Bernshtam, V., Matacotta, F.C., "Characterization of a channel spark discharge and the generated electron beam" (2006) *Journal of Applied Physics*, 99 (6), art. no. 063303

[5] Witke, T., Lenk, A., Siemroth, P., "Channel spark discharges for thin film technology" (1997) *IEEE Transactions on Plasma Science*, 25 (4), pp. 758-762.

[6] Dewald, E., Frank, K., Hoffmann, D.H.H., Tauschwitz, A., "Plasma development in the low-pressure channel spark for pulsed intense electron beam generation" (2002) *IEEE Transactions on Plasma Science*, 30 (1 III), pp. 363-374.

[7] Wyndham, E., Aliaga-Rossel, R., Chuaqui, H., Favre, M., Mitchell, I.H., Choi, P., "X-ray and plasma dynamics of an intermediate size capillary discharge" (2002) *IEEE Transactions on Plasma Science*, 30 (1 III), pp. 401-407.

[8] Wyndham, E., Favre, M., Aliaga-Rossel, R., Chuaqui, H., Mitchell, I., Choi, P., "Formation and dynamics of a Z pinch in a high current capillary discharge in initial vacuum" (2003) *Journal of Applied Physics*, 94 (9), pp. 5537-5542.

[9] Dewald, E., Frank, K., Hoffmann, D.H.H., Stark, R., Ganciu, M., Mandache, B.N., Nistor, M.G., Pointu, A.-M., Popescu, I.-I., "Pulsed intense electron beams generated in transient hollow cathode discharges: fundamentals and applications" (1997) *IEEE Transactions on Plasma Science*, 25 (2), pp. 272-278.

[10] Dewald, E., Frank, K., Hoffmann, D.H.H., Tauschwitz, A., "Comparative studies on intense electron beams generated in transient hollow-cathode discharges" (2002) *IEEE Transactions on Plasma Science*, 30 (5 I), pp. 1820-1826.

[11] Rosier, O., Apetz, R., Bergmann, K., Jonkers, J., Wester, R., Neff, W., Pankert, J., "Frequency scaling in a hollow-cathode-triggered pinch plasma as radiation source in the extreme ultraviolet" (2004) *IEEE Transactions on Plasma Science*, 32 (1 II), pp. 240-246.

[12] Boggasch, E., Rhee, M.J., "High-brightness pseudospark-produced electron beam" (1990) *Applied Physics Letters*, 56 (18), pp. 1746-1748.

[13] Jain, K.K., Boggasch, E., Reiser, M., Rhee, M.J., "Experimental investigation of a pseudospark-produced high-brightness electron beam" (1990) *Physics of Fluids B*, 2 (10), pp. 2487-2491.

[14] Korolev, Y.D., Frank, K., "Discharge formation processes and glow-to-arc transition in pseudospark switch" (1999) *IEEE Transactions on Plasma Science*, 27 (5), pp. 1525-1537.

[15] Bochkov, V.D., Dyagilev, V.M., Ushich, V.G., Frants, O.B., Korolev, Yu.D., Shemyakin, I.A., Frank, K., "Sealed-off pseudospark switches for pulsed power applications (current status and prospects)" (2001) *IEEE Transactions on Plasma Science*, 29 (5 I), pp. 802-808.

[16] Jiang, C., Kuthi, A., Gundersen, M.A., "Toward ultracompact pseudospark switches" (2005) *Applied Physics Letters*, 86 (2), art. no. 024105, pp. 024105-1-024105-3.

[17] Bergmann, K., Lebert, R., Kiefer, J., Neff, W., "Triggering a radial multichannel pseudospark switch using electrons emitted from material with high dielectric constant" (1997) *Applied Physics Letters*, 71 (14), pp. 1936-1938.

[18] Yin, H., Cross, A.W., He, W., Phelps, A.D.R., Ronald, K., "Pseudospark experiments: Cherenkov interaction and electron beam post-acceleration," (2004) *IEEE Transactions on Plasma Science*, 31 (1), pp. 233- 239.

[19] Yin, H., Cross, A.W., He, W., Phelps, A.D.R., Ronald, K., Bowes, D., Robertson, C.W., "Millimeter wave generation from a pseudospark-sourced electron beam" (2009) *Physics of Plasmas*, 16 (6), art. no. 063105.

[20] Yin, H., Robb, G.R.M., He, W., Phelps, A.D.R., Cross, A.W., Ronald, K., "Pseudospark-based electron beam and Cherenkov maser experiments" (2000) *Physics of Plasmas*, 7 (12), pp. 5195-5205.

[21] Muntz, E.P., Kunc, J.A., Erwin, D.A., "A pulsed electron-photon fluoresence technique for temperature and specie concentration measurement at points in relatively dense, unseeded air flows" (1987) AIAA-87-1526. *AIAA Thermophysics Conference*, 22 nd, Honolulu, Hawaii.

[22] Lufty, F.M., Muntz, E.P., "Initial experimental study of pulsed electron beam fluorescence", (1996) *AIAA Journal*, Vol. 34, No. 3, pp. 478-482.

[23] Macheret, S. O., Shneider, M. N., Miles, R. B., "Modeling of air plasma generation by electron beams and high-voltage pulses," (2000) AIAA-2000-2569, *AIAA Plasmadynamics and Lasers Conference*, 31st, Denver, CO.

[24] Macheret, S. O., Miles, R. B., Nelson, G. L., Macheret, S. O., Miles, . B., Nelson, G. L., "Feasibility study of a hybrid MHD/radiatively driven facility for hypersonic ground testing," (1997) AIAA-1997-2429, *AIAA Plasmadynamics and Lasers Conference*, 28th, Atlanta, GA.

[25] Macheret, S. O., Shneider, M. N., Miles, R. B., "Electron beam generated plasmas in hypersonic MHD channels," (1999) AIAA-1999-3635, *AIAA Thermophysics Conference*, 33rd, Norfolk, VA.

[26] Macheret, S. O., Shneider, M. N., Miles, R. B., Lipinski, R. J., "Electron-Beam-Generated Plasmas in Hypersonic Magnetohydrodynamic Channels," (2001) *AIAA Journal*, 0001-1452, Vol. 39, No. 6, pp 1127-1138.

[27] Ramaswamy, K., Destler, W.W., Rodgers, J., "A high-voltage triggered pseudospark discharge experiment" (1996) *Journal of Applied Physics*, 80 (9), pp. 4887-4895.

[28] Lieberman, M.A., Lichtenber, A.J., 1994 *Principles of plasma discharges and materials processing* (New York, N. Y.: Wiley)

[29] Jiang, C., Kuthi, A., Gundersen, M.A., Hartmann, W., "Pseudospark electron beam as an excitation source for extreme ultraviolet generation" (2005) *Applied Physics Letters*, 87 (13), art. no. 131501, pp. 1-3.

[30] Ding, B.N., Myers, T.J., Rhee, M.J., "Time-resolved energy spectrum of a pseudospark-produced electron beam" (1993) *Review of Scientific Instruments*, 64 (6), pp. 1442-1444.

[31] Liu, C.J., Rhee, M.J., "Experimental study of post-acceleration and transport of a pseudospark-produced electron beam" (1993) *Proceedings of the IEEE Particle Accelerator Conference*, 1, pp. 688-690.

[32] Modreanu, G., Mandache, N.B., Pointu, A.M., Ganciu, M., Popescu, I.I., "Time-resolved measurement of the energy distribution function of an electron beam created by a transient hollow cathode discharge", (2000) *Journal of Physics D: Applied Physics*, 33 (7), pp. 819-825.

[33] Hu, J., Rovey, J.L., "Faraday cup with nanosecond response and adjustable impedance for fast electron beam characterization" (2011) *Review of Scientific Instruments*, 82 (7), art. no. 073504.

[34] Zou, Y., Cui, Y., Haber, I., Reiser, M., O'Shea, P.G., "Longitudinal space-charge effects in a retarding field energy analyzer", (2003) *Physical Review Special Topics - Accelerators and Beams*, 6 (11), pp. 1-10.

[35] Boeuf, Jean-Pierre, Pitchford, Leanne C., "Pseudospark discharges via computer simulation" (1991) *IEEE Transactions on Plasma Science*, 19 (2), pp. 286-296.

[36] Miller, R.B., 1982 *An introduction to the physics of intense charged particle beams* (New York, N.Y.: Plenum Press)

[37] Hartmann, W., Gundersen, M.A., "Origin of anomalous emission in superdense glow discharge", (1988) *Physical Review Letters*, 60 (23), pp. 2371-2374.

[38] Jain, K.K., Boggasch, E., Reiser, M., Rhee, M.J., "Experimental investigation of a pseudospark-produced high-brightness electron beam" (1990) *Physics of Fluids B*, 2 (10), pp. 2487-2491.

# 4. SUMMARY AND RECOMMENDATIONS FOR FUTURE WORK

The main emphasis of this dissertation is the experimental investigation of the pseudospark discharge properties and intense electron beams generated by pseudospark device. This dissertation consists of introduction of pseudospark discharge, literature reviews of previous research work and application interest on pseudospark in a variety of areas in chapter 1, introduction of the design and construction of a high voltage pseudospark discharge experiment setup and diagnostic system in chapter 2, and three journal articles which have been published or under review presented in chapter 3. Based on research work completed in this dissertation, the following issues are recommended for future work.

## 4.1 TRIGGER SOURCE IN THE HOLLOW CATHODE REGION

Pseudospark discharge can be operated under self-trigger mode, and external trigger mode [1-4]. Trigger is an important issue in low pressure discharge, since in the low pressure pulsed discharge of high E/N, the gas density is comparatively low to $10^{13}$-$10^{14}$/cm$^3$. At such low gas density, the initial ionization which is originated in the hollow cathode region may be random in some cases. In many previous research work, it has been shown that the introduction of trigger source in hollow cathode region can improve the performance of stable operation in given pseudospark device [5-7]. The trigger methods of pseudospark discharge includes optical trigger [5], high voltage pulse trigger [6], and surface discharge over insulators [7].

In addition to the improvement of device performance, the introduction of trigger can provide more accurate time-resolved information of development and process of pseudospark discharge, which is of great importance for the fundamental gas discharge physics. Electron beam generation by pseudospark discharge is also dependent on the stable ionization counts originated in hollow cathode region [2]. Thus the introduction of trigger source in hollow cathode also may improve the stable production of electron beams from pseudospark device. The trigger mechanism and efficient trigger method for the pseudospark device in this work are recommended for future work.

## 4.2 MODELING AND SIMULATION OF INTENSE PULSED ELECTRON BEAMS INTERACTING WITH NEUTRAL GAS

As discussed in Chapter 1, the intense pulsed electron beam generated from pseudospark has a variety of applications or potential applications in different areas. The experimental investigations results completed in this dissertation have focused on determinations of discharge properties and electron beam characteristics. But more information can not be obtained by experimental work currently, thus the modeling and particle simulations are required for assistance with experimental investigations and multiple applications. An example is the plasma generation by intense pulsed electron beam interacting with neutral gas [8-12]. The capacity of pulsed energetic electron beams to generate plasma is of great research interest for many applications, while the experimental investigations on this issue is very limited and challenging [12]. Thus the theoretical modeling and simulations on the interaction of neutral gas with intense energetic electrons is necessary [8-11]. XOOPIC, an X11 based Object Oriented Particle-In-Cell code, can be applied to simulate such processes. The accurate determination of time structure and electron energy distribution spectrum completed in this dissertation provides necessary input information for the simulation work, which can greatly improve the accuracy of simulation work. Thus the modeling of development of intense pulsed electron beams interacting with neutral gas, and the ionization process by energetic electrons with neutral gas under various pressures by XOOPIC is recommended for future work and under progress currently.

## 4.3 OPERATIONS OF PSEUDOSPARK DISCHARGE UNDER HIGHER VOLTAGES

In this dissertation, a high voltage pseudospark discharge experiment consisting of high voltage charging and transmission, vacuum pumping, gas flow controller, electron beam diagnostics is designed and constructed for high voltage operation. The construction and calibration of high voltage operation and transmission system are

summarized in chapter 2. The presented experiment setup is operated under voltage up to 20 kV in this dissertation. The experiment results presented in this dissertation show that the electron output, energy transformation efficiency and discharge properties are improved with increasing applied voltage on pseudospark device. Thus the operation of pseudospark discharge under higher applied voltages is recommended for future work to improve the electron generation capacity of the device.

## BIBLIOGRAPHY

[1] Gundersen M.A. and Schaerfer G., (eds) 1990 *Physics and Applications of Pseudosparks* (New York, N.Y.: Plenum Press)

[2] Schaefer, G., Kristiansen, M. and Guenther, A. (eds) 1990 *Gas Discharge Closing Switches* (New York, N.Y.: Plenum Press)

[3] Boeuf, Jean-Pierre, Pitchford, Leanne C., "Pseudospark discharges via computer simulation", (1991) *IEEE Transactions on Plasma Science*, 19 (2), pp. 286-296.

[4] Mehr, Thomas, Arenz, Hartmuth, Bickel, Peter, Christiansen, Jens, Frank, Klaus, Goertler, Andreas, Heine, Frank, Hofmann, Detlef, Kowalewicz, Roland, Schlaug, Martin, Tkotz, Rupert, "Trigger devices for pseudospark switches", (1995) *IEEE Transactions on Plasma Science*, 23 (3), pp. 324-329.

[5] Jiang, C., Kuthi, A., Gundersen, M.A. "Toward ultracompact pseudospark switches", (2005) *Applied Physics Letters*, Vol. 86, No. 2, art. no. 024105, pp. 024105-1-024105-3.

[6] Jain, K.K., Ding, B.N., Rhee, M.J., "Scaling study of pseudospark produced electron beam", (1991) *Conference Record of the Particle Accelerator Conference, Accelerator Science and Technology., IEEE*, Vol. 3, pp.1972-1974.

[7] Goertler, Andreas, Christiansen, Jens, Dotzer, Robert, Frank, Klaus, "Investigations of pulsed surface flashovers for the triggering of pseudospark high-power switches", (1989) *IEEE Transactions on Plasma Science*, 17 (5), pp. 762-765.

[8] Macheret, S. O., Shneider, M. N., Miles, R. B., and Lipinski, R. J., "Electron-Beam-Generated Plasmas in Hypersonic Magnetohydrodynamic Channels", (2001) *AIAA Journal*, 0001-1452, Vol. 39, No. 6, pp 1127-1138.

[9] Macheret, S. O., Miles, . B., Nelson, G. L., "Feasibility study of a hybrid MHD/radiatively driven facility for hypersonic ground testing", (1997) *AIAA-1997-2429, Plasmadynamics and Lasers Conference*, 28th, Atlanta, GA.

[10] Macheret, S. O., Shneider, M. N., Miles, R. B., "Modeling of air plasma generation by electron beams and high-voltage pulses", (2000) *AIAA-2000-2569, AIAA Plasmadynamics and Lasers Conference*, 31st, Denver, CO.

[11] Macheret, S. O., Shneider, M. N., Miles, R. B., "Electron beam generated plasmas in hypersonic MHD channels", (1999) *AIAA-1999-3635, AIAA Thermophysics Conference*, 33rd, Norfolk, VA.

[12] Vidmar, R. J., Seeley, M. V., Serdyuchenko, A., Stalder, K. R., "Electrical, RF, and optical diagnostics in E-beam excited air plasma", (2008) *AIAA 2008-1111, AIAA Aerospace Sciences Meeting and Exhibit*, 46th, Reno, NV.

# VITA

Jing Hu was born in Hubei, China. She received her Bachelor of Engineering degree in Electrical Engineering in 2004 from Xi'an Institute of Telecommunications, Xi'an, China. In 2007, she received her Master of Science degree in Atomic and Molecular Physics from Chinese Academy of Sciences, China. She joined the Ph.D degree program in Aerospace Engineering at Missouri University of Science and Technology in Rolla, Missouri in Fall semester, 2008. And she received her Doctor of Philosophy in Aerospace Engineering from Missouri University of Science and Technology in December 2012. Her research interests include high voltage pulse power technology, gas discharge physics, fast signal measurements, and charge particle diagnostics.